

THE EXTRAGALACTIC DISTANCE SCALE KEY PROJECT. IV. THE DISCOVERY OF CEPHEIDS AND A NEW DISTANCE TO M100 USING THE HUBBLE SPACE TELESCOPE¹

LAURA FERRARESE,² WENDY L. FREEDMAN,³ ROBERT J. HILL,³ ABHIJIT SAHA,⁴ BARRY F. MADORE,⁵
ROBERT C. KENNICUTT JR.,⁶ PETER B. STETSON,⁷ HOLLAND C. FORD,² JOHN A. GRAHAM,⁸
JOHN G. HOESSEL,⁹ MINGSHENG HAN,⁹ JOHN HUCHRA,¹⁰ SHAUN M. HUGHES,¹¹
GARTH D. ILLINGWORTH,¹² DANIEL KELSON,¹² JEREMY R. MOULD,¹³ RANDY PHELPS,³
N. A. SILBERMANN,⁵ SHOKO SAKAI,⁵ ANNE TURNER,⁶ PAUL HARDING,⁶
AND FABIO BRESOLIN⁶

Received 1995 September 8; accepted 1995 December 15

ABSTRACT

We report on observations of Cepheids in the Virgo spiral galaxy M100, based on data obtained with the Wide Field and Planetary Camera 2 (WFPC2) on board the *Hubble Space Telescope* (*HST*). The observations are part of the *HST* Key Project on the Extragalactic Distance Scale, which aims to provide a measurement of the Hubble constant H_0 with 10% accuracy. A total of 12 epochs were obtained using the F555W filter (transformed to Johnson V), and 4 epochs using the F814W filter (transformed to Cousins I). Photometry on the data was performed using two independent packages, DoPHOT and DAOPHOT II/ALLFRAME; a total of 52 Cepheids, with periods ranging from about 10 to 70 days, were identified based on both sets of photometry.

We have fitted V and I period-luminosity relations and derived apparent V and I distance moduli assuming a Large Magellanic Cloud distance modulus and mean color excess of $\mu_{\text{LMC}} = 18.50 \pm 0.10$ mag and $E(B-V) = 0.10$ mag, respectively. Using the extinction law given by Cardelli, Clayton, & Mathis, and adopting our most recent WFPC2 (“long-exposure”) zero-point calibration, we obtain a true distance modulus for M100 of $\mu_0 = 30.04 \pm 0.17$ mag, corresponding to a distance $d = 16.1 \pm 1.3$ Mpc, and a total (Galactic plus internal) mean color excess $E(B-V) = 0.10 \pm 0.06$ mag.

When compared with the preliminary distance of 17.1 ± 1.8 Mpc derived by Freedman et al. from the same set of data, the results presented here benefit from a larger sample size, refinements in the zero-point calibration, and improvements in the software packages used for the photometry. The two results agree to within their quoted errors.

Subject headings: Cepheids — galaxies: distances and redshifts — galaxies: individual (M100)

1. INTRODUCTION

M100 (=NGC 4321) is one of the most conspicuous spiral galaxies in the Virgo cluster, located 3.9° from the central Virgo giant elliptical M87. Seen nearly face-on (Warmels 1988), the galaxy has been classified as Sc(s)I by Sandage & Tammann (1981), and as SAB(s)bc by de Vaucouleurs, de Vaucouleurs, & Corwin (1976), although recent H I and optical images suggest that M100 may in fact be a

barred spiral (Knapen et al. 1993). According to Sandage & Tammann (1981), the recession velocity, relative to the centroid of the local group (using the standard IAU correction), is 1501 ± 4 km s⁻¹, and the integrated blue magnitude is $B_T = 10.11$. M100 is poorly resolved from the ground, but from space a color-magnitude diagram has been obtained from high-resolution *Hubble Space Telescope* (*HST*) B , V , and R images, identifying the brightest stars, several young clusters, and associations in the spiral arms (Freedman et al. 1994b).

There is considerable debate in the literature regarding the distance to the Virgo cluster, with estimates ranging from 15 Mpc (Jacoby, Ciardullo, & Ford 1990) up to 28 Mpc (Sandage 1993). The distance to M100 itself is no exception to this debate: Schmidt et al. (1994) quote a distance of 15 ± 4 Mpc by applying the Expanding Photosphere Method (EPM) to the bright Type II supernova SN 1979C, although the Baade Method applied to the same supernova yielded a distance of 23 ± 3 Mpc (Branch et al. 1981). A distance of 18.4 ± 2.2 Mpc was derived based on the Tully-Fisher relation (Pierce & Tully 1988) and then revised in a subsequent paper (Pierce 1994) to 14.5 ± 1.1 Mpc. These distances are in satisfactory agreement, but more extreme values are found in the literature. By assuming that M100 has the same diameter as M101, Sandage (1993) calculated a distance of 27.7 Mpc, while de Vaucouleurs (1982) derived a distance to M100 of 11.8 by comparing the relative positions of 37 spirals in the Virgo

¹ Based on observations with the NASA/ESA *Hubble Space Telescope*, obtained at the Space Telescope Science Institute, which is operated by AURA, Inc., under NASA contract NAS 5-26555.

² Johns Hopkins University and Space Telescope Science Institute, Baltimore, MD 21218.

³ Carnegie Observatories, Pasadena, CA 91101.

⁴ Space Telescope Science Institute, Baltimore, MD 21218.

⁵ NASA/IPAC Extragalactic Database and California Institute of Technology, Pasadena, CA 91125.

⁶ Steward Observatory, University of Arizona, Tucson, AZ 85721.

⁷ Dominion Astrophysical Observatory, Victoria, BC, V8X 4M6 Canada.

⁸ Department of Terrestrial Magnetism, Carnegie Institutions of Washington, Washington, DC 20015.

⁹ University of Wisconsin, Madison, WI 53706.

¹⁰ Harvard-Smithsonian Center for Astrophysics, Cambridge, MA 02138.

¹¹ Royal Greenwich Observatory, Cambridge CB3 OHA, UK.

¹² Lick Observatory, University of California, Santa Cruz, CA 95064.

¹³ Mount Stromlo and Siding Spring Observatories, Institute of Advanced Studies, ANU, ACT 2611, Australia.

cluster based on a variety of secondary distance indicators available at that time.

Based on *HST* observations of a sample of 20 Cepheids in M100, Freedman et al. (1994c) derived a preliminary distance of 17.1 ± 1.8 Mpc, in good agreement with the value inferred from SN 1979C via EPM and the Tully-Fisher relation. Since the publication of the Freedman et al. (1994c) paper, we have completed a more comprehensive analysis of the *HST* observations of M100; the zero-point calibration has been improved, and improvements have been made to the software packages used to measure magnitudes. In this paper, we present the details of the data analysis and refine our measurements of the M100 distance using a larger sample of 52 Cepheids. In a companion paper (Hill et al. 1996), we present details of the photometric reduction and calibration, and color-magnitude diagrams of the resolved stellar population.

Cepheids have a well-known and very successful history as distance indicators. The period-luminosity (PL) relation, as applied to Cepheids discovered in M31 and M33, led to the conclusion that these systems were located far beyond the boundaries of the Milky Way (Hubble 1925), a discovery that laid the basis for Hubble's remarkable work on the extragalactic distance scale. Since then, the PL relation has undergone many revisions and refinements (e.g., Feast & Walker 1987; Walker 1988; Madore & Freedman 1991), and Cepheid distances have been determined for several late-type spirals and irregular galaxies in the Local Group, including the SMC, LMC, M31, M33, IC 1613, NGC 6822, and WLM, as well as for more distant galaxies, including NGC 2403 and the M81 group, NGC 300, Sextans A, Sextans B, Leo A, Pegasus, and M101. To date, the most distant Cepheids discovered with ground-based facilities are reported at the Canada-France-Hawaii Telescope by Pierce et al. (1994), who discovered four candidate Cepheids in the Virgo galaxy NGC 4571, placing it at a distance of 14.1 Mpc.

A new era in detecting and measuring Cepheids began with *HST*. The telescope has proved to be extremely effective in discovering Cepheids when compared to ground-based facilities. The telescope resolution (a factor 5–10 improvement when compared with the best conditions at ground-based sites) significantly reduces the problems of crowding and confusion that ultimately limit the ground-based detections. A second, but no less important, advantage is the ability to schedule observations so as to maximize the probability of detecting Cepheids over a broad range of periods, with optimum coverage of the light curves, within a single observing season. Ground-based efforts, in contrast, are continually compromised by weather, variable seeing, day–night cycles, phases of the moon, and scheduled instrument changes.

Distance measurements to three nearby galaxies are now available based on *HST* observations obtained before the 1993 December mission that corrected for the spherical aberration affecting the *HST* primary mirror. Freedman et al. (1994a) reported on the discovery of 30 new Cepheids in M81 (only two Cepheids with well-determined periods had been detected previously from the ground, e.g., Freedman & Madore 1988), which yielded a distance of 3.63 ± 0.34 Mpc. Saha et al. (1994) discovered 28 Cepheids in the nearby Sdm galaxy IC 4182, giving a distance of 4.7 ± 0.2 Mpc. Based on 11 Cepheids, Sandage et al. (1994) determined a distance of 4.1 ± 0.1 Mpc to the galaxy NGC 5253. With *HST* now

restored to its full capabilities, the search for Cepheids has moved to the Virgo cluster with the discovery of Cepheids in M100.

The observations presented in this paper are part of an extensive *HST* project, which aims to provide an absolute calibration for the extragalactic distance scale by measuring Cepheid distances to approximately 20 galaxies within a redshift of approximately 1500 km s^{-1} . The project, known as The *HST* Key Project on the Extragalactic Distance Scale, has been described elsewhere (Freedman et al. 1994a, 1994b, 1994c; Mould et al. 1996; Kennicutt, Freedman, & Mould 1995) and will lead to a determination of the Hubble constant H_0 to within 10% accuracy by providing an accurate absolute calibration for a number of secondary distance indicators, such as the Tully-Fisher relation, the Planetary Nebula Luminosity Function, the Surface Brightness Fluctuation Method, the Expanding Photosphere Method, the Globular Cluster Luminosity Function, and the Type Ia supernova standard candle.

This paper is organized as follows: Section 2 describes the data and the preliminary reduction. Sections 3 and 4 deal with the photometric reduction and the variable star search. The results from §§ 3 and 4 are compared in § 5. The *V* and *I* PL relations and the apparent distance moduli are discussed in § 6, while § 7 deals with the extinction and the true distance modulus. The conclusions are drawn in § 8.

2. OBSERVATIONS AND DATA REDUCTION

2.1. Observing Strategy

The *HST* observations of M100 began on 1994 April 23 using the Wide Field and Planetary Camera 2 (WFPC2). A total of 25 F555W images, divided among 12 epochs, were obtained within a 57 day period, with the sequence ending on 1994 June 19. The F555W filter has a bandpass close to the Johnson *V*. In the same time interval, nine additional images, divided into four epochs, were obtained using the F814W filter, which is similar to Cousins *I*. All of the observations were carried out at the same telescope pointing and roll angle.

A detailed description of the WFPC2 and its capabilities can be found in the *HST* WFPC2 Instrument Handbook, Version 2.0 (Burrows et al. 1994). Briefly, the WFPC2 consists of four separate 800×800 CCD detectors. Three of these are the Wide Field Camera (WFC) chips, with a pixel size of $0''.10$ and a field of view of $1.3'' \times 1.3''$ per chip. The fourth CCD is the higher resolution Planetary Camera (PC1), with a pixel size of $0''.046$ and a field of view of $36'' \times 36''$. The gain and readout noise are about $7 \text{ e}^- \text{ DN}^{-1}$ and 7 e^- , respectively. All observations were obtained with the telescope guiding in fine lock, which has a nominal pointing stability of about 3 mas. The WFPC2 field of view is illustrated in Figure 1 (Plate 16), superimposed on a *V* band image of M100 obtained by R. Peletier at the prime focus of the INT at La Palma.

The summary of observations and exposure times is given in Table 1. The sampling strategy has been discussed by Freedman et al. (1994a). The spacing between observations was chosen in order to maximize the probability of detecting Cepheids with periods between 3 and 60 days, allowing at the same time for an optimum sampling of the light curves and reducing the possibility of aliasing. Due to technical reasons (the first visit was canceled and then rescheduled at the end of the sequence due to a telescope safing

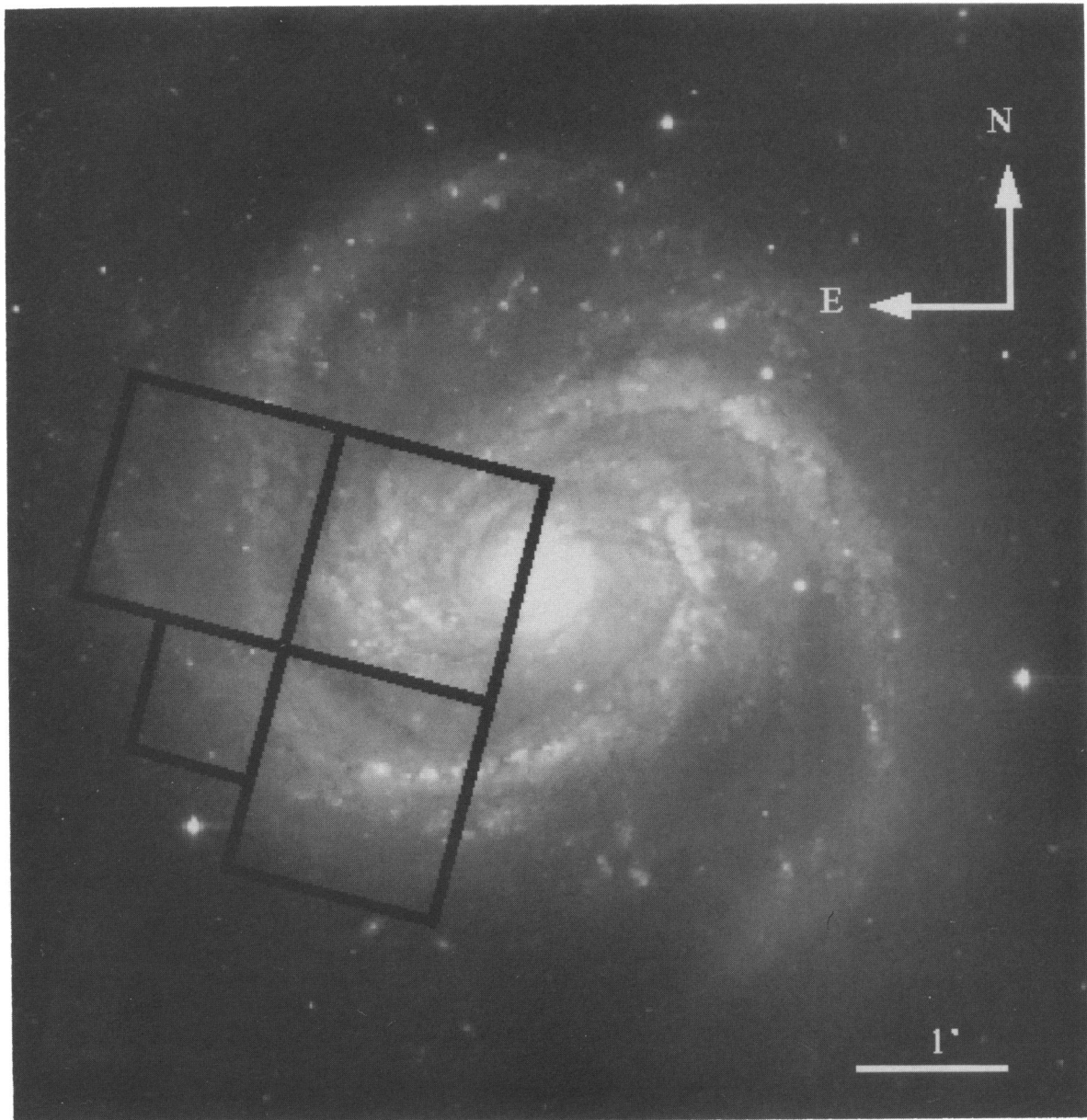


FIG. 1.—*V*-band ground-based image of M100, obtained by R. Peletier at the prime focus of the INT, La Palma. Superimposed is the *HST*/WFPC2 field of view.

FERRARESE et al. (see 464, 569)

TABLE 1
LOG OF OBSERVATIONS

Observation Date (1)	JD (2)	Exposure Time (s) (3)	Filter (4)
94 Apr 23	2449465.781	1800 + 1800	F555W
	2449465.909	2100 + 1500	F814W
94 May 4	2449476.707	1800 + 1800	F555W
94 May 6	2449478.986	1800 + 1800	F555W
94 May 9	2449482.401	2100 + 1500	F555W
94 May 12	2449485.216	2100 + 1500 + 350	F555W
	2449485.349	1900 + 1700 + 350	F814W
94 May 16	2449489.037	2100 + 1500	F555W
94 May 20	2449493.528	2100 + 1500	F555W
94 May 26	2449498.824	2100 + 1500	F555W
94 May 31	2449503.852	2100 + 1500	F555W
94 Jun 7	2449510.819	1800 + 1800	F555W
	2449510.811	2100 + 1500	F814W
94 Jun 17	2449520.949	1800 + 1800	F555W
94 Jun 19	2449522.959	1800 + 1800	F555W
	2449523.093	2100 + 1500	F814W

NOTES.—Log of the *HST*/WFPC2 observations of M100. At least two images of the same field were taken at each epoch, in order to facilitate removal of cosmic rays. The Julian Date reported in col. (2) refers to the middle of the observing sequence for each epoch.

The following are the reference files used in the calibration of the F555W exposures (see § 2.2). The name conventions are the ones adopted by the STScI in the header of the science data, except for the bias and dark frames that were provided by the WFPC2 IDT. MASKFILE = e2112084u.r0h, ATODFILE = dbu1405iu.r1h; BIASFILE = biasapr94.r2h (for 1994 April 23 exposures, both F555W and F814W), BIASFILE = biasmay94.r2h (for exposures other than the 1994 April 23, both F555W and F814W); DARKFILE = darkapr94.r3h (for 1994 April 23 exposures, both F555W and F814W), DARKFILE = darkmay94.r3h (for exposures other than the 1994 April 23, both F555W and F814W); FLATFILE = e380935cu.r4h (for F555W exposures), FLATFILE = e391434fu.r4h (for F814W exposures); SHADFILE = e371355eu.r5h (shutter A) or e371355iu.r5h (shutter B), depending on the shutter in place at the beginning of the exposure; GRAPHTAB = dc614258m.tmg; COMPTAB = dc614242rm.tmc.

event), the actual observations did not follow exactly the intended sampling. The solid line in Figure 2 represents the probability that a variable with period P is detected given the temporal sampling of our observations, under the assumption that all initial phases are equally likely, following the lines given in Saha et al. (1994). In the figure, the incompleteness due to magnitude-dependent selection effects has not been taken into account. The probability of detection is reasonably stable over the range between 3 and 60 days, with a minimum at 22 days and maximum peaks at 25, 30, and 50 days, but the probability of finding variables with periods larger than 60 days, which coincides with the length of the observing window, decreases rapidly with increasing period. For comparison, the dashed line in Figure 2 shows what the probability of discovery would have been if the proposed scheduling had been adopted.

2.2. Data Reduction

HST data are routinely calibrated using a standard pipeline maintained by the Space Telescope Science Institute (STScI). The reduction steps are performed in the following order: correction of small analog-to-digital (A/D) errors; subtraction of a bias level for each chip; subtraction of a superbias frame; subtraction of a dark frame; and correction for shutter shading effects and division by a flat field. The reduction procedure is described in detail by Holtzman et al. (1995). During the period spanned by the M100 observations, substantial improvements to the routine cali-

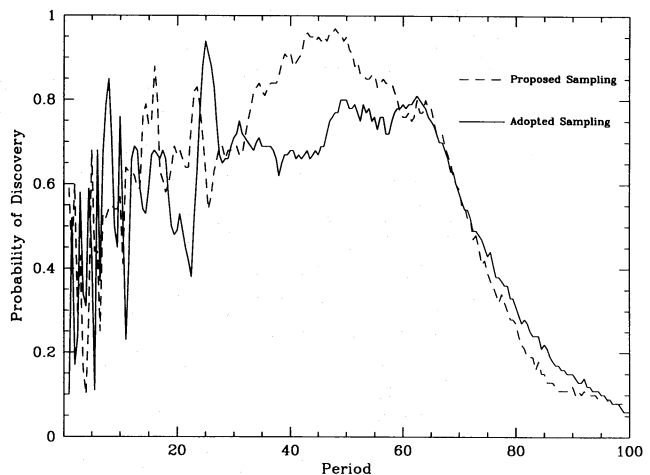


FIG. 2.—The solid line represents the probability that a variable with period P is detected given the temporal sampling of our observations, under the assumption that all initial phases are equally likely. The incompleteness due to magnitude-dependent selection effects has not been taken into account. The dashed line shows what the probability of discovery would have been if the proposed scheduling had been adopted.

bration files were made. In particular, the introduction of a new generation of bias and dark frames was made available by the WFPC2 Instrument Definition Team (IDT). In order to produce an homogeneous data set, all observations of M100 were reprocessed using the new calibration files. The STScI names of the reference files used for the recalibration are listed in the notes to Table 1.

It is known that the WFPC2 suffers from a growth in the number of hot pixels with time (Holtzman et al. 1995). The problem was reduced, but not eliminated, by lowering the CCD operating temperature from -77°C to -88°C on 1994 April 23. The first of the M100 epochs was taken at the higher (-77°C) temperature, while all subsequent epochs were taken at the lower (-88°C) temperature. The IDT dark frames used in the re-reduction of the M100 exposures, known as the “superdarks,” are made from many individual dark frames taken over several months at the two operating temperatures. Unfortunately, during this time interval, several hundred new hot pixels appeared. As a consequence, the use of the superdarks can leave many hot pixels uncorrected. To solve the problem, J. Holtzman (1994, private communication) has made available sets of “delta darks,” each made from three to five individual dark frames taken within a week, and from which the superdark has been subtracted. The hot pixels that are not removed by the superdark can largely be eliminated by subtracting the delta dark, which is taken as close as possible to the image itself, from the calibrated image. As will be clear in § 3, the few hot pixels that may still be left after this procedure do not pose a serious problem to the photometry, since they are easily distinguishable from stellar objects.

Another potential problem is the so-called “charge transfer effect” (Holtzman et al. 1995). At the CCD operating temperature of -77°C , a 10%–15% gradient in the photometry has been measured across each chip due to charge transfer inefficiencies, in the sense that a star appears fainter at higher row numbers. The effect depends on the apparent magnitude of the star, being more severe for fainter objects, as well as on the specific chip and on the filter used. Fortunately, as noted above, only the first epoch was taken at the higher operating temperature. At -88°C , the problem is

much reduced, with the effect being 3%–4% peak to peak across the chip, corresponding to an additional error of about 0.01 mag in the photometry if no correction is attempted. In addition, the charge transfer effect becomes less pronounced with increasing background level. Analysis of the data (Hill et al. 1996) shows that the effect is likely to be smaller than 1% peak to peak for the M100 images. Therefore, as will be discussed extensively in § 7, the impact of the charge transfer effect on the distance modulus is negligible compared with other sources of error.

3. PHOTOMETRIC REDUCTION

Photometric analysis of the data was performed independently by L. F. and A. S. at the Johns Hopkins University and STScI in Baltimore, using a variant of DoPHOT (Schechter, Mateo, & Saha 1993; see also Saha et al. 1994), and by R. H. and W. L. F. at the Carnegie Observatories, Pasadena, using DAOPHOT II and ALLFRAME (Stetson 1994). A critical and detailed comparison of the DoPHOT and DAOPHOT photometry is presented in a companion paper (Hill et al. 1996), and we only summarize the highlights below.

The philosophies behind the DoPHOT and DAOPHOT II/ALLFRAME programs are entirely different. DoPHOT uses a point-spread function (PSF) derived from the brightest and most isolated stars in the image being analyzed, while the PSFs used in the DAOPHOT reduction are constructed a priori from independent images of uncrowded fields. To aid the photometry, both DoPHOT and DAOPHOT resort to a template file containing a close to complete list of stars to be found in each image, created by running the programs on a deep frame obtained by averaging all of the images belonging to different epochs. However, while DoPHOT is then run independently on each image, ALLFRAME simultaneously reduces all the single images, identifying as real only objects appearing in a significant fraction of the frames. This makes DAOPHOT II/ALLFRAME very robust in identifying cosmic-ray events, while DoPHOT is more easily run on images from which cosmic rays have been removed. Because of the fundamental differences in the way DoPHOT and DAOPHOT handle the data, comparing the sets of photometry that are output by the two programs provides an independent check of the results and is a very powerful tool for revealing systematic errors that could be present in the measured magnitudes, and would most likely go unnoticed if only one of the two programs was used.

Removal of the cosmic rays is easily done in the case of M100 since a pair of images with the same orientation are available for each epoch. The two images can be combined, and cosmic rays flagged, by comparing the difference in values between pairs of corresponding pixels with a local σ calculated from the combined effects of Poisson statistics and local noise (see Hill et al. 1996). The version of DoPHOT used to reduce the resulting 12 V and 4 I frames is a variant of the one described in Schechter et al. (1993) and was developed to handle the peculiarities of the *HST* data and PSFs. Briefly, a template list of stars is first created by running DoPHOT on deep V and I frames obtained by averaging all the V and I images, and then used as an input object list for the reduction of the single epochs. The DoPHOT output magnitudes are based simply on the height of the fitted PSFs and can be transformed to “real” magnitudes m_{DoPHOT} by applying an aperture correction

that DoPHOT calculates from observations of uncrowded fields in Leo I (Hill et al. 1996). The magnitudes thus obtained can be converted to the “ground system” magnitudes F555W and F814W as defined in Holtzman et al. (1996) using the zero points derived from observations of ω Cen (Hill et al. 1996). Finally, F555W and F814W magnitudes can be converted to V and I magnitudes following the procedure outlined by Holtzman et al. (1996). Table 2 summarizes the various steps taken that lead from DoPHOT magnitudes to V and I magnitudes.

We estimate that, in the period range of interest for the Cepheids (V magnitudes between 24.5 and 26.5 mag), the rms error on the final DoPHOT magnitudes amounts to 0.04 mag in V and 0.05 mag in I . This error takes into account the uncertainty in the determination of the DoPHOT aperture corrections.

In the case of the DAOPHOT/ALLFRAME reductions, PSFs were derived from WFPC2 exposures of the Galactic globular clusters ω Cen, NGC 2419, and Pal 4 (Hill et al. 1996); the implicit assumption made here is that the PSF for a given chip/filter combination does not change with time. Since the PSFs were derived independently of the M100 data, no attempt was made to remove cosmic rays and each of the cosmic-ray split pairs of images were reduced independently. Preliminary reductions with ALLSTAR were used to provide a starlist on which the final ALLFRAME (Stetson 1994) reductions were made. A final instrumental magnitude for each epoch was then obtained by averaging the magnitudes obtained for each cosmic-ray split pair of images. The photometric errors for the mean magnitudes of stars spanning the range of magnitudes covered by the Cepheids are estimated to be ± 0.04 mag in V and ± 0.05 mag in I . The transformation to the standard VI system was made using the calibration presented in Hill et al. (1996); the calibration equations are listed in Table 2. More detailed descriptions of both the DoPHOT and DAOPHOT reductions and the calibration process are given by Hill et al. (1996).

4. VARIABLE STAR SEARCH

4.1. *DoPHOT Variables and Light Curves*

The search for variable stars was performed on the V -band images following the procedure described in Saha & Hoessel (1990), the main points of which are summarized below. We required that a star be detected in at least 10 of the 12 frames to be checked for variability. We also excluded all stars in crowded regions by rejecting candidates with a companion contributing more than 50% of the total light within a 2 pixel radius. Each star meeting these requirements was first tested for variability using a χ^2 test. The reduced χ^2_r is defined by

$$\chi^2_r = \frac{1}{n-1} \sum_i^n \frac{(m_i - \bar{m})^2}{\sigma_i^2}, \quad (1)$$

where m_i and σ_i are the magnitude and rms error of a particular star as measured in the i th epoch, \bar{m} is the magnitude of the star averaged over all epochs, and n is the number of epochs in which the star is detected. A star was always flagged as variable if $\chi^2_r \geq 8$. Stars shown as variables at a 99% confidence level (as defined in Saha & Hoessel 1990) but with $\chi^2_r < 8$ were checked for periodicity using a variant of the Lafler & Kinman (1965) method of phase dispersion minimization, in the period range between 3 and 100 days.

TABLE 2
WFPC2 ZERO POINTS

Chip	Transformation Equations for DoPHOT
PC1	$F555W = m_{DoPHOT}^{F555W} + 2.5 \log_{10} t - 7.630$ $F814W = m_{DoPHOT}^{F814W} + 2.5 \log_{10} t - 8.536$
WF2.....	$F555W = m_{DoPHOT}^{F555W} + 2.5 \log_{10} t - 7.536$ $F814W = m_{DoPHOT}^{F814W} + 2.5 \log_{10} t - 8.381$
WF3.....	$F555W = m_{DoPHOT}^{F555W} + 2.5 \log_{10} t - 7.554$ $F814W = m_{DoPHOT}^{F814W} + 2.5 \log_{10} t - 8.436$
WF4.....	$F555W = m_{DoPHOT}^{F555W} + 2.5 \log_{10} t - 7.559$ $F814W = m_{DoPHOT}^{F814W} + 2.5 \log_{10} t - 8.441$
All	$V = F555W - 0.045(V-I) + 0.027(V-I)^2$ $I = F814W - 0.067(V-I) + 0.025(V-I)^2$
Chip	Transformation Equations for DAOPHOT
PC1	$F555W = m_{DAOPHOT}^{F555W} + 2.5 \log_{10} t - 24.974$ $F814W = m_{DAOPHOT}^{F814W} + 2.5 \log_{10} t - 24.979$ $V = F555W - 0.052(V-I) + 0.027(V-I)^2 + 5.629$ $I = F814W - 0.063(V-I) + 0.025(V-I)^2 + 4.883$
WF2.....	$F555W = m_{DAOPHOT}^{F555W} + 2.5 \log_{10} t - 24.965$ $F814W = m_{DAOPHOT}^{F814W} + 2.5 \log_{10} t - 24.971$ $V = F555W - 0.052(V-I) + 0.027(V-I)^2 + 5.640$ $I = F814W - 0.063(V-I) + 0.025(V-I)^2 + 4.952$
WF3.....	$F555W = m_{DAOPHOT}^{F555W} + 2.5 \log_{10} t - 24.956$ $F814W = m_{DAOPHOT}^{F814W} + 2.5 \log_{10} t - 24.971$ $V = F555W - 0.052(V-I) + 0.027(V-I)^2 + 5.637$ $I = F814W - 0.063(V-I) + 0.025(V-I)^2 + 4.937$
WF4.....	$F555W = m_{DAOPHOT}^{F555W} + 2.5 \log_{10} t - 24.935$ $F814W = m_{DAOPHOT}^{F814W} + 2.5 \log_{10} t - 24.946$ $V = F555W - 0.052(V-I) + 0.027(V-I)^2 + 5.650$ $I = F814W - 0.063(V-I) + 0.025(V-I)^2 + 4.932$

NOTE.—The zero-point calibration adopted for DoPHOT and DAOPHOT, as described in Hill et al. 1996. m_{DoPHOT}^{F555W} and m_{DoPHOT}^{F814W} are defined as $-2.5 \log_{10} (\text{DN})$, where DN is the total number of counts for a given star in a single image with exposure time t , in the F555W and the F814W filter, respectively.

Stars with $\Lambda \geq 3$ were flagged as variables, where Λ is as used in Saha & Hoessel (1990), following the definition by Lafler & Kinman (1965).

Several spurious variables are detected in this procedure as a consequence of non-Gaussian sources of error (Saha & Hoessel 1990), various anomalies in the images (e.g., residual cosmic ray events), and crowding. Therefore, each star selected on the basis of the χ^2 and the Λ tests was visually inspected by blinking several of the individual frames against each other. This allowed us to select from the original list a total of 63 bona fide Cepheids and one nova, which is discussed separately in Ferrarese et al. 1996. The best period for each variable was selected by phasing the data for all periods between 3 and 100 days in incremental steps of 0.01 days. Although in most cases the final period adopted corresponds to the minimum value of the phase dispersion, in a few cases an obvious improvement of the light curve was obtained for a slightly different period. The light curves for each variable star were checked independently by three of us (L. F., J. A. G., and A. S.) for the best periods, and excellent agreement was found in all cases. Because of the careful sampling of the data, aliasing does not present a serious problem, and we were always able to determine a preferred period for all variables. However, because of the length of the observing window, periods of Cepheids larger than about 50 days cannot be determined

accurately. For some of these Cepheids, observations of M100 taken in 1993 December and 1994 January can come to the rescue. These images, described in Freedman et al. (1994b), are part of the *HST* Early Release Observation (ERO) program and were taken with a different orientation than the ones described in this paper, so that only about a one-third of the Cepheids can be found in the ERO field of view. For those Cepheids though, the EROs have been incorporated in the photometry and, in some cases, were useful in resolving period aliases and narrowing down the period range of the long-period Cepheids.

4.2. DAOPHOT Variables and Light Curves

Two independent methods were used to search for variable stars based on the DAOPHOT photometry. The first method was described by Freedman et al. (1994a) in their search for Cepheids in M81. Candidate variables were identified on the basis of a statistic defined by the ratio σ of the average absolute deviation from the mean to the mean error in the observations for that star. To flag a star as a variable candidate, σ had to exceed a value of 1.5 and measured ALLFRAME magnitudes were required for at least 10 out of 12 V epochs. In practice, all of the variables turned out to have been measured at all 12 epochs. No light curves were generated for obviously spurious variables where only one data point contributed to a high measured dispersion. The Cepheids were selected from the candidate variable lists after visual inspection of both the phased light curves and the images. As described in Freedman et al. (1994a), periods were determined using a modified version of the Lafler & Kinman (1965) statistic that weights individual phase points by their errors. The data were initially phased for all periods between 2 and 400 days in steps of 0.1 days; these periods were then refined by doing the search in increments of 0.01 days within a narrower window. The light curves were inspected and the periods determined by W. L. F. and L. F. (and, in most cases, also independently by J. A. G.). As in the case for the DoPHOT photometry, the ERO data proved useful in some cases in resolving period aliases for the longer period Cepheids.

In the second method, an experimental prototype version of an automatic variable-detection scheme (Stetson 1996) was used. The candidate lists generated by the two methods were in good agreement. The highest probability candidates were identified using both methods about 90% of the time. It is hoped that tests such as these will eventually lead to a refined automatic package that will be as effective as more astronomer-intensive variable-detection schemes.

In conclusion, the two methods described in the previous paragraphs produced a total of 60 variables (59 bona fide Cepheids and the nova) based on the DAOPHOT photometry; 52 Cepheids are in common between the DAOPHOT and DoPHOT list. A complete list of all the Cepheids identified in M100 is given in Table 3. The Cepheids are numbered in order of decreasing period. Period aliases are noted in the last column, while generic comments on the field around each Cepheid are given in the notes to the table.

4.3. Mean Magnitudes

The mean magnitude for each Cepheid has been defined in two different ways: (1) intensity average magnitude,

$$m = -2.5 \log_{10} \sum_{i=1}^n \frac{1}{n} 10^{-0.4 \times m_i}, \quad (2)$$

TABLE 3A
MEAN *V* PHOTOMETRY OF THE M100 CEPHEIDS

ID (1)	R.A. (2000) (2)	Decl. (2000) (3)	P_{Dop} (4)	$V_{\text{Dop}}^{\text{av}}$ (5)	$V_{\text{Dop}}^{\text{ph}}$ (6)	χ^2_{Dop} (7)	P_{DAO} (8)	$V_{\text{DAO}}^{\text{av}}$ (9)	$V_{\text{DAO}}^{\text{ph}}$ (10)	σ_{DAO} (11)	Chip (12)	Comments (13)
C1	12:23:00.24	15:48:47.7	85.0	24.97	24.95	10.5	85.0	25.01	25.00	1.8	WF2	$P > 85d$
C2	12:23:01.73	15:50:12.5	76.3	25.19	25.15	13.9	56.0	25.29	25.26	1.4	WF4	$P > 57d$
C3	12:23:02.01	15:49:28.3	63.5	25.01	25.04	3.2	60.8	25.09	25.11	1.5	WF4	$P > 58.4d$
C4	12:23:03.32	15:50:25.4	53.1	25.16	25.22	13.9	55.0	25.16	25.22	1.5	WF4	$P > 48d$
C5	12:22:58.03	15:49:54.7	52.8	25.08	25.06	8.0	54.0	25.31	25.26	1.5	WF3	
C6	12:23:00.67	15:48:12.6	52.0	25.12	25.20	16.6	52.0	25.16	25.23	1.9	WF2	$46d < P < 55d$
C7	12:23:04.51	15:49:45.5	51.0	24.79	24.78	12.5	50.3	24.77	24.76	1.5	WF4	
C8	12:23:01.58	15:50:05.8	50.3	25.01	24.98	5.7	50.2	25.05	25.03	1.5	WF4	
C9	12:23:03.69	15:48:41.5	50.3	25.97	25.90	4.5	50.0	25.89	25.82	2.1	PC1	$47d < P < 55d$
C10	12:23:04.72	15:49:49.0	50.0	24.79	24.72	22.9	50.0	24.83	24.77	2.8	WF4	$46d < P < 54d$
C11	12:23:03.82	15:50:13.5	48.0	25.49	25.49	18.7	48.0	25.47	25.48	2.4	WF4	$P > 42d$
C12	12:22:57.77	15:47:47.9	47.9	25.24	25.31	9.5	WF2	$46d < P < 53d$
C13	12:23:04.18	15:50:06.5	47.0	25.54	25.50	14.9	47.0	25.52	25.49	1.5	WF4	
C14	12:22:58.87	15:50:03.5	46.5	24.96	24.91	15.9	45.6	25.04	25.00	2.6	WF3	$P > 42d$
C15	12:23:04.61	15:49:45.7	44.0	25.39	25.46	25.2	43.5	25.35	25.42	2.6	WF4	
C16	12:22:57.82	15:50:02.5	42.9	24.95	24.95	7.7	40.7	25.05	25.02	1.7	WF3	
C17	12:22:59.73	15:48:50.3	42.9	24.97	25.00	5.2	40.5	25.01	25.04	1.5	WF2	
C18	12:23:04.95	15:49:20.2	42.3	25.26	25.20	24.6	41.7	25.27	25.25	2.3	WF4	
C19	12:22:57.70	15:48:02.3	41.7	25.71	25.75	5.1	31.0	25.87	25.89	1.4	WF2	$P_{\text{DAO}} = 41.0d$
C20	12:23:03.03	15:48:55.6	41.6	26.26	26.18	1.5	WF4	
C21	12:22:59.88	15:48:01.2	41.5	25.32	25.32	9.4	39.9	25.37	25.37	1.5	WF2	
C22	12:23:03.41	15:48:41.8	41.5	25.49	25.50	2.2	PC1	
C23	12:23:00.35	15:49:53.5	41.1	25.58	25.63	6.4	38.3	25.80	25.83	1.6	WF4	
C24	12:22:59.85	15:48:28.3	36.4	26.00	25.89	6.1	WF2	
C25	12:23:03.27	15:48:42.0	34.7	25.84	25.81	3.1	35.5	25.91	25.92	1.5	PC1	
C26	12:23:02.99	15:48:59.8	34.1	25.67	25.62	1.8	WF2	
C27	12:22:58.04	15:47:50.0	33.9	26.24	26.20	7.0	34.3	26.40	26.31	1.5	WF2	
C28	12:23:03.12	15:50:21.1	33.1	25.59	25.62	2.0	WF4	
C29	12:23:02.71	15:49:04.6	33.0	25.67	25.63	1.7	WF2	
C30	12:23:01.70	15:48:36.3	32.4	26.17	26.09	1.9	WF2	
C31	12:23:02.49	15:48:46.2	32.0	25.48	25.50	12.9	29.9	25.46	25.45	3.2	PC1	
C32	12:23:03.42	15:50:11.6	31.7	26.06	26.09	11.4	30.1	26.17	26.19	2.3	WF4	
C33	12:22:58.48	15:49:58.4	31.6	25.73	25.76	12.2	31.6	25.81	25.83	2.4	WF3	
C34	12:23:02.68	15:48:55.4	30.4	26.25	26.26	1.9	WF4	
C35	12:22:57.39	15:47:34.5	30.0	26.19	26.16	17.0	29.5	26.27	26.27	1.8	WF2	
C36	12:23:01.33	15:48:26.9	29.7	25.39	25.40	5.0	WF2	
C37	12:23:02.24	15:50:06.6	29.7	26.15	26.19	4.2	28.2	26.27	26.25	1.8	WF4	
C38	12:22:59.33	15:47:49.8	28.8	25.39	25.36	6.8	WF2	
C39	12:23:00.46	15:48:27.4	28.8	26.09	26.15	8.0	28.2	26.11	26.14	1.5	WF2	
C40	12:23:01.03	15:48:15.7	28.2	26.08	26.14	4.7	29.6	26.08	26.10	1.5	WF2	
C41	12:22:58.46	15:47:58.8	28.2	24.91	24.89	12.1	26.3	24.86	24.86	1.5	WF2	
C42	12:23:01.45	15:49:58.4	26.5	25.81	25.86	21.0	25.7	25.77	25.80	2.5	WF4	
C43	12:22:58.17	15:48:28.7	26.4	25.54	25.54	7.6	22.5	25.57	25.52	1.8	WF2	$P_2 = 26.9d, P_3 = 19.5d$
C44	12:22:57.92	15:47:47.0	25.7	26.34	26.33	3.1	WF2	*
C45	12:23:01.14	15:47:58.4	25.5	25.68	25.69	16.0	26.1	25.66	25.64	1.8	WF2	
C46	12:23:04.37	15:49:45.9	25.3	25.33	25.35	27.7	26.6	25.36	25.38	1.5	WF4	
C47	12:23:03.75	15:49:50.9	25.3	26.16	26.15	5.3	26.0	26.22	26.21	1.5	WF4	
C48	12:23:03.43	15:49:50.9	25.1	25.97	25.95	11.1	24.3	25.86	25.84	1.8	WF4	
C49	12:22:57.14	15:47:39.7	24.8	26.29	26.30	9.5	24.0	26.44	26.41	1.5	WF2	$P_2 = 30.6d$
C50	12:23:02.73	15:48:38.6	24.5	26.19	26.18	11.4	25.5	26.21	26.16	2.4	PC1	
C51	12:23:00.40	15:50:01.8	24.0	25.92	26.05	21.8	23.9	25.96	26.11	2.6	WF4	
C52	12:23:01.91	15:48:41.8	22.4	26.50	26.50	10.9	24.4	26.42	26.38	2.4	PC1	
C53	12:23:02.64	15:48:44.4	21.8	26.52	26.57	3.8	21.9	26.46	26.51	1.5	PC1	
C54	12:23:03.13	15:49:56.4	21.3	26.09	26.20	14.7	WF4	
C55	12:23:02.39	15:48:59.8	21.0	26.50	26.52	4.7	24.0	26.53	26.54	1.5	PC1	
C56	12:23:04.34	15:50:04.5	21.0	26.30	26.32	28.4	21.6	26.24	26.25	2.3	WF4	
C57	12:22:59.85	15:47:51.4	20.2	26.50	26.43	3.4	WF2	
C58	12:22:59.30	15:48:03.8	19.9	25.83	25.74	7.9	WF2	
C59	12:23:01.05	15:48:01.8	19.0	25.49	25.40	15.1	19.0	25.51	25.42	1.6	WF2	$P_{\text{DAO}} = 25.9d$
C60	12:23:01.44	15:49:57.6	18.8	26.21	26.17	4.1	15.5	26.08	26.11	1.5	WF4	$P_{\text{DAO}} = 19.2d$
C61	12:23:01.42	15:48:44.4	18.4	26.19	26.24	1.7	WF3	
C62	12:23:02.55	15:49:33.6	17.7	26.06	26.15	12.8	18.0	26.09	26.20	1.9	WF4	
C63	12:23:03.67	15:50:25.6	17.6	26.05	26.13	6.6	17.7	26.10	26.14	1.7	WF4	
C64	12:22:57.44	15:48:20.4	17.0	25.78	25.79	7.9	17.1	25.80	25.81	1.5	WF2	
C65	12:22:58.00	15:48:39.9	15.7	25.88	25.93	3.4	14.8	25.68	25.76	1.9	WF2	
C66	12:23:02.40	15:48:41.0	15.5	26.35	26.26	10.7	15.9	26.41	26.33	1.5	PC1	
C67	12:23:01.79	15:48:41.5	14.1	26.52	26.49	3.0	PC1	
C68	12:22:57.24	15:47:37.8	10.9	26.00	25.91	8.5	10.9	26.06	25.99	1.7	WF2	$P_2 = 22.5d$
C69	12:23:02.43	15:48:45.4	9.2	26.38	26.45	3.2	PC1	
C70	12:23:02.94	15:48:40.7	7.3	26.32	26.36	9.0	7.5	26.38	26.37	1.7	PC1	$P_2 = 14.6d, P_3 = 4.3d$
N1	12:23:03.52	15:49:41.7	N/A	N/A	N/A	N/A	N/A	N/A	N/A	N/A	WF4	Nova

TABLE 3B
NOTES TO TABLE 3A

ID	Description
C1	Bright and isolated
C2	Fainter companion 2 pixels away
C3	Two fainter companions 3 and 6 pixels away
C4	Fainter companion 4 pixels away
C5	Fainter companion 4 pixels away
C6	Fainter companion 2 pixels away
C7	Crowded, 4 fainter companions within 4 pixels
C8	Isolated
C9	Bright and isolated
C10	Bright and isolated
C11	Fainter companion 6 pixels away, brighter companion 9 pixels away
C12	Crowded, brighter companion 3 pixels away
C13	Two fainter companions 3 pixels away
C14	Fainter companion 3 pixels away
C15	Brighter companion 6 pixels away
C16	Fainter companion 5 pixels away
C17	Crowded, fainter companion 3 pixels away
C18	Fainter companion 3 pixels away
C19	Crowded, several fainter companions within 4 pixels
C20	Isolated
C21	Two fainter companions 4 pixels away
C22	Bright and isolated
C23	Crowded, two brighter companions 5 pixels away
C24	Variable background
C25	Two fainter companions 4 pixels away
C26	Bright companion 4 pixels away, 2 fainter companions 6 pixels away
C27	Crowded, two fainter companions 3 pixels away
C28	Fainter companion 4 pixels away, brighter companion 6 pixels away
C29	Brighter companion 4 pixels away
C30	Variable background, companion 4 pixels away
C31	Bright and isolated
C32	Isolated
C33	Fainter companion 5 pixels away
C34	Fainter companion 3 pixels away
C35	Crowded, brighter companion 4 pixels away
C36	Crowded, fainter companion 4 pixels away
C37	Two fainter companions 3 pixels away
C38	Brighter companion 4 pixels away
C39	Two fainter companions 3 pixels away
C40	Isolated
C41	Isolated
C42	Isolated
C43	Crowded, three fainter companions 4 pixels away
C44	Crowded, brighter companion 4 pixels away, several fainter companions within 4 pixels
C45	Crowded, brighter companion 4 pixels away
C46	Two fainter companions 5 pixels away, <i>V</i> light curve is flat-bottomed
C47	Brighter companion 5 pixels away
C48	Brighter companion 3 pixels away, two fainter companions 3 pixels away
C49	Crowded, variable background
C50	Bright and isolated
C51	Isolated
C52	Companion 4 pixels away, noisy <i>V</i> light curve
C53	Isolated
C54	Isolated
C55	Isolated
C56	Isolated
C57	Fainter companion 2 pixels away
C58	Crowded, several fainter companions within 5 pixels
C59	Two fainter companions 3 pixels away
C60	Isolated
C61	Isolated
C62	Isolated
C63	Isolated
C64	Fainter companion 2 pixels away
C65	Crowded, two fainter companions 3 pixels away
C66	Brighter companion 5 pixels away
C67	Companion 3 pixels away, noisy <i>V</i> light curve
C68	Crowded, fainter companion 3 pixels away, brighter companion 4 pixels away
C69	Fainter companion 4 pixels away
C70	Two fainter companions 5 pixels away

and (2) phase weighted magnitude (Saha & Hoessel 1990),

$$m = -2.5 \log_{10} \sum_{i=1}^n 0.5(\phi_{i+1} - \phi_{i-1}) 10^{-0.4 \times m_i}, \quad (3)$$

where n is the total number of observations, and m_i and ϕ_i are the magnitude and phase of the i th observation in order of increasing phase.

For variable stars with uniformly sampled light curves, equations (2) and (3) coincide; however, whenever the phase coverage of the light curves is not uniform, phase weighting provides a more accurate estimate of the mean magnitude than simple intensity average. Unlike the intensity averaged magnitude, the phase weighted magnitude depends on the distribution of the epoch of observations within the cycle, since it is a function of the spacing between subsequent phase points. For the variables in our sample, the difference between the intensity averaged and phase weighted magnitudes is rarely larger than 0.1 mag and, as expected, is more acute for those variables with poorly sampled light curves. Typically, differences are of the order of 0.02 or 0.03 mag, therefore, as will be shown later (§ 7 and Table 8), using phase weighted magnitudes or intensity averaged magnitudes does not impact the distance modulus, a conclusion that also applies to the Cepheids in M101 (Kelson et al. 1996) and NGC 925 (Silbermann et al. 1996).

Since only four epochs have been observed in the I band, the poor phase coverage makes both the intensity averaged magnitude and the phase weighted magnitude inaccurate representations of the mean I magnitude. However, Freedman (1988) found that there is very good correspondence between the V and I light curves; in the sense that, at least as a first approximation, one can be mapped into the other by simple scaling. The ratio of the V to I amplitude is found by Freedman (1988) to be 1:0.51. Therefore, we calculated a correction to the mean I magnitudes by first calculating the difference between the mean V magnitude obtained using the complete (up to 12 points) data set and the same magnitude calculated using only the data points in common with the I observations (up to 4, minimum 2), and then by scaling the difference by the 1:0.51 amplitude ratio. The result is then summed to the mean I magnitude. Of course, the correction has to be calculated separately for the intensity averaged and phase weighted I magnitudes, and the size of the correction depends on how well the I data sample the light curve. We found corrections ranging from about -0.10 to 0.10 mag, the average absolute value being 0.05 mag. This technique of correcting I magnitudes derived from only a few data points by using knowledge of a better sampled light curve in a different band has previously been applied to the Cepheids in M81 (Freedman et al. 1994a) and M101 (Kelson et al. 1996). All of the DoPHOT Cepheids selected on the basis of the V photometry were observed in

at least three of the I epochs, except for C26, observed in only two epochs, and C44, detected in only one epoch. For C44, the I mean magnitude cannot be calculated, and the color index needed for the photometric calibration of the V and I data (see Table 2) has been assumed to be $(V-I) = 1.0$ (Hill et al. 1996). The V light curve for C26 shows a bright isolated point, and hence the mean V magnitude is unreliable. Neither of these two Cepheids was detected based on the DAOPHOT photometry, and, therefore, as discussed in § 5, they will not be considered in fitting the PL relations.

The list of variable stars, their periods, and intensity averaged and phase weighted mean magnitudes are listed in Table 3 (cols. [4]–[6] for DoPHOT, cols. [8]–[10] for DAOPHOT) for the V -band exposures and in Table 4 (cols. [2]–[4] for DoPHOT, cols. [7]–[9] for DAOPHOT) for the I exposures. The I magnitudes reported in Table 4 have already been corrected as described in the previous paragraph, using the corrections reported in columns (5), (6), (10), and (11). Also listed in Table 3 are the right ascension and declination at equinox J2000 for each variable star. The coordinates have been derived using the pointing information provided in the image header by STScI and are believed to be accurate to within $0''5$, corresponding to the uncertainty in the guide star positions. The χ_r^2 (eq. [1]) is reported in column (7) for DoPHOT, while the DAOPHOT σ is listed in column (11). Under the comments in Table 3, we have noted whenever an alternative period cannot be excluded for the analysis of the light curve. Generic comments on the field surrounding each Cepheid (such as presence of nearby companions or background irregularities) can be found in the notes to Table 3.

The newly discovered variable stars are identified in each of the WFPC2 chips in Figures 3a–3d (Plates 17–20). The Cepheids are identified by white circles and numbered following the convention given in Table 3; the nova is marked on WF4.

5. COMPARISON BETWEEN THE TWO SETS OF CEPHEIDS AND THE FINAL SAMPLE

As can be drawn from Table 3, the overlap between the DoPHOT and DAOPHOT Cepheid lists is very good. Only seven of the DAOPHOT Cepheids were not selected on the basis of the DoPHOT photometry; three of these (C30, C20, and C34) were detected in fewer than 10 of the DoPHOT frames and, therefore, were not considered for variability (see § 4.1), while, for the others, χ_r^2 and Δ are just below the accepted threshold. These Cepheids would have been flagged if the χ_r^2 and Δ limits were lowered in the algorithm that automatically selects the Cepheids from the DoPHOT photometry files; on the other hand, the number of spurious candidates that would also be flagged as a con-

TABLE 3B—Continued

NOTES.—The mean V photometry for the total sample of 70 Cepheids identified from either the DoPHOT or DAOPHOT photometry. The Cepheids' identification is listed in col. (1). The Cepheids are numbered in order of decreasing period. The chip where each Cepheid was found is listed in col. (12). The right ascension (in hours, minutes, and seconds of time) and declination (in degrees, minutes, and seconds of arc) at equinox J2000 are reported in cols. (2) and (3). The period, intensity averaged and phase weighted V magnitudes, and χ_r^2 derived from the DoPHOT photometry are reported in cols. (4), (5), (6), and (7), respectively. Cepheids that are flagged from the DAOPHOT photometry but are not selected based on the DoPHOT photometry have a blank entry in these columns. The period, intensity averaged and phase weighted V magnitudes, and σ derived from the ALLFRAME photometry are listed in cols. (8), (9), (10), and (11). Cepheids that are flagged from the DoPHOT photometry but are not selected based on the DAOPHOT photometry have a blank entry in these columns. Finally, whenever the light curve phases for more than one period, the alternative periods are reported in col. (13) as P_2 , P_3 , etc.; for Cepheids that vary on scales longer than about 50 days, often only a period window can be determined. A star in col. (13) indicates that no mean DoPHOT I magnitude is available for that star and the V DoPHOT magnitude has been calculated assuming $V-I = 1.0$.

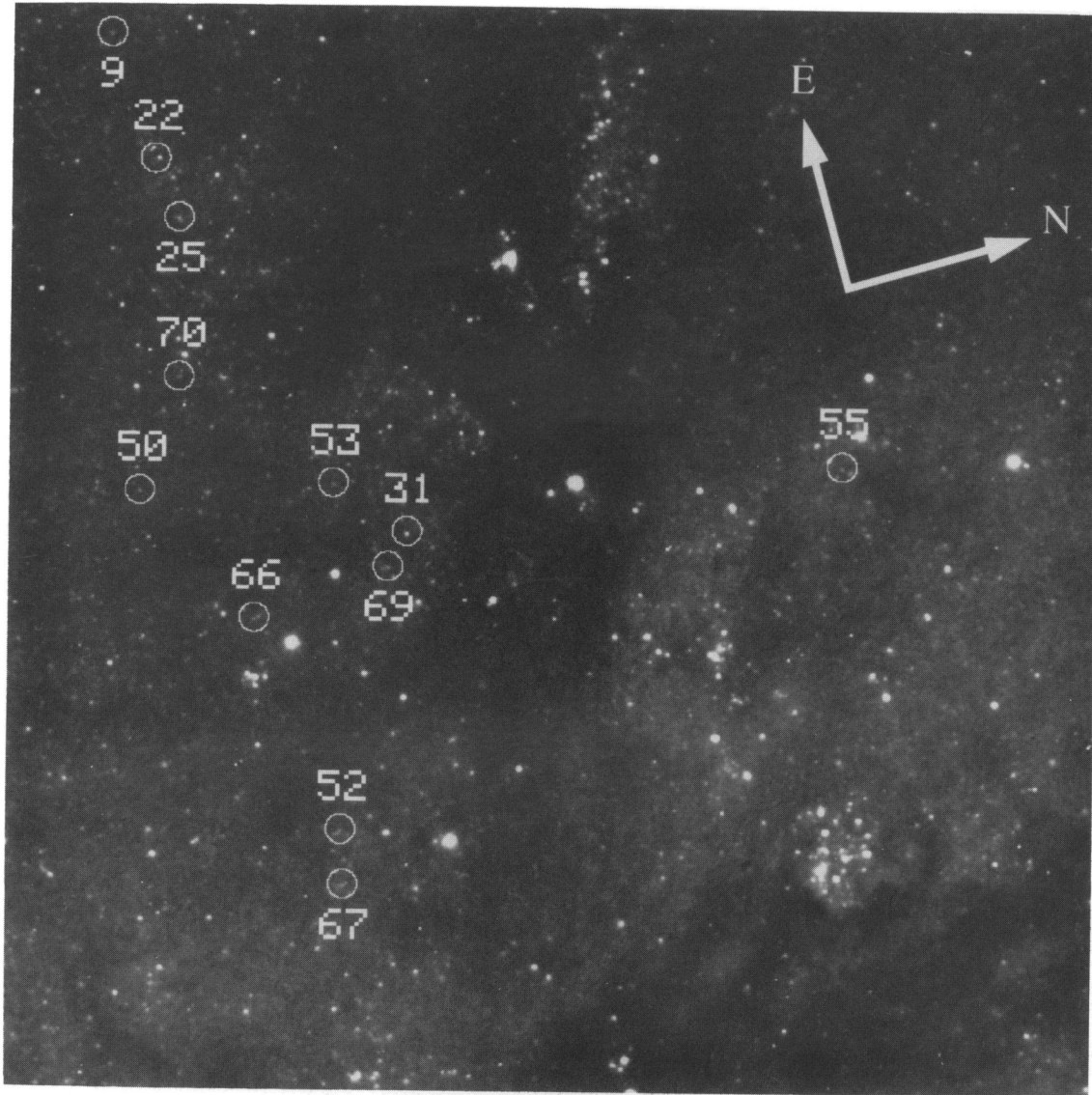


FIG. 3a

FIG. 3.—(a-d) HST/WFPC2 images of M100. The images were obtained by averaging 20 of the F555W frames (all epochs except the first and the tenth) and rejecting cosmic rays in the process. (a) PC1 ($36'' \times 36''$), while (b) WF2, (c) WF3, and (d) WF4 (the field of view for each WFC chip is $1.3'' \times 1.3''$). Each chip is oriented the same way, the direction of the north and east is shown in each figure. The Cepheids are identified by white circles and labeled following the convention adopted in Tables 3 and 4. Also marked in WF4 is the position of the nova.

FERRARESE et al. (see 464, 575)

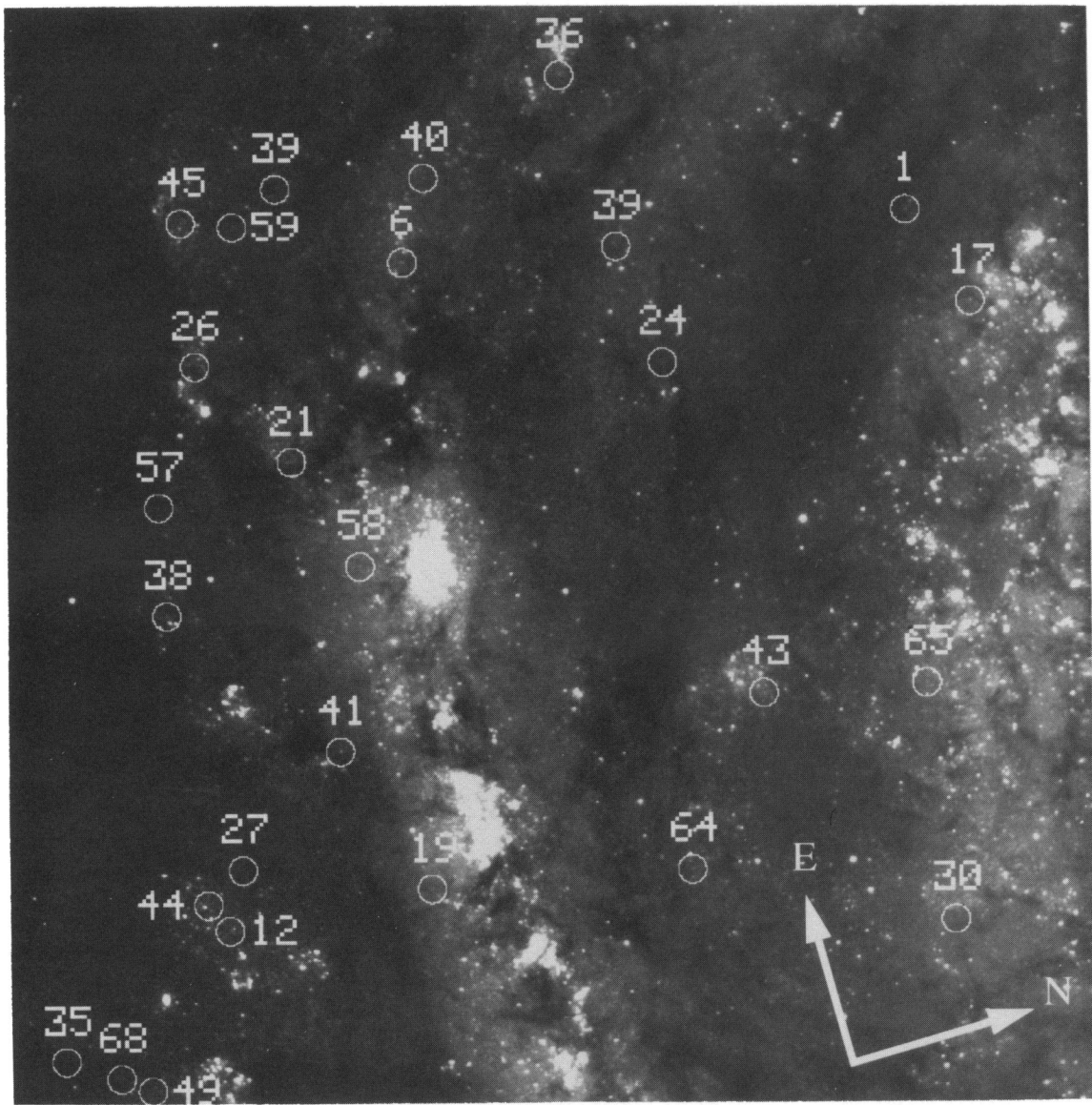


FIG. 3b

FERRARESE et al. (see 464, 575)

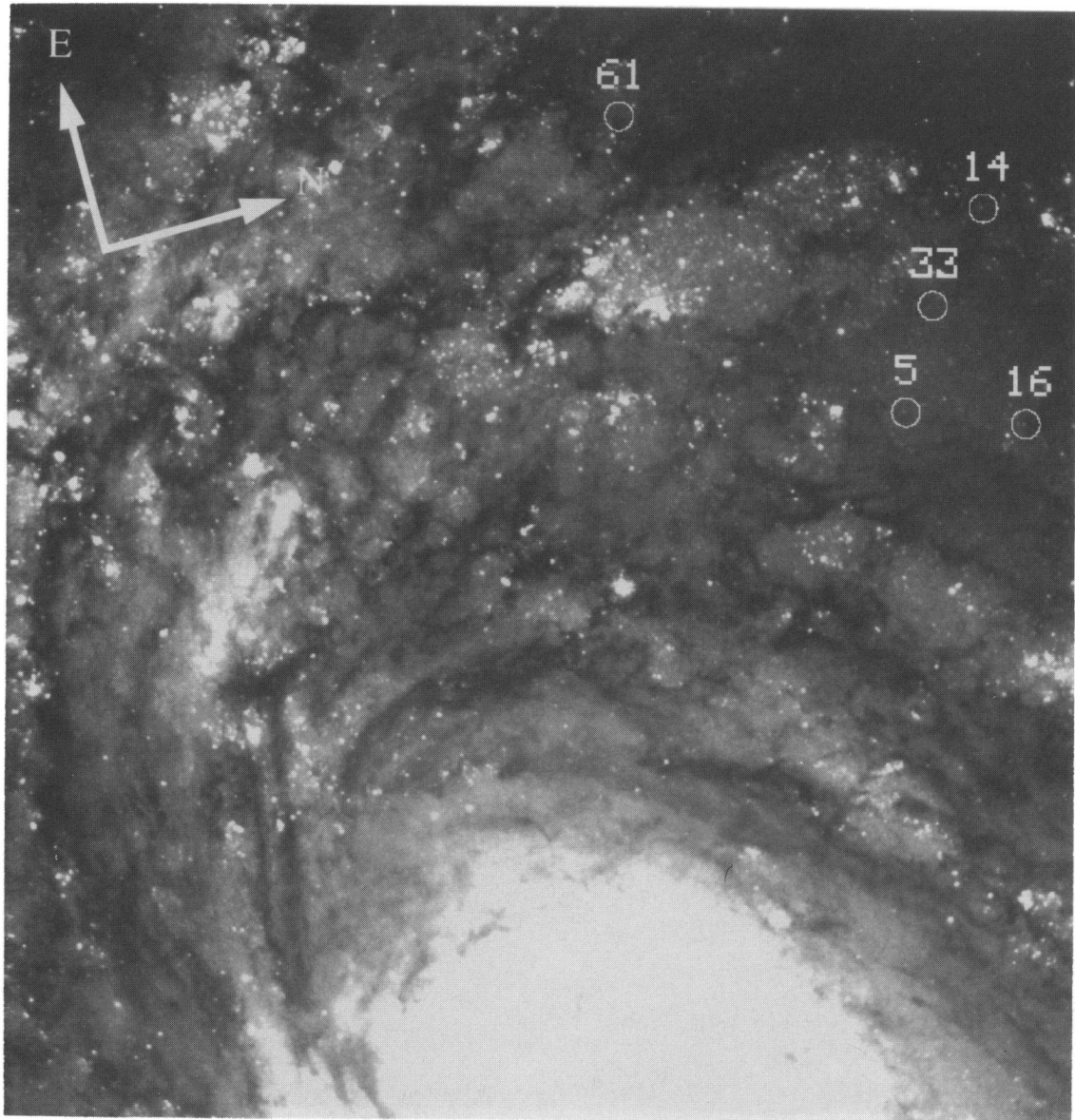


FIG. 3c

FERRARESE et al. (see 464, 575)

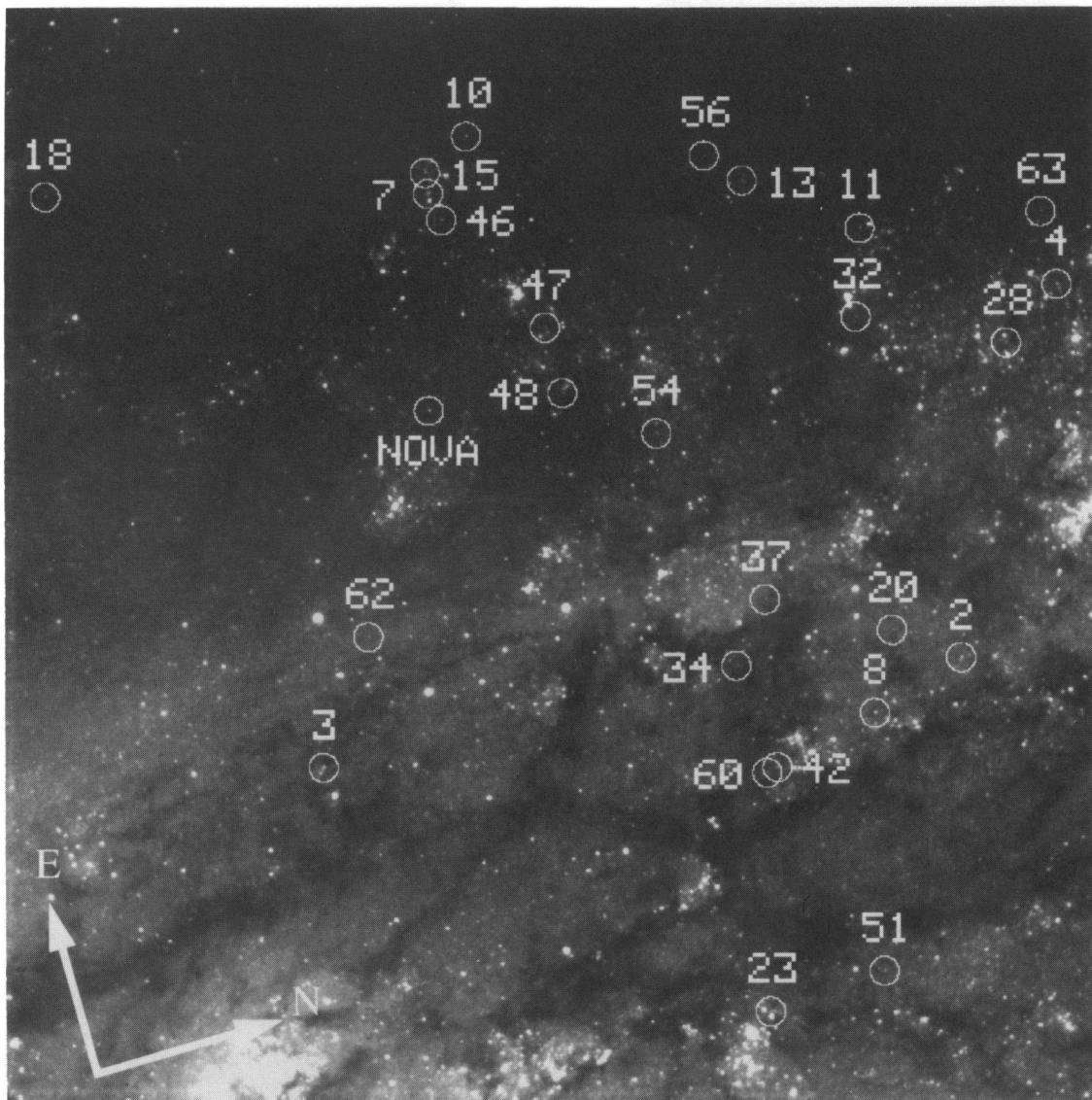


FIG. 3d

FERRARESE et al. (see 464, 575)

TABLE 4
MEAN *I* PHOTOMETRY OF THE M100 CEPHEIDS

ID (1)	P_{DoP} (2)	$I_{\text{DoP}}^{\text{av}}$ (3)	$I_{\text{DoP}}^{\text{ph}}$ (4)	$\Delta I_{\text{DoP}}^{\text{av}}$ (5)	$\Delta I_{\text{DoP}}^{\text{ph}}$ (6)	P_{DAO} (7)	$I_{\text{DAO}}^{\text{ph}}$ (8)	$I_{\text{DAO}}^{\text{ph}}$ (9)	$\Delta I_{\text{DAO}}^{\text{av}}$ (10)	$\Delta I_{\text{DAO}}^{\text{ph}}$ (11)
C1	85.0	23.91	23.88	-0.01	-0.01	85.0	23.78	23.78	-0.01	0.00
C2	76.3	23.86	23.84	0.03	0.01	56.0	23.98	23.96	0.05	0.03
C3	63.5	23.94	23.94	-0.04	0.00	60.8	24.04	24.03	-0.03	0.00
C4	53.1	23.94	23.97	0.02	0.01	55.0	24.03	24.05	0.02	0.02
C5	52.8	23.95	23.95	0.05	0.02	54.0	24.13	24.11	0.06	0.03
C6	52.0	24.47	24.48	-0.04	0.02	52.0	24.50	24.48	-0.03	-0.01
C7	51.0	23.86	23.87	0.09	0.06	50.3	23.93	23.87	0.10	0.06
C8	50.3	24.03	24.04	0.04	0.02	50.2	24.11	24.07	0.05	0.02
C9	50.3	24.93	24.92	-0.01	-0.05	50.0	24.83	24.80	0.04	0.04
C10	50.0	23.77	23.75	-0.05	-0.09	50.0	23.80	23.89	-0.05	-0.09
C11	48.0	24.38	24.38	-0.02	0.03	48.0	24.52	24.48	-0.04	0.02
C12	47.9	23.89	23.94	-0.05	0.02
C13	47.0	24.28	24.26	-0.07	-0.11	47.0	24.29	24.32	-0.05	-0.07
C14	46.5	23.91	23.89	-0.06	-0.05	45.6	24.02	24.03	-0.05	-0.03
C15	44.0	24.37	24.37	-0.09	-0.03	43.5	24.44	24.43	-0.04	0.03
C16	42.9	23.83	23.84	0.07	0.06	40.7	24.02	23.97	0.05	0.04
C17	42.9	23.81	23.83	0.04	0.04	40.5	23.84	23.86
C18	42.3	24.25	24.23	0.02	-0.02	41.7	24.34	24.33	0.02	0.00
C19	41.7	24.79	24.80	0.01	0.05	31.0	24.92	24.88	0.06	0.04
C20	41.6	24.20	24.33	-0.13	-0.15
C21	41.5	24.34	24.34	0.06	0.06	39.9	24.30	24.23	0.06	0.07
C22	41.5	24.74	24.75	0.01	-0.01
C23	41.1	24.62	24.62	0.04	0.06	38.3	24.86	24.80	0.06	0.05
C24	36.4	24.76	24.70	-0.03	-0.08
C25	34.7	25.26	25.23	-0.01	-0.02	35.5	25.13	25.10	0.02	0.03
C26	34.1	24.18	24.23	-0.06	-0.07
C27	33.9	25.09	25.04	-0.02	-0.04	34.3	25.07	25.11	-0.07	-0.06
C28	33.1	24.77	24.77	0.02	0.04
C29	33.0	24.59	24.56	0.01	0.01
C30	32.4	25.27	25.10	0.12	0.09
C31	32.0	24.74	24.76	0.05	0.04	29.9	24.46	24.49	0.05	0.03
C32	31.7	25.07	25.06	0.04	0.01	30.1	25.08	25.04	0.09	0.07
C33	31.6	24.71	24.71	0.13	0.14	31.6	25.09	25.03	0.11	0.07
C34	30.4	25.06	25.06	0.03	0.02
C35	30.0	24.81	24.82	-0.10	-0.10	29.5	24.86	24.90	-0.05	-0.03
C36	29.7	24.84	24.80	0.00	0.00
C37	29.7	24.86	24.86	0.00	-0.01	28.2	24.98	24.94	0.05	0.02
C38	28.8	24.42	24.41	-0.09	-0.09
C39	28.8	24.92	24.95	0.03	0.09	28.2	25.00	24.94	0.03	0.07
C40	28.2	25.06	25.10	0.06	0.08	29.6	25.13	25.12	0.04	0.03
C41	28.2	24.16	24.13	-0.06	-0.06	26.3	24.19	24.25	-0.07	-0.07
C42	26.5	24.99	24.97	-0.01	0.04	25.7	24.83	24.76	-0.01	0.05
C43	26.4	24.97	25.00	0.09	0.05	22.5	24.85	24.75	0.14	0.06
C44	25.7
C45	25.5	24.67	24.69	-0.03	0.03	26.1	24.95	24.92	-0.03	0.00
C46	25.3	24.84	24.85	-0.06	0.00	26.6	24.94	24.90	-0.04	0.01
C47	25.3	25.15	25.18	0.07	0.04	26.0	25.49	25.54	0.03	0.02
C48	25.1	24.89	24.83	0.09	0.04	24.3	24.95	24.86	0.08	0.03
C49	24.8	25.30	25.33	0.00	0.01	24.0	25.08	25.01	-0.07	-0.05
C50	24.5	25.30	25.29	-0.04	-0.03	25.5	25.28	25.30	-0.03	-0.05
C51	24.0	25.00	25.08	-0.03	0.12	23.9	25.26	25.20	-0.03	0.12
C52	22.4	25.52	25.56	0.10	0.01	24.4	25.47	25.43	0.12	0.07
C53	21.8	25.67	25.72	0.06	0.07	21.9	25.34	25.33	0.04	0.06
C54	21.3	24.98	25.12	-0.02	0.06
C55	21.0	25.20	25.17	-0.09	-0.09	24.0	25.16	25.27	-0.11	-0.05
C56	21.0	25.27	25.23	0.03	-0.06	21.6	25.44	25.52	0.04	-0.04
C57	20.2	25.20	25.21	0.03	0.04
C58	19.9	25.35	25.33	0.06	0.08
C59	19.0	24.65	24.68	0.11	0.12	19.0	24.56	24.43	0.12	0.12
C60	18.8	24.98	24.95	-0.02	0.04	15.5	25.15	25.23	-0.02	-0.04
C61	18.4	25.08	25.19	0.07	0.06
C62	17.7	25.04	25.06	0.08	0.09	18.0	25.11	25.06	0.09	0.10
C63	17.6	24.97	25.01	0.05	0.06	17.7	25.28	25.28	0.08	0.06
C64	17.0	25.35	25.41	-0.01	-0.01	17.1	25.41	25.46	-0.02	-0.02
C65	15.7	25.28	25.28	-0.03	-0.02	14.8	25.34	25.35	0.04	-0.04
C66	15.5	25.87	25.83	0.10	0.06	15.9	25.83	25.76	0.04	0.03
C67	14.1	25.25	25.24	-0.08	-0.06
C68	10.9	24.78	24.78	-0.02	-0.01	10.9	24.84	24.85	-0.04	-0.02
C69	9.2	25.86	25.80	0.02	0.01
C70	7.3	25.69	25.70	0.06	0.04	7.5	25.38	25.36	0.16	0.14

sequence would be unreasonably large (several hundred) and the result unmanageable. For coherence with our selection criteria, we do not publish the DoPHOT photometry for these stars; however, when the photometry for these DAOPHOT Cepheids is extracted manually from the DoPHOT photometry files, they all show good Cepheid-like light curves and excellent agreement, both in period and magnitude, with their DAOPHOT counterparts.

Eleven candidates that met the DoPHOT criteria for classification as Cepheids failed to meet the criteria set for the DAOPHOT candidates. In three of those cases, the stars fell very close to the cutoff limit of $\sigma = 1.5$. However, in the other eight cases, the stars fell significantly short of the cutoff criterion, i.e., $\sigma \ll 1.5$. Hence, the internal errors estimated by DAOPHOT for these stars were large compared with their magnitude dispersion. Furthermore, there was no convincing minimum in the Lafler-Kinman statistic as a function of period; instead, plots of the Lafler-Kinman statistic for these stars were extremely noisy. In all but two of the cases, using the period determined by the DoPHOT analysis, a reasonable (although generally very noisy) light curve could be obtained.

For the 52 Cepheids in common between the DoPHOT and DAOPHOT lists, the agreement in period is excellent. A marginal disagreement is present only for C19, which has a DoPHOT period of 41.7 days, while the best phasing DAOPHOT light curve is obtained at 31.0 days but presents an alias at 41 days.

In Table 5, we present the final sample of Cepheids that will be used for fitting the PL relations and calculating the distance modulus to M100. Of the 70 Cepheids listed in Tables 3 and 4, we kept only the 52 in common between the DoPHOT and DAOPHOT lists; this protects us from uncertainties in the determination of the periods and small (about 0.1 mag) systematic errors in the photometry (larger errors have already been excluded, see Hill et al. 1996) that cannot be avoided for Cepheids for which photometry by only one of the methods was available. For the common Cepheids, we calculated a “mean” period by averaging the DoPHOT and DAOPHOT periods, and “mean” V and I magnitudes by averaging the DoPHOT and DAOPHOT mean V and I magnitudes. The resulting list of Cepheids, periods, and V and I magnitudes are reported in Table 5. In the Table, identifications are the same as in Tables 3 and 4. The errors associated with the mean periods are given as half the sum in quadrature of the errors associated with the DoPHOT and DAOPHOT periods, which in turn are estimated as the width of the window in period around the minimum of the phase dispersion in which the light curve phases; for some of the longer period Cepheids, only a lower limit on the period can be determined. This has been noted in the table by placing a plus sign after the period. The errors in the mean magnitudes will be considered in §§ 6 and 7 and Table 9.

Finding charts for the selected variable stars are given in Figures 4a–4i (Plates 21–29). These finding charts cover a $4'' \times 4''$ region (40×40 pixels for the WFC and 93×93

TABLE 5
FINAL SAMPLE OF CEPHEIDS: V AND I PHOTOMETRY

ID (1)	$P \pm \epsilon P$ (2)	V^{av} (3)	V^{ph} (4)	I^{av} (5)	I^{ph} (6)	Chip (7)
C1	85.0 +	24.99	24.98	23.85	23.83	WF2
C2	66.2 $^{+9}_{-9}$	25.24	25.21	23.92	23.90	WF4
C3	62.1 $^{+4}_{-6}$	25.05	25.07	23.99	23.98	WF4
C4	54.0 $^{+4}_{-6}$	25.16	25.22	23.98	24.01	WF4
C5	53.4 \pm 3.0	25.19	25.16	24.04	24.03	WF3
C6	52.0 $^{+3}_{-6}$	25.14	25.21	24.48	24.48	WF2
C7	50.6 \pm 3.0	24.78	24.77	23.90	23.87	WF4
C8	50.2 \pm 3.0	25.03	25.01	24.07	24.05	WF4
C9	50.1 $^{+5}_{-3}$	25.93	25.86	24.88	24.86	PC1
C10.....	50.0 \pm 4.0	24.81	24.74	23.78	23.82	WF4
C11.....	48.0 \pm 6.0	25.48	25.48	24.45	24.43	WF4
C13.....	47.0 \pm 2.0	25.53	25.49	24.28	24.29	WF4
C14.....	46.0 \pm 4.0	25.00	24.96	23.96	23.96	WF3
C15.....	43.8 \pm 2.0	25.37	25.44	24.41	24.40	WF4
C16.....	41.8 \pm 2.0	25.00	24.99	23.92	23.91	WF3
C17.....	41.7 \pm 2.0	24.99	25.02	23.82	23.84	WF2
C18.....	42.0 \pm 2.0	25.26	25.22	24.30	24.28	WF4
C19.....	36.4 \pm 5.4	25.79	25.82	24.86	24.84	WF2
C21.....	40.7 \pm 2.0	25.34	25.34	24.32	24.29	WF2
C23.....	39.7 \pm 1.5	25.69	25.73	24.74	24.71	WF4
C25.....	35.1 \pm 1.5	25.88	25.87	25.20	25.17	PC1
C27.....	34.1 \pm 1.5	26.32	26.25	25.08	25.07	WF2
C31.....	30.9 \pm 1.5	25.47	25.48	24.60	24.62	PC1
C32.....	30.9 \pm 1.5	26.12	26.14	25.07	25.05	WF4
C33.....	31.6 \pm 1.5	25.77	25.80	24.90	24.87	WF3
C35.....	29.8 \pm 1.5	26.23	26.21	24.84	24.86	WF2
C37.....	28.9 \pm 1.5	26.21	26.22	24.92	24.90	WF4
C39.....	28.5 \pm 1.5	26.10	26.14	24.96	24.95	WF2
C40.....	28.9 \pm 1.5	26.08	26.12	25.09	25.11	WF2
C41.....	27.2 \pm 1.5	24.88	24.88	24.18	24.19	WF2
C42.....	26.1 \pm 1.5	25.79	25.83	24.91	24.87	WF4
C43.....	24.4 \pm 3.0	25.55	25.53	24.91	24.88	WF2
C45.....	25.8 \pm 1.5	25.67	25.66	24.81	24.80	WF2
C46.....	26.0 \pm 1.5	25.34	25.36	24.89	24.88	WF4
C47.....	25.6 \pm 1.5	26.19	26.18	25.32	25.36	WF4
C48.....	24.7 \pm 1.0	25.92	25.90	24.92	24.84	WF4
C49.....	24.4 \pm 1.0	26.37	26.36	25.19	25.17	WF2
C50.....	25.0 \pm 1.0	26.20	26.17	25.29	25.30	PC1
C51.....	23.9 \pm 1.0	25.94	26.08	25.13	25.14	WF4
C52.....	23.4 \pm 1.0	26.46	26.44	25.49	25.49	PC1
C53.....	21.9 \pm 1.0	26.49	26.54	25.51	25.53	PC1
C55.....	22.5 \pm 1.0	26.51	26.53	25.18	25.22	PC1
C56.....	21.3 \pm 1.0	26.27	26.28	25.36	25.38	WF4
C59.....	19.0 \pm 1.0	25.50	25.41	24.61	24.56	WF2
C60.....	17.1 \pm 2.0	26.15	26.14	25.06	25.09	WF4
C62.....	17.9 \pm 1.0	26.07	26.17	25.08	25.06	WF4
C63.....	17.6 \pm 1.0	26.07	26.13	25.13	25.15	WF4
C64.....	17.1 \pm 1.0	25.79	25.80	25.38	25.44	WF2
C65.....	15.2 \pm 1.0	25.78	25.84	25.31	25.32	WF2
C66.....	15.7 \pm 1.0	26.38	26.29	25.85	25.80	PC1
C68.....	10.9 \pm 1.0	26.03	25.95	24.81	24.82	WF2
C70.....	7.4 \pm 1.0	26.35	26.37	25.54	25.53	PC1

NOTES.—The final sample of Cepheids, which were flagged on the basis of both the DoPHOT and DAOPHOT photometry. The Cepheids' identification is the same as in Tables 3 and 4 and in Figs. 3–5. The periods (col. [2]) and phase weighted and intensity averaged V and I magnitudes (cols. [4]–[6]) are simple averages of the DoPHOT and DAOPHOT values. The errors associated with the mean periods are given as the square root of one-half the sum in quadrature of the errors associated to the DoPHOT and DAOPHOT periods; for some of the longer period Cepheids, only a lower limit on the period can be determined; this has been noted in the table by placing a plus sign after the period.

TABLE 4—Continued

NOTES.—The mean I photometry for the total sample of 70 Cepheids identified from either the DoPHOT or DAOPHOT photometry. The periods and intensity averaged and phase weighted magnitudes are listed in cols. (2), (3), and (4) for DoPHOT, and cols. (7), (8), and (9) for DAOPHOT. The I magnitudes have been corrected as described in § 4.3, using the corrections reported in cols. (5), (6), (10), and (11).

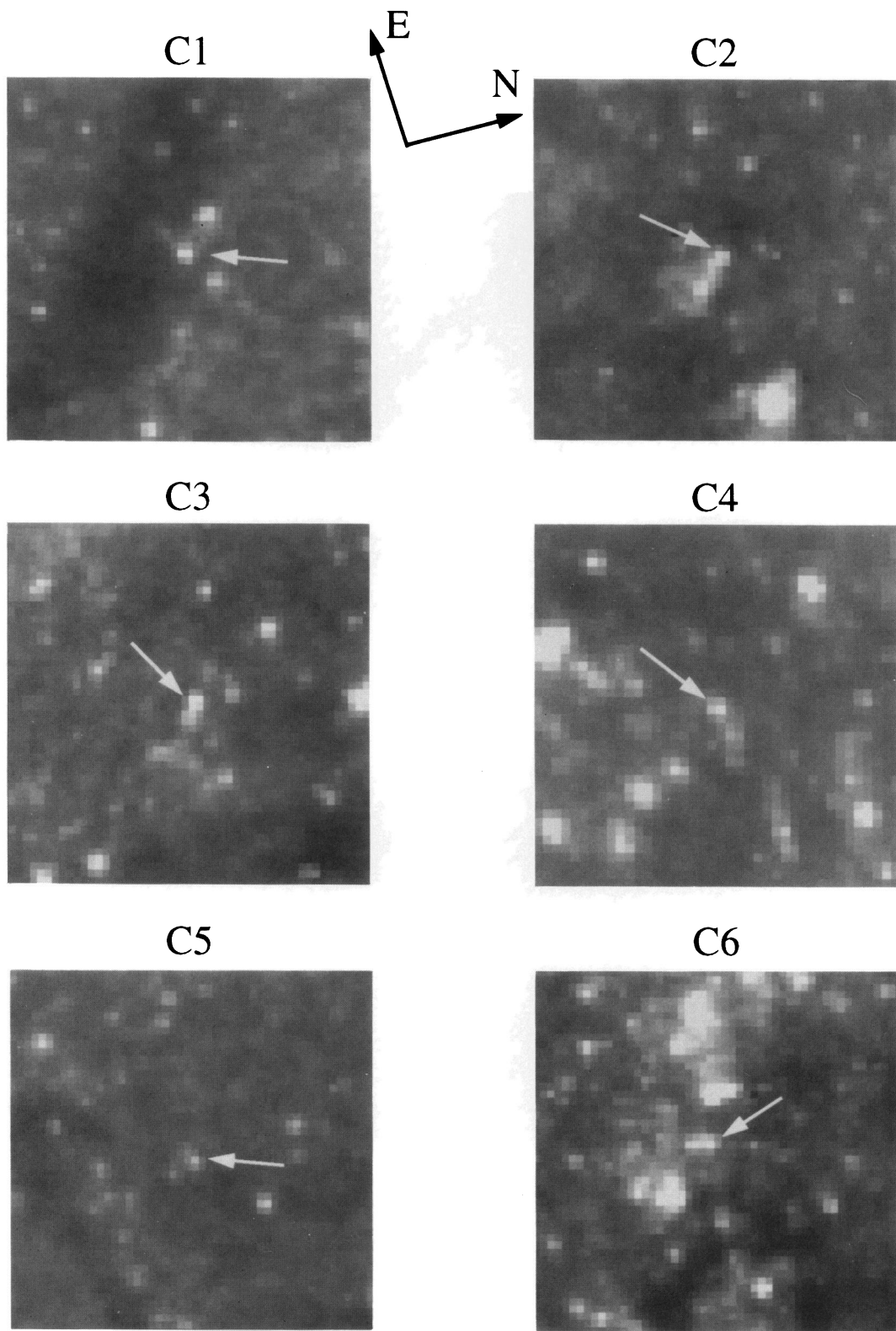


FIG. 4a

FIG. 4.—(a-i) Finding charts for the variable stars that were identified from both the DoPHOT and DAOPHOT photometry. Each finding chart covers a region $4'' \times 4''$ and is oriented as the chips in Figs. 3a-3d. The arrow marks the position of the Cepheid. Finding charts for the Cepheids found by only one of the two photometry packages can be found in the Appendix (Figs. 10a-10c).

FERRARESE et al. (see 464, 577)

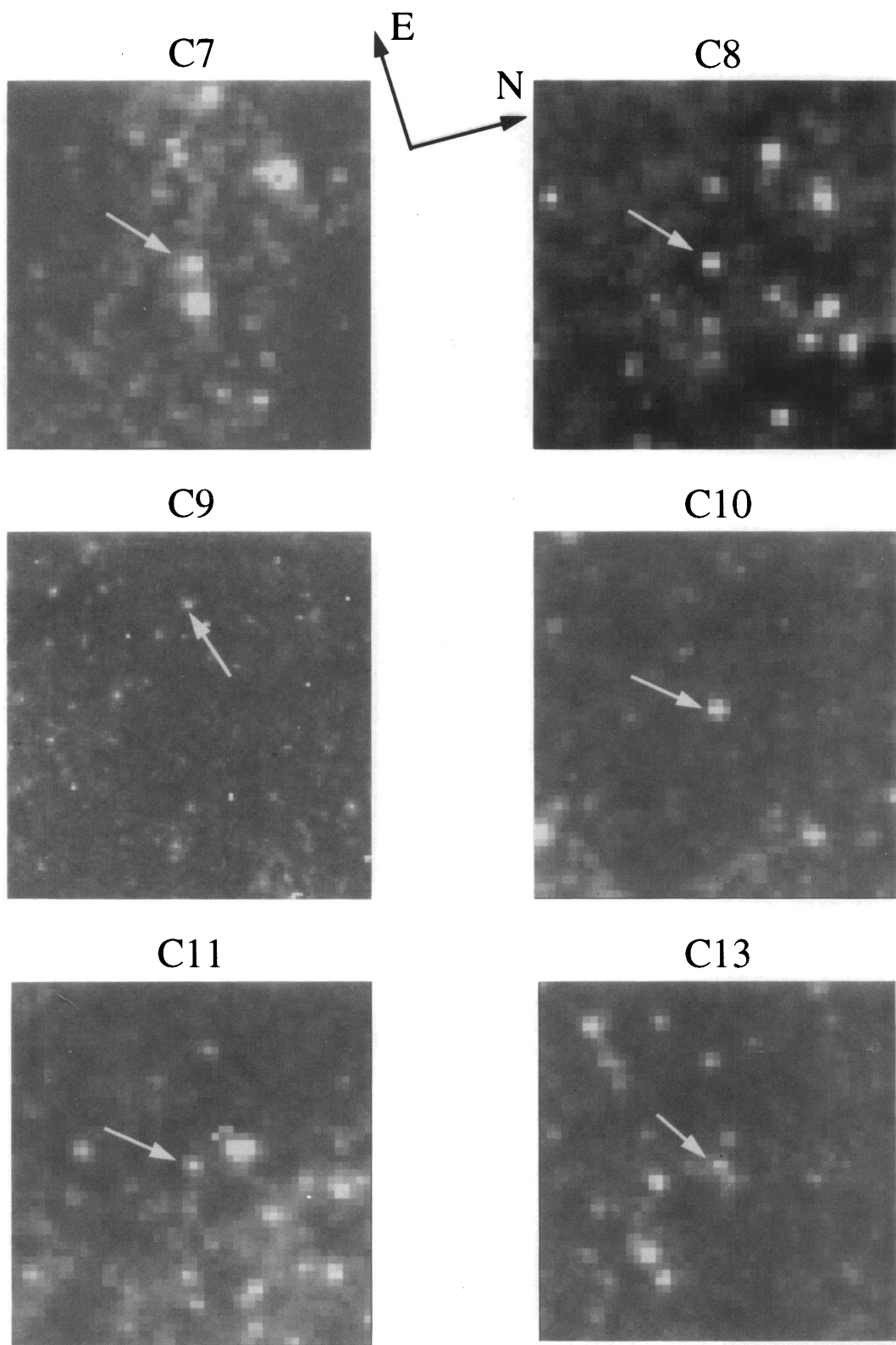


FIG. 4b

FERRARESE et al. (see 464, 577)

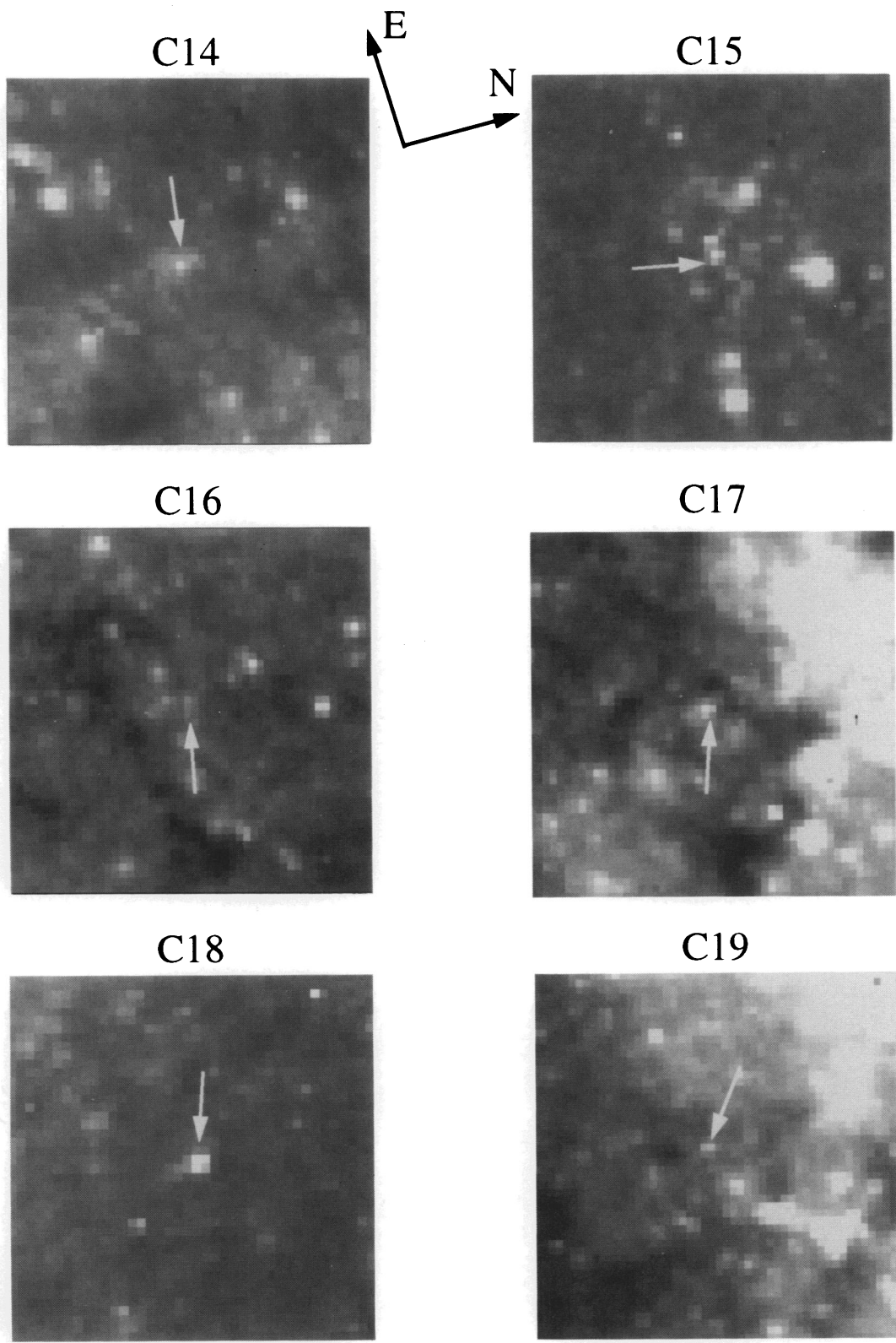


FIG. 4c

FERRARESE et al. (see 464, 577)

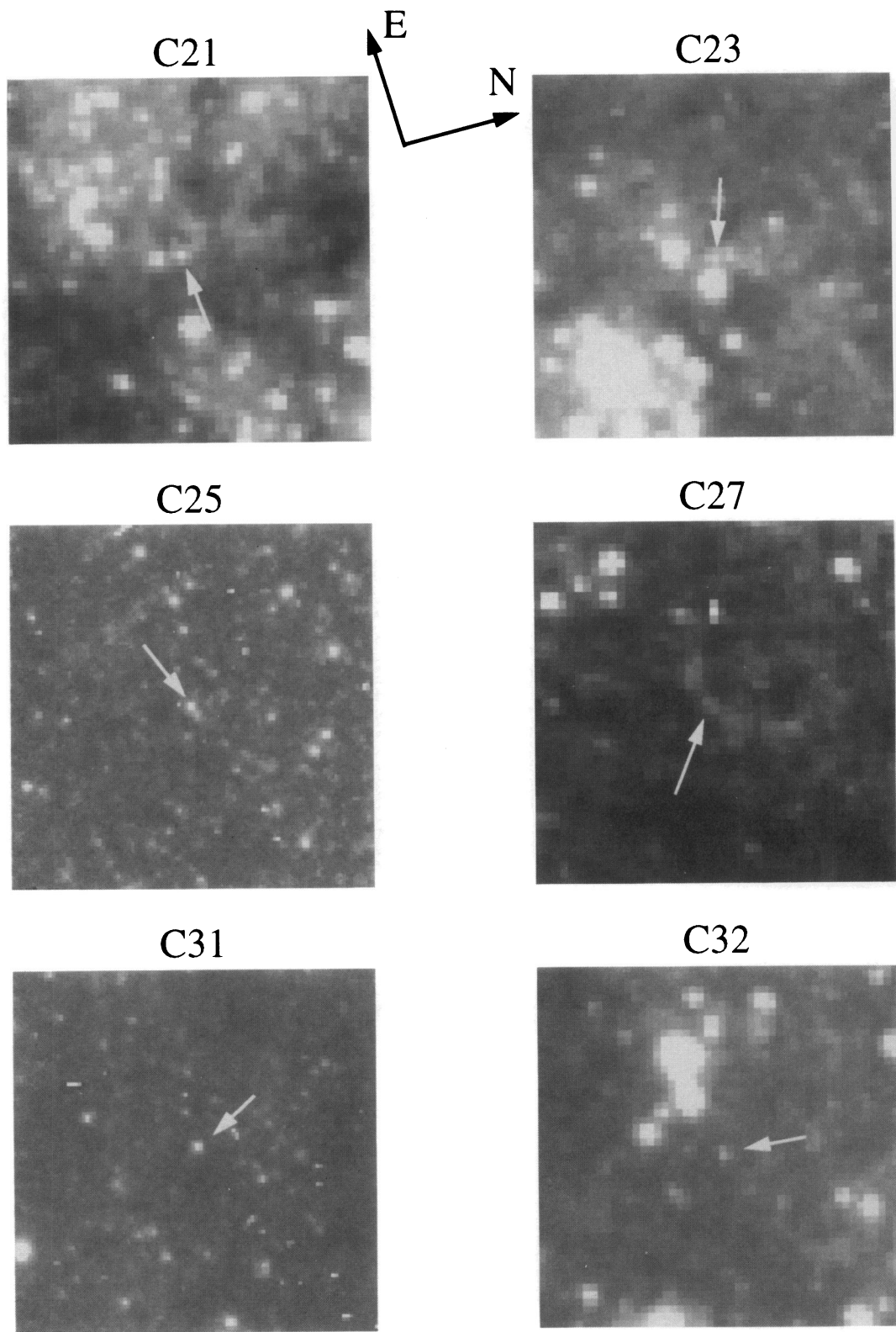


FIG. 4d

FERRARESE et al. (see 464, 577)

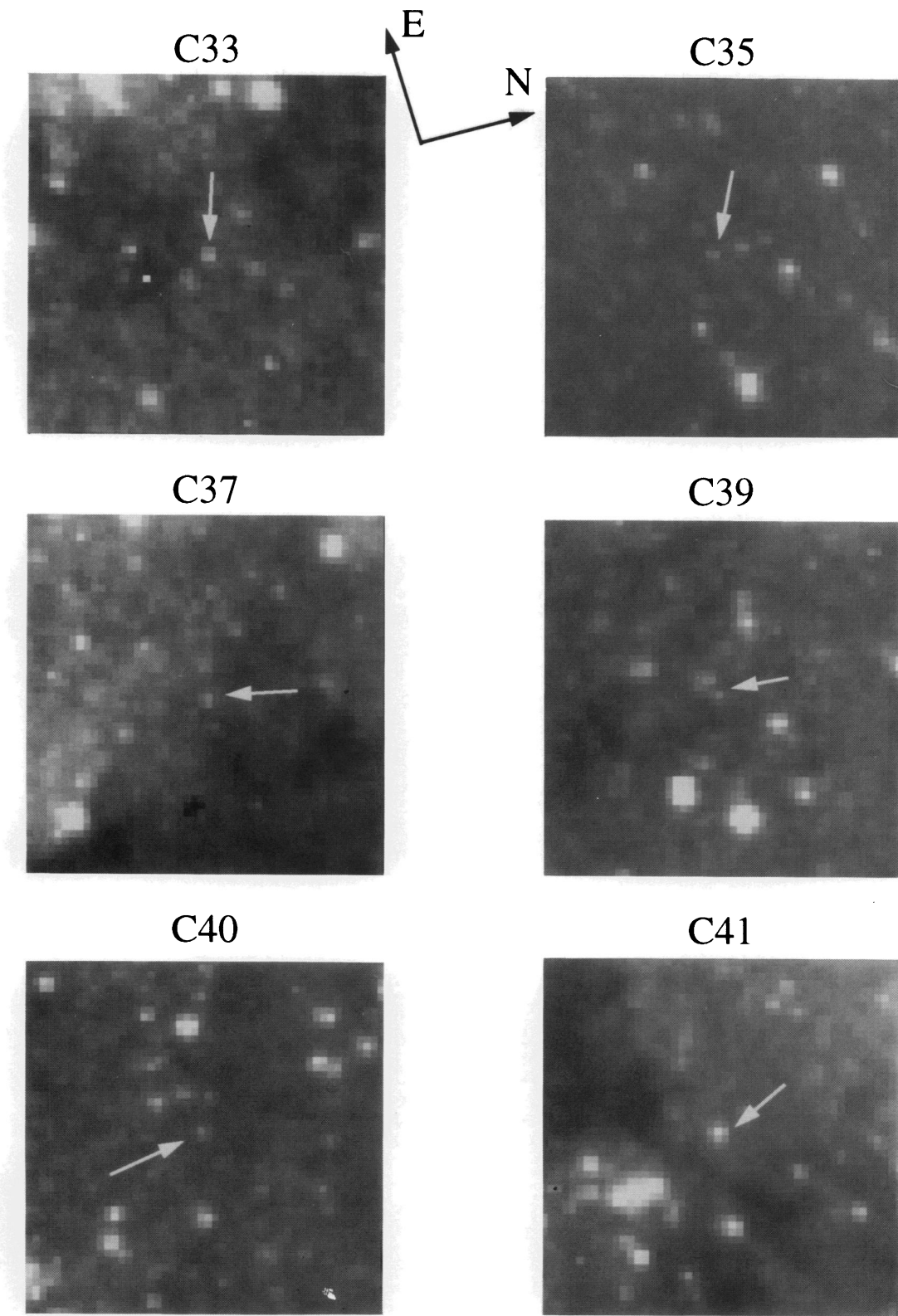


FIG. 4e

FERRARESE et al. (see 464, 577)

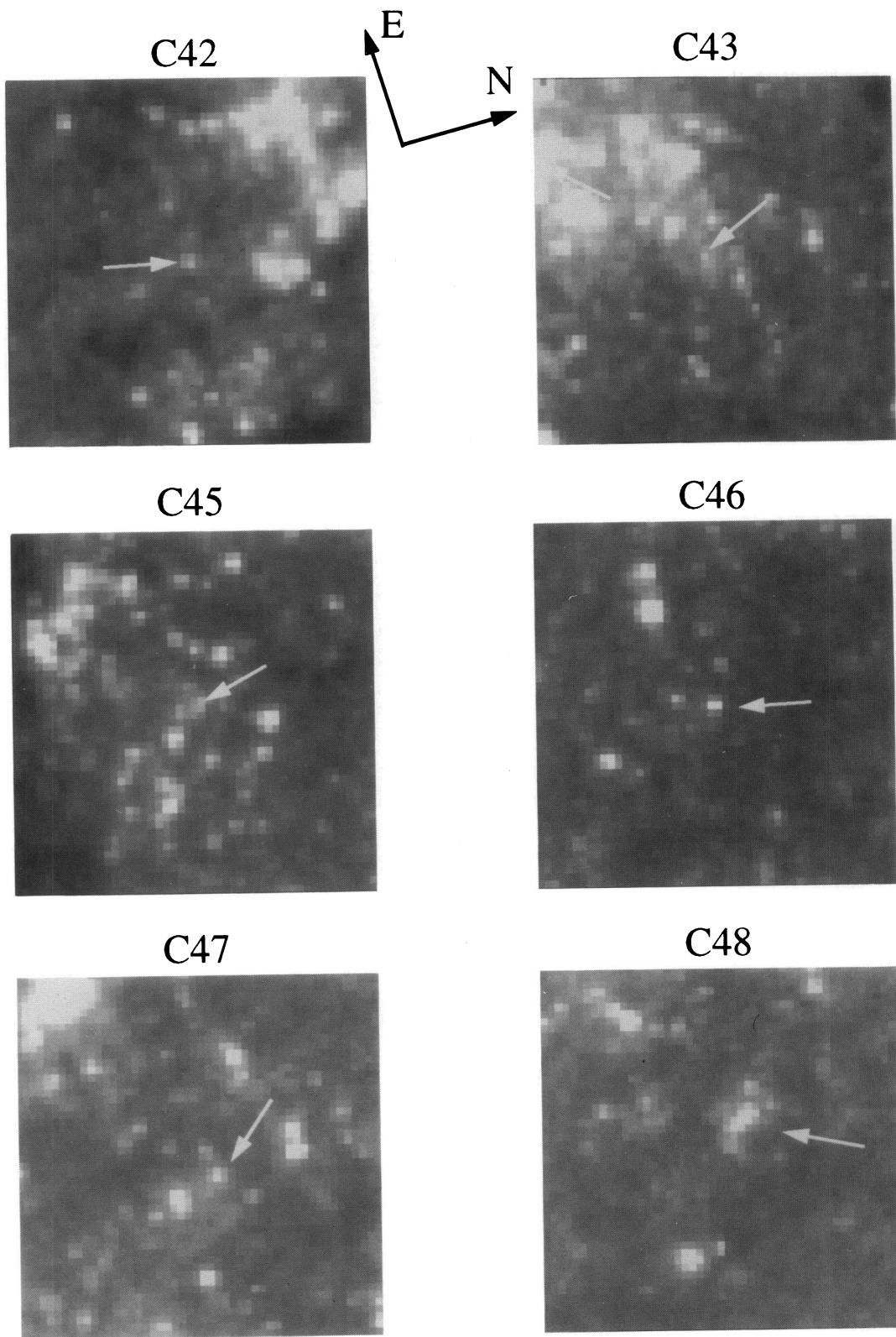


FIG. 4f

FERRARESE et al. (see 464, 577)

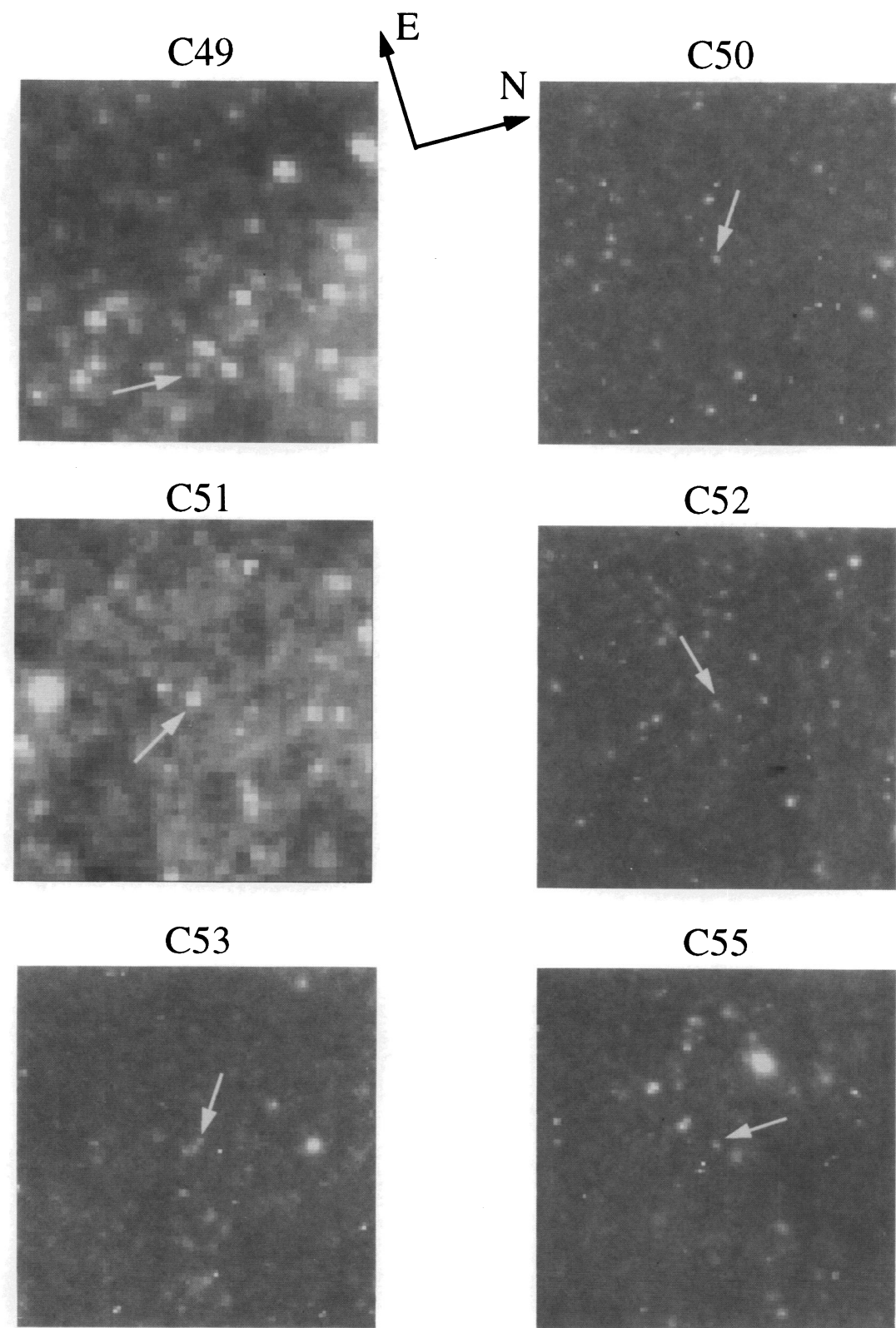


FIG. 4g

FERRARESE et al. (see 464, 577)

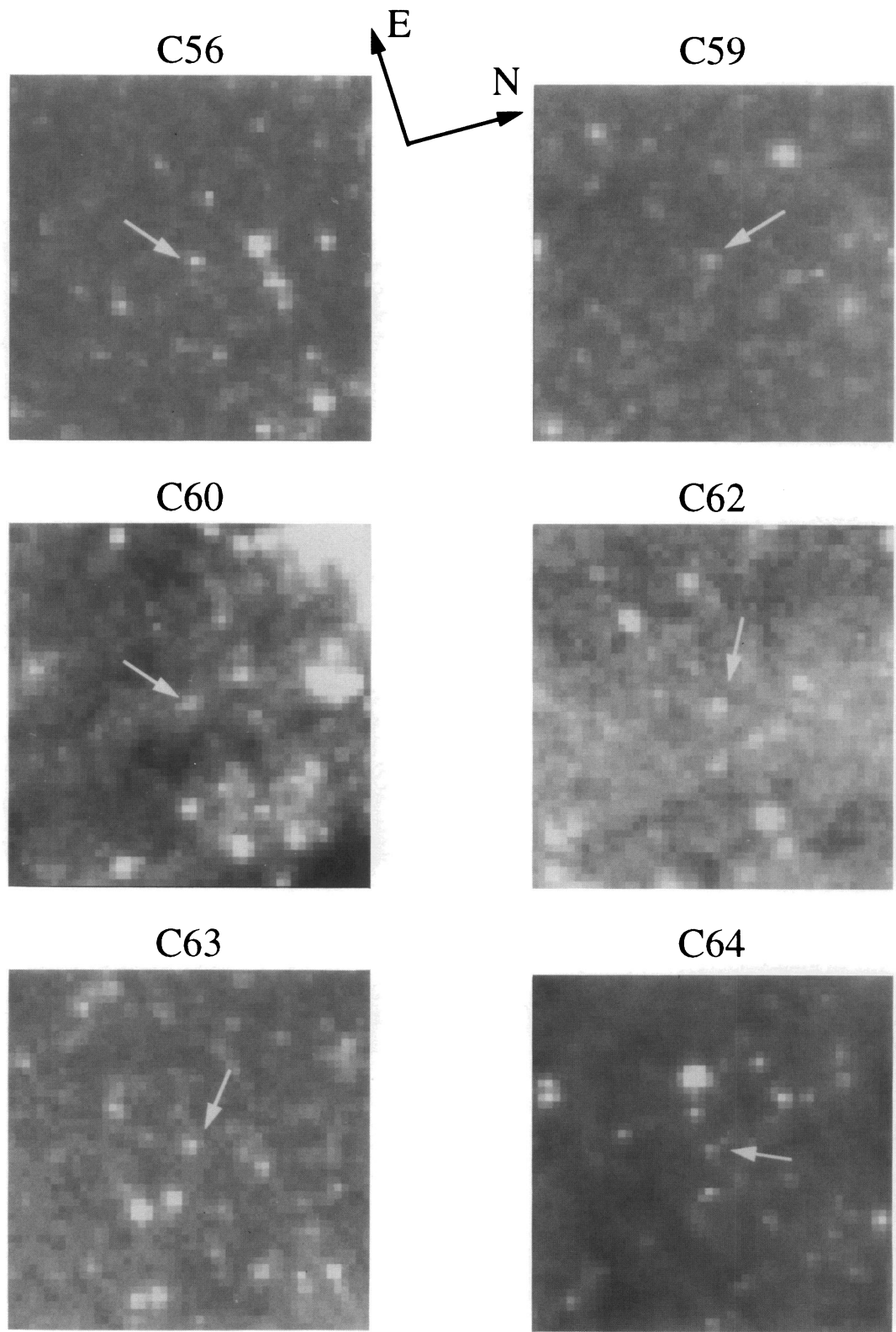
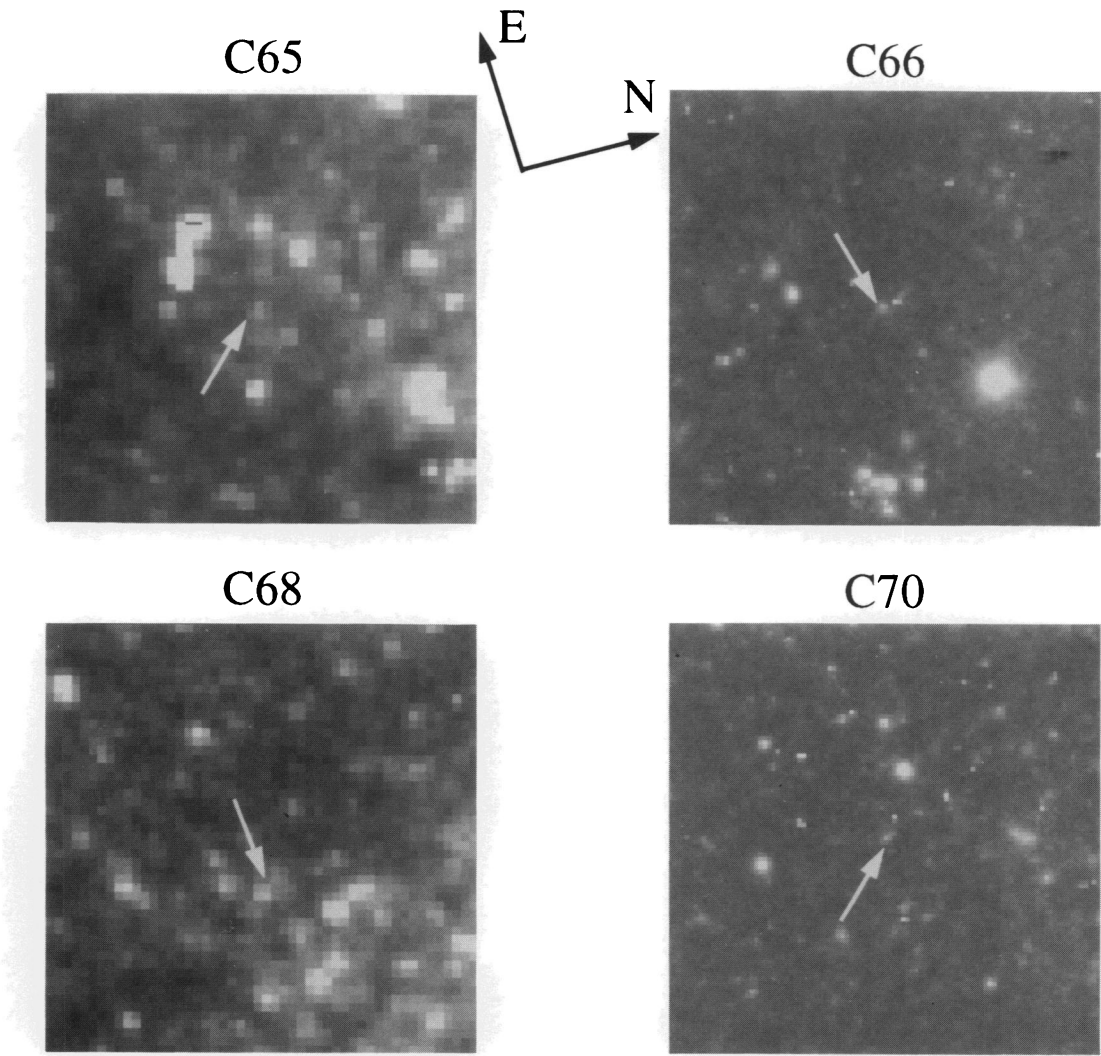


FIG. 4*h*

FERRARESE et al. (see 464, 577)

FIG. 4*i*

FERRARESE et al. (see 464, 577)

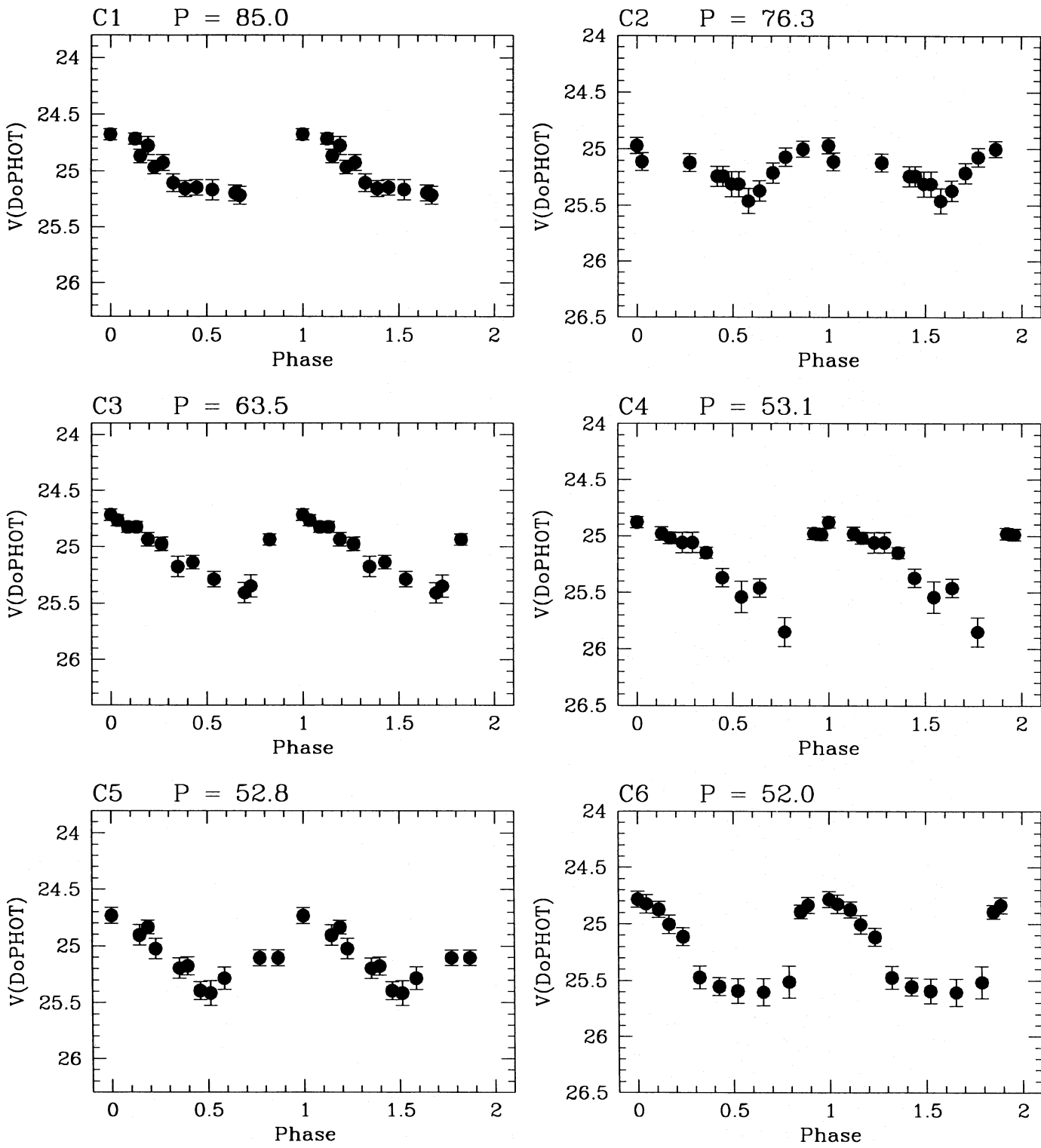


FIG. 5a

FIG. 5.—(a–i) Light curves for the 52 Cepheids that were identified from both the DoPHOT and DAOPHOT photometry. The data presented are from the DoPHOT photometry. Variables in the plots are labeled with their identification numbers and DoPHOT periods. Light curves for the Cepheids found by only one of the two photometry packages can be found in the Appendix (Figs. 11a–11c).

pixels for the PC1) and have the same orientation as the corresponding image displayed in Figures 3a–3d. The contrast and intensity level have been adjusted differently for each finding chart; therefore, the relative brightness of the Cepheids cannot be inferred from them. The light curves for the common Cepheids are presented in Figures 5a–5i and are derived from the DoPHOT photometry in all cases.

Variables in the plots are labeled with their identification number and DoPHOT period. In Table 6, we present the V photometry for the Cepheids: For each epoch, we list the Julian Date of the observation and the corresponding DoPHOT V magnitude and the error. The DoPHOT I photometry is reported in Table 7. The period listed in the table's headings is the DoPHOT period (from Table 3). The

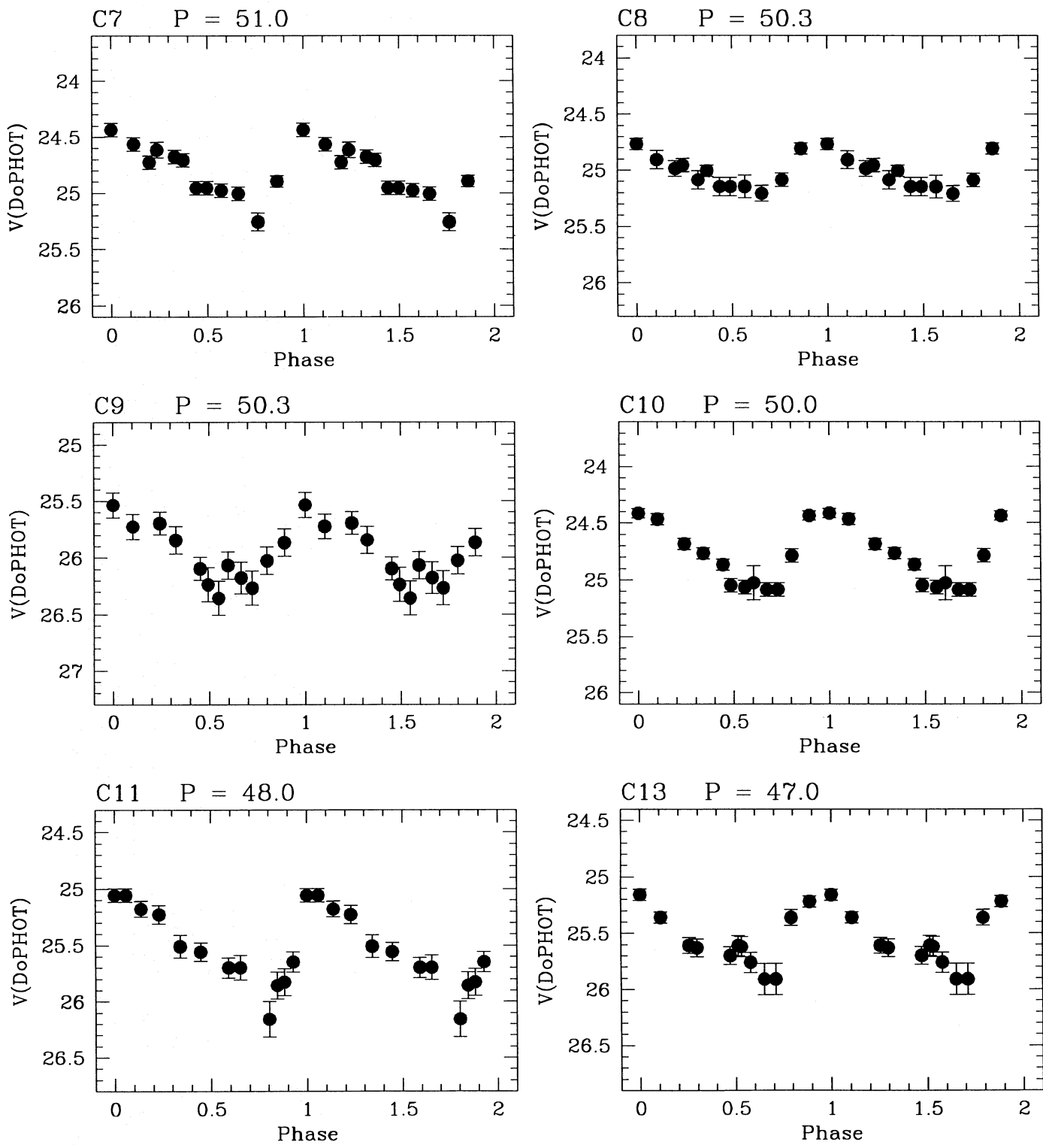


FIG. 5b

DAOPHOT light curves and photometry for each Cepheid are available upon request.

The DoPHOT and DAOPHOT phase weighted mean magnitudes for the common Cepheids are compared in Figure 6. In the figure, Cepheids belonging to different chips are marked differently. The mean V magnitudes agree very well for all chips except for WF3: the mean value of the difference between the DoPHOT and DAOPHOT V magnitudes is (in the sense of DoPHOT-DAOPHOT)

0.01 ± 0.01 for PC1, -0.03 ± 0.01 for WF2, -0.11 ± 0.02 for WF3, and 0.02 ± 0.01 for WF4. The mean I magnitudes for WF2 are in perfect agreement, but the same cannot be said for the other chips: The mean value of the difference between the DoPHOT and DAOPHOT I magnitudes is 0.16 ± 0.02 for PC1, 0.01 ± 0.01 for WF2, -0.19 ± 0.02 for WF3, and -0.10 ± 0.01 for WF4. These values are largely consistent with the values quoted by Hill et al. (1996) for the difference between the DoPHOT and DAOPHOT photo-

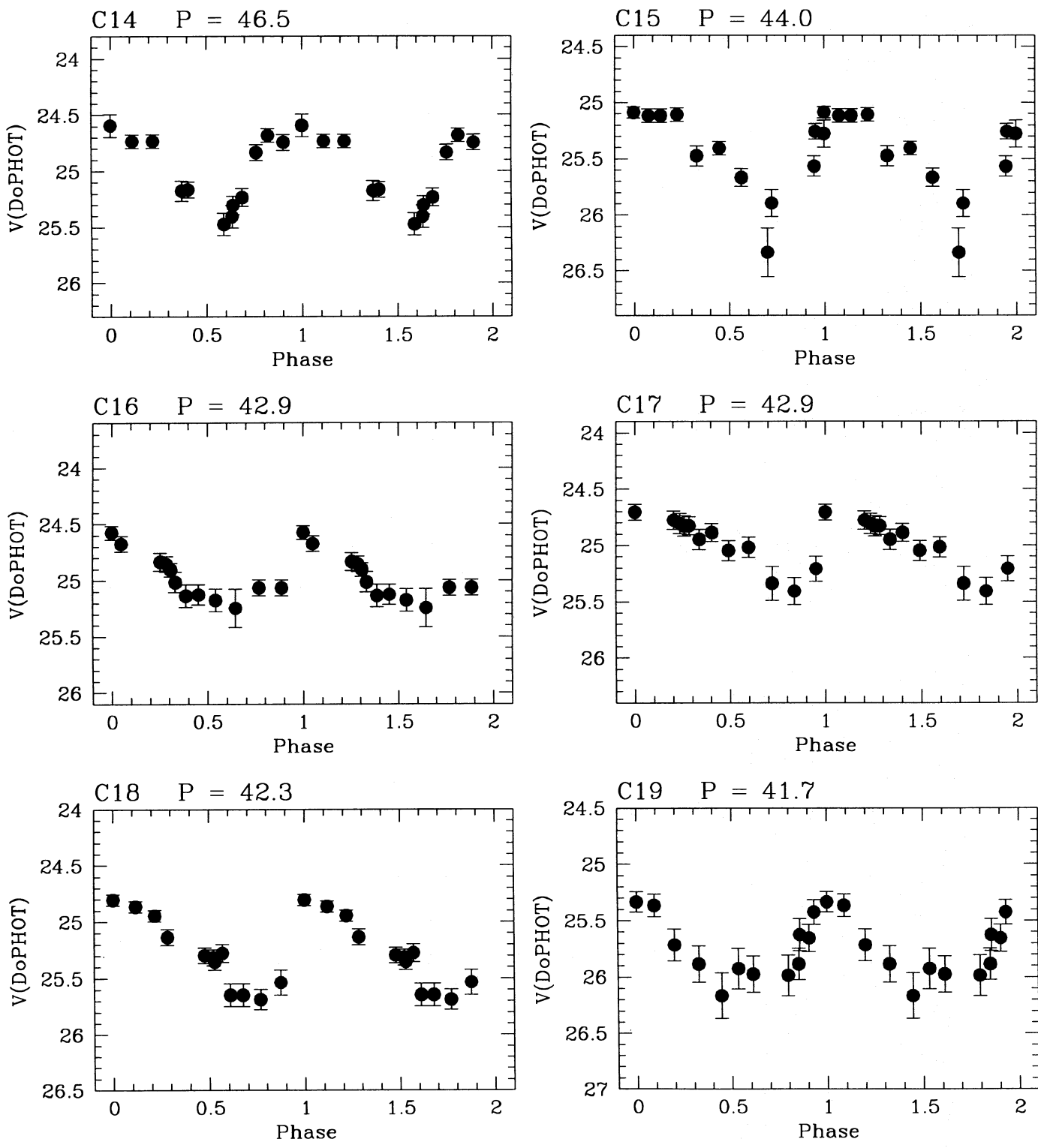


FIG. 5c

metry for the brightest stars in each chip. The large differences found for WF3 are discussed in detail in Hill et al. (1996).

In the Appendix, we will discuss further the separate samples of DoPHOT and DAOPHOT Cepheids. There, the two samples will be treated separately, PL relations will be fitted and distance moduli derived for both. This exercise shows that our result is not sensitive to the particular choice of the sample of Cepheids. Also in the Appendix, we give the

photometry, finding charts, and light curves for the Cepheids that were identified by only one of two photometric packages.

To conclude this section, we would like to point out that the sample of Cepheids presented in this paper is not complete. Apart from the obvious limits due to the lower magnitude cutoff of the data, enough observations must exist near both maximum and minimum of the light curve for the star to be flagged as variable; therefore, the probability of detec-

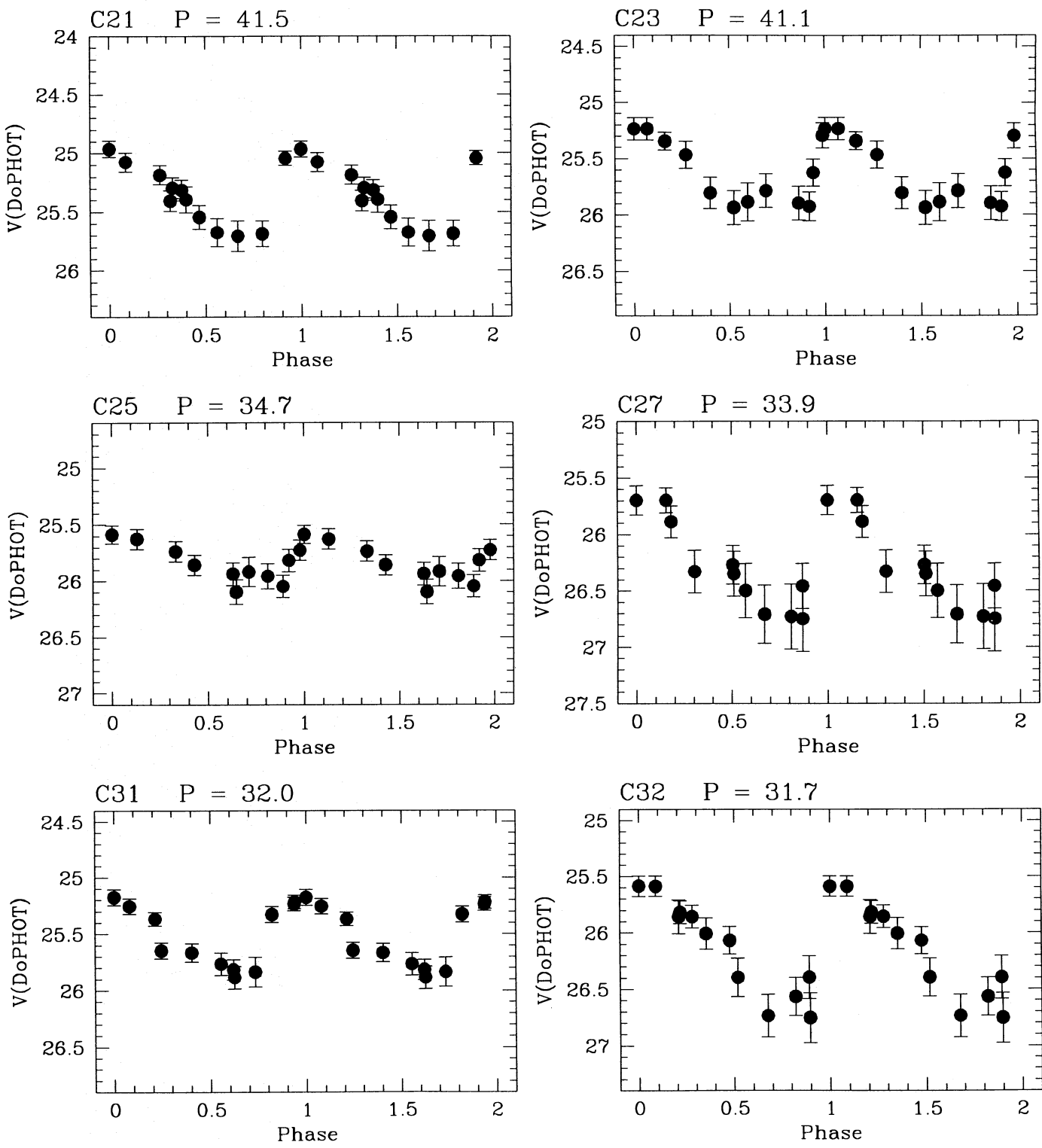


FIG. 5d

tion is a function of the period of the object, as explained in § 2.1. In addition, there is a strong dependence of the probability of detection with location in the galaxy, since a star is less likely to be found and measured accurately in crowded regions. As a consequence, more variables are found in the less crowded regions (PC1 or WF4 rather than WF2 or WF3).

6. THE PL RELATION AND THE APPARENT DISTANCE MODULI TO M100

In keeping with other papers in this series (Freedman et al. 1994a; Kelson et al. 1996; Silbermann et al. 1996), the apparent V and I distance moduli to M100 are derived using a standard application of the published V and I PL

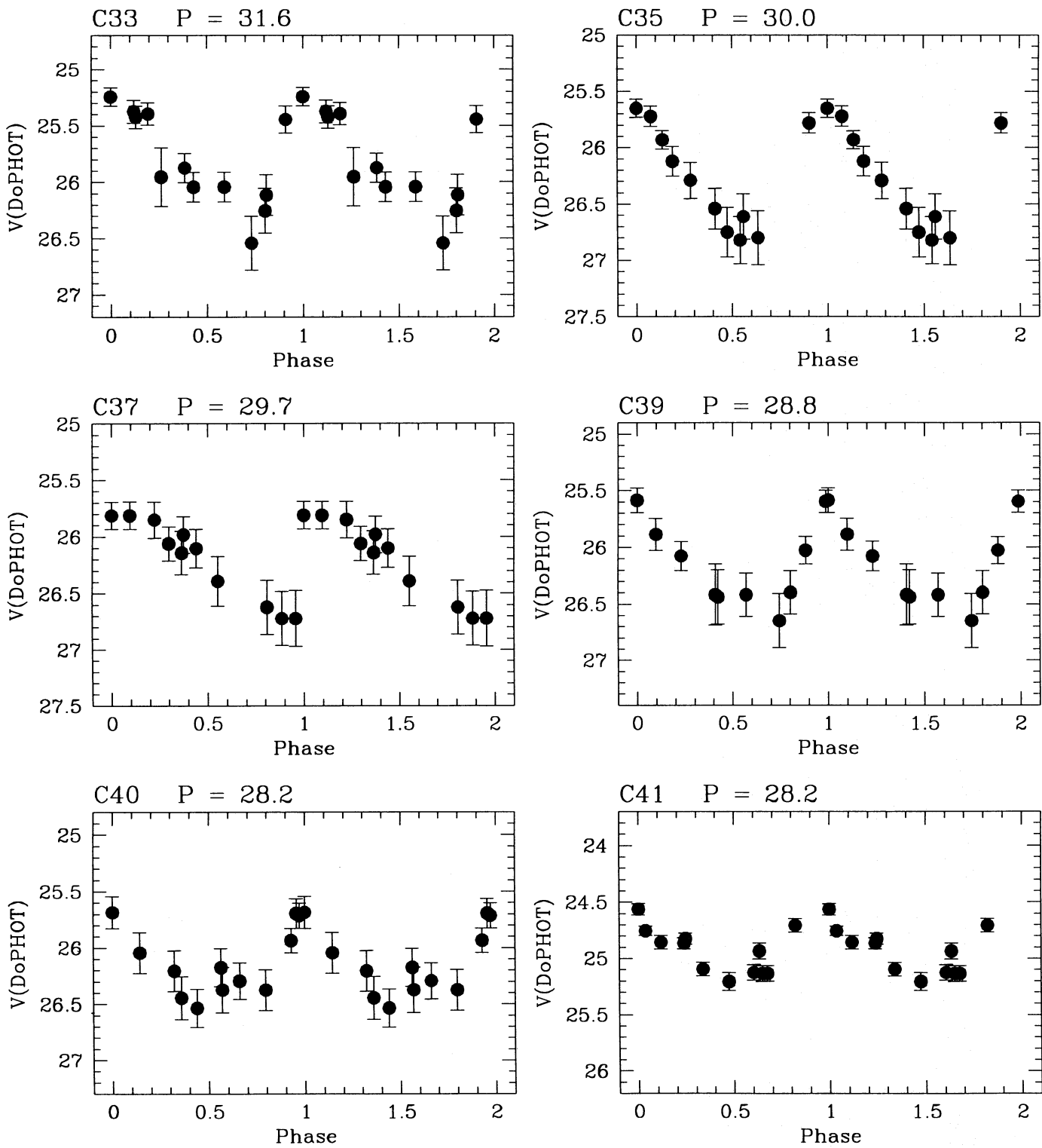


FIG. 5e

relations listed by Madore & Freedman (1991). These PL relations, which are based on LMC Cepheid data scaled to a true modulus of 18.50 ± 0.10 and corrected for an average line-of-sight reddening of $E(B-V) = 0.10$ mag, give

$$M_V = -2.76[\log_{10}(P) - 1.0] - 4.16, \quad (4)$$

and

$$M_I = -3.06[\log_{10}(P) - 1.0] - 4.87. \quad (5)$$

In fitting the M100 data, we have followed the procedure outlined in Freedman et al. (1994a): In order to avoid any bias in a slope fitted to M100 itself, due to incompleteness at short periods, the slope of the fit is fixed to the Madore & Freedman (1991) values quoted above. Only the M100 Cepheids with periods between 8 and 70 days have been considered in the fits, since Cepheids with periods shorter than about 8 days are likely to be oscillating in the first harmonic (Smith et al. 1992), while the validity of the PL relation for

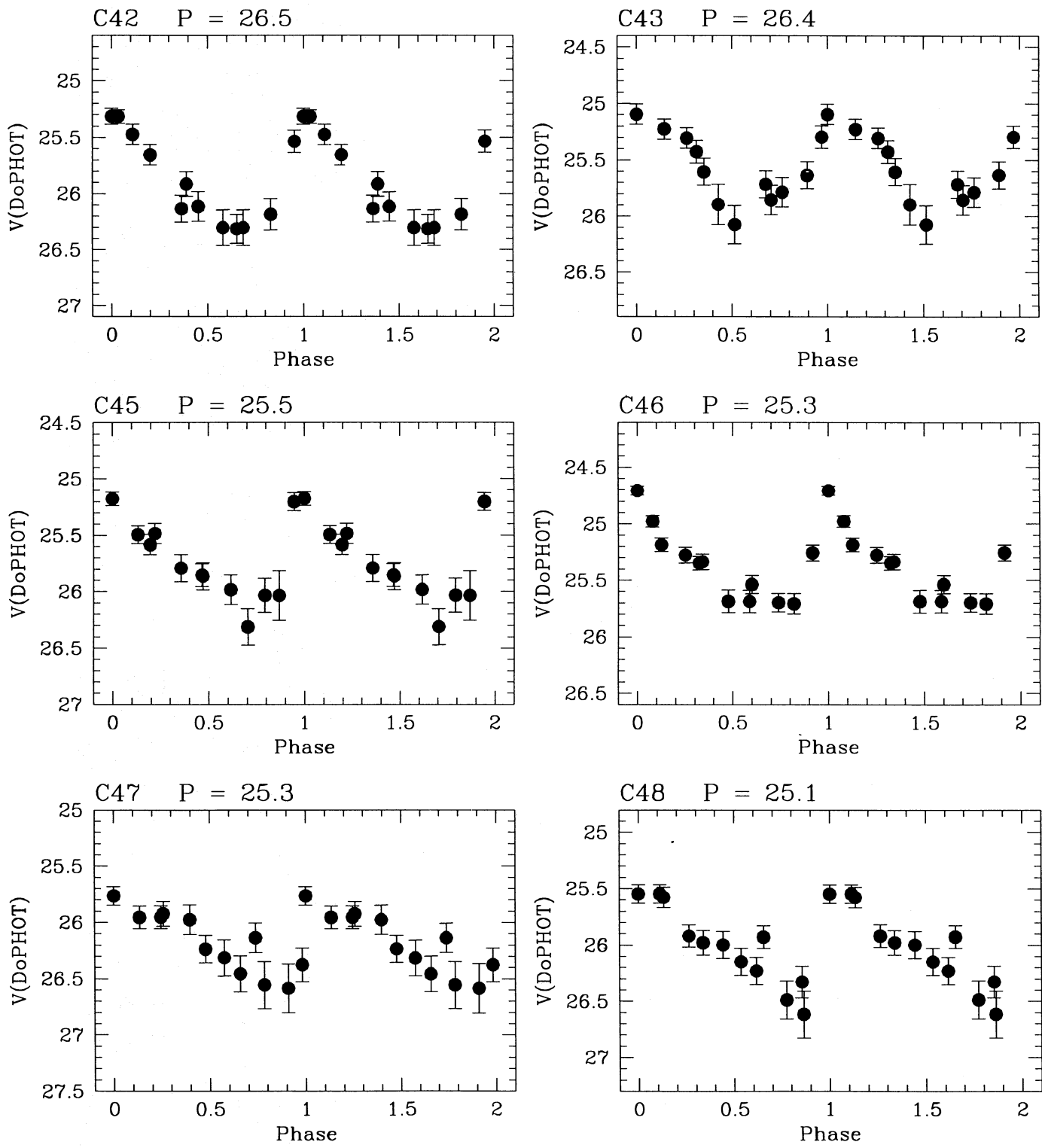


FIG. 5f

Cepheids with period longer than 70 days is controversial (Freedman 1988). Several fits to the combined M100 and LMC sample are performed, each time sliding the LMC data in the y -direction in increments of 0.01 mag, until the rms of the fit is minimized. The magnitude shift resulting in the minimum rms represents the apparent relative distance modulus between the LMC and M100. The V and I PL relations for the common sample of Cepheids (Table 5) are

plotted in Figures 7 and 8, respectively. Phase weighted magnitudes have been used in plotting the data. The solid line in each figure represents the best fitting PL relation for Cepheids with period between 20 and 70 days (this choice of period range will be justified below). The dashed lines, drawn at ± 0.54 mag for the V PL plot and ± 0.36 mag for the I PL plot, reflect the finite width of the Cepheids instability strip and thus the expected intrinsic scatter around

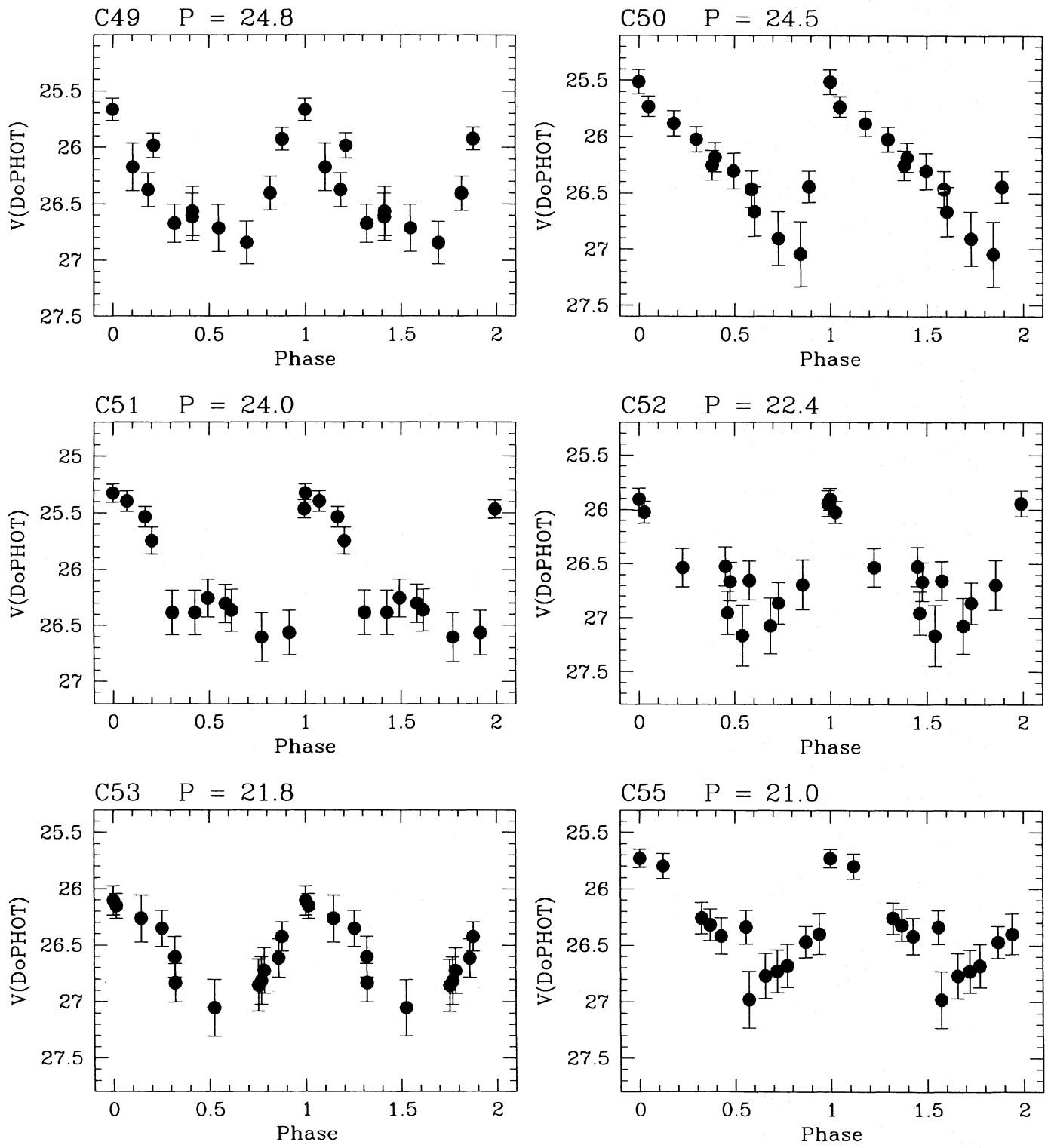


FIG. 5g

the best fitting PL relation. The open circles represent outliers falling more than 4σ away from the mean in either the V or I PL plots.

Due to the faint end limiting magnitude (Hill et al. 1996), and to the intrinsic width of the PL relation, only the brightest of the short-period Cepheids are detected. This incompleteness will produce a lower apparent distance modulus since the slope of the fitted PL relation is fixed. In

order to study the effects of this bias, we have imposed several lower limit cutoffs to the data and have fitted PL relations independently for samples of Cepheids with periods larger than 8, 20, 25, 30, and 35 days, using phase weighted mean magnitude (we will return to the question of mean magnitudes later in this section). This exercise will allow us to determine in which period range the Cepheid sample does not suffer from magnitude incompleteness. The

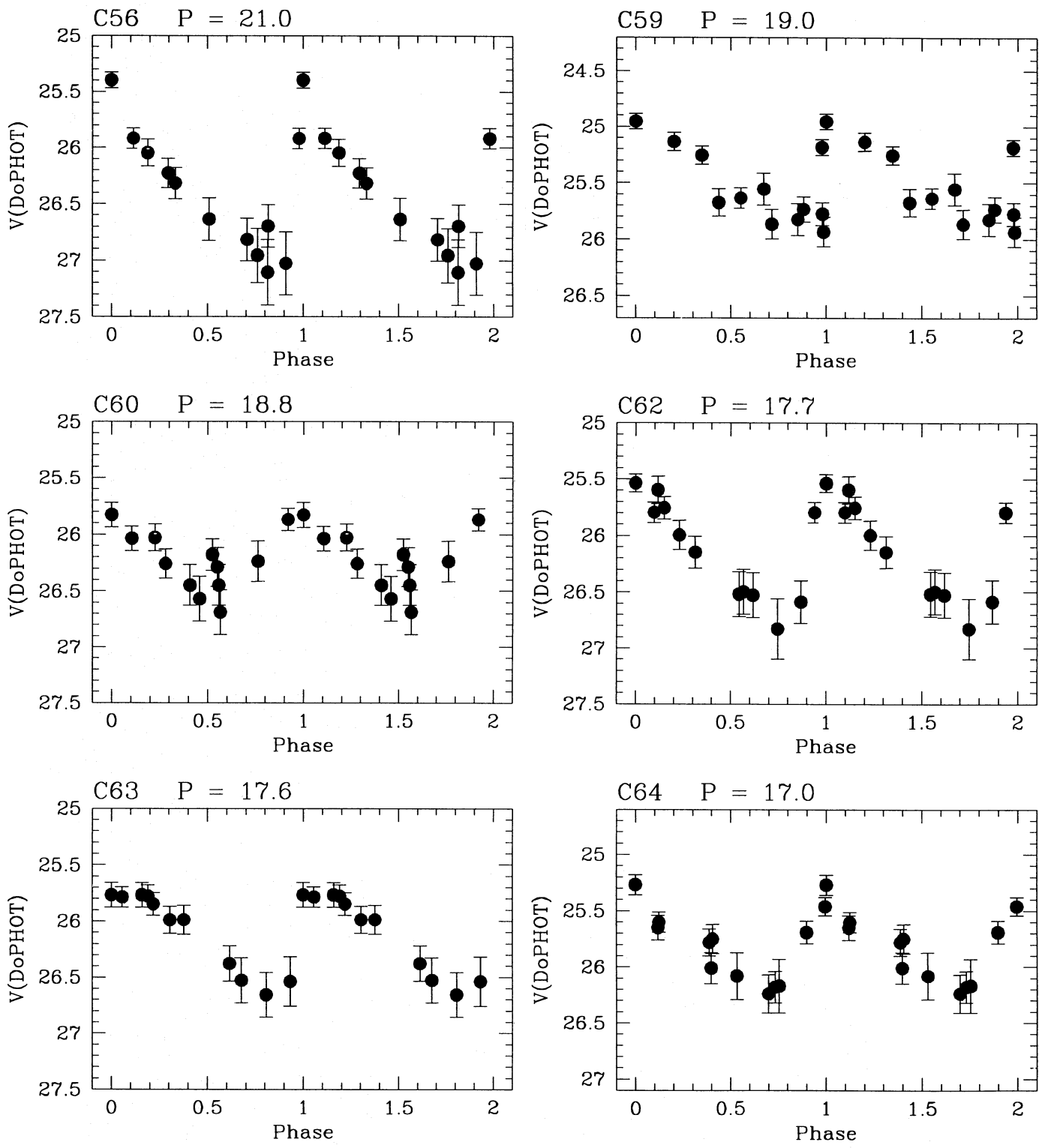
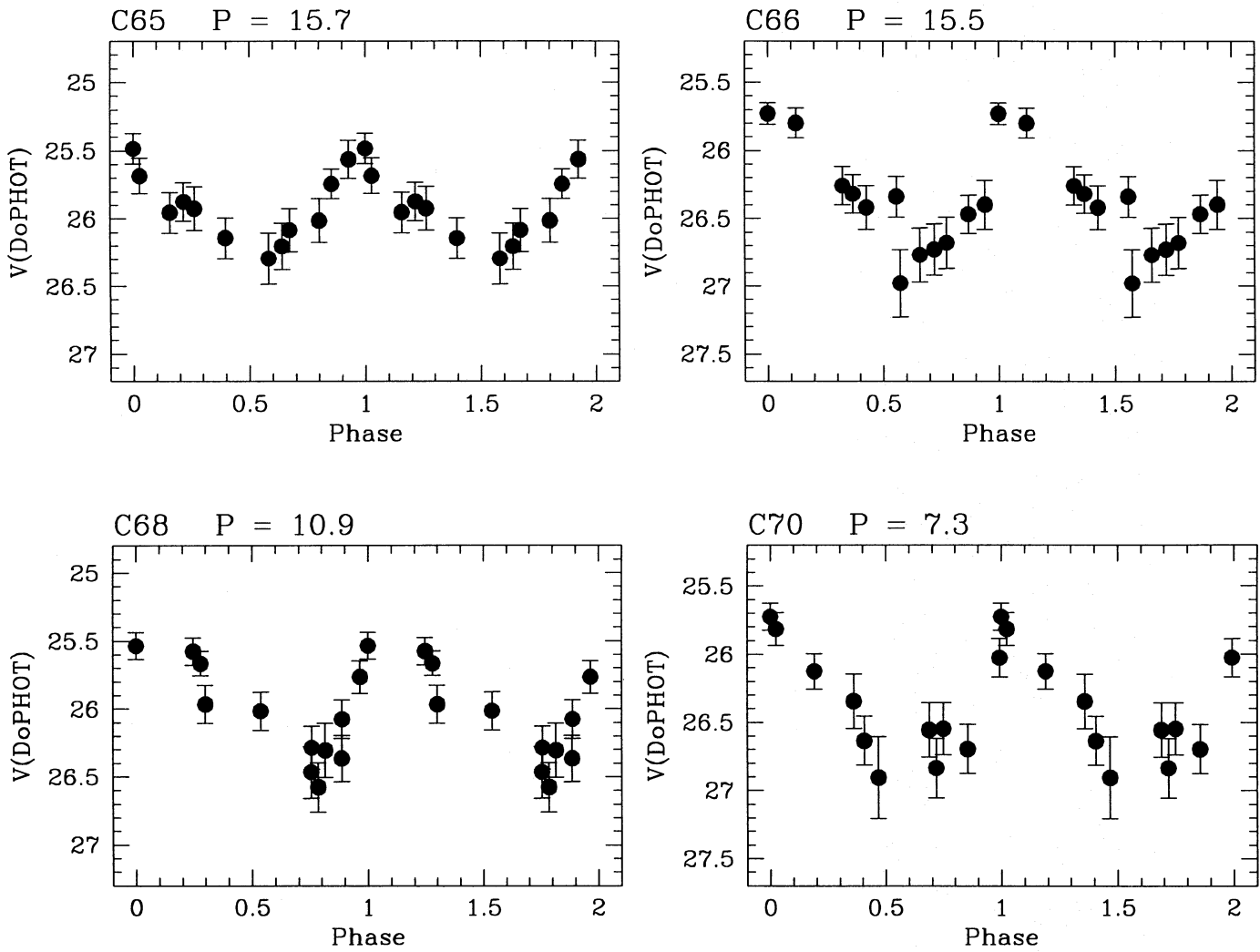


FIG. 5h

result is shown in Table 8. The rms for each fit (calculated for the M100 data alone, not for the combined M100 and LMC samples) is also reported in Table 8. The errors associated with the apparent distance moduli, μ_V and μ_I , are derived from the fits themselves, as $\sigma/(n - 1)^{1/2}$. The true distance modulus μ_0 and its error will be discussed in the following section.

There is a modest tendency for the distance modulus to

increase if a higher cutoff is imposed on the period: For the fit to the complete sample of Cepheids, the true distance modulus in V increases by 0.1 mag when the lower cutoff on the period is increased from 8 to 20 days, showing the existence of a magnitude-related selection effect for Cepheids with periods between 8 and 20 days, and acting in a way that only the brighter Cepheids are detected. Increasing the period cutoff to 35 days does not further increase the dis-

FIG. 5*i*

tance modulus; we therefore conclude that a magnitude bias is not present for Cepheids with periods longer than 20 days.

Another source of concern is the possibility of systematic differences between the distance moduli derived from Cepheids belonging to different chips. These differences may be due to intrinsic differences in the photometric zero point between chips, to errors in the flat fields, or, since some of the chips (WF2 and WF3) are more crowded than others, to errors in the background determination in crowded regions. Therefore, we have divided the Cepheids into four groups, according to the chip in which they were found, and fitted PL relations separately to each group. As is the case for the complete sample, within each chip a magnitude-related selection effect is present for Cepheids with periods lower than 20 days, while the distance modulus remains stable for longer period Cepheids. In Table 8, we report the apparent V and I distance moduli, the true distance modulus, and reddening for the four samples of Cepheids belonging to the four different WFPC2 chips, and with periods between 20 and 70 days. No significant differences in the distance modulus are present. The WF2 and WF4 samples are the best defined ones, containing the largest number of Cepheids, and the distance moduli inferred from these two samples agree very well between themselves and with the

sample including Cepheids from all chips (not surprisingly, since, in all period groups, about 70% of the Cepheids are in WF2 and WF4). The samples consisting of the PC1 and WF3 Cepheids are obviously not very significant, since they contain only seven and four objects, respectively, but lead to a true distance modulus consistent, within the errors, with the ones derived from the WF2 and WF4 samples.

A quick look at the light curves plotted in Figures 5*a*–5*i* will show that most, if not all, of the M100 Cepheids have very well defined light curves, with very uniform phase coverage. Therefore, we expect that the distance modulus will not depend on whether intensity average or phase weighted mean magnitudes are used. In Table 8, we list the distance moduli for the complete sample of Cepheids with period, between 20 and 70 days, obtained using intensity averaged mean magnitudes. As expected, the result is virtually identical to the one obtained from the same sample using phase weighted mean magnitudes. Also, we do not expect any changes in the final result if weights are assigned to each Cepheid prior to fitting the PL relation, to reflect the fact that some of the objects are higher confidence variables than others. In Table 8, we report the distance moduli derived from the weighted fits obtained by assigning to each Cepheid weights proportional to the inverse of the DoPHOT χ^2 (eq. [1]) and to the inverse of the DAOPHOT

TABLE 6
 V PHOTOMETRY FOR THE FINAL SAMPLE

JD	$V \pm \Delta V$						
	C1 $P = 85.0$	C2 $P = 76.3$	C3 $P = 63.5$	C4 $P = 53.1$	C5 $P = 52.8$	C6 $P = 52.0$	C7 $P = 51.0$
2449465.78	24.67 ± 0.05	25.12 ± 0.08	24.94 ± 0.05	24.98 ± 0.05	24.90 ± 0.09	25.51 ± 0.14	24.56 ± 0.06
2449476.71	24.71 ± 0.05	25.24 ± 0.09	24.72 ± 0.05	24.98 ± 0.06	25.19 ± 0.09	24.78 ± 0.07	24.67 ± 0.06
2449478.99	24.86 ± 0.06	25.24 ± 0.09	24.77 ± 0.05	25.02 ± 0.05	25.17 ± 0.08	24.82 ± 0.08	24.70 ± 0.06
2449482.40	24.77 ± 0.08	25.31 ± 0.11	24.83 ± 0.05	25.06 ± 0.09	25.39 ± 0.08	24.87 ± 0.07	24.95 ± 0.06
2449485.22	24.96 ± 0.06	25.31 ± 0.11	24.83 ± 0.05	25.06 ± 0.09	25.41 ± 0.11	25.00 ± 0.08	24.95 ± 0.06
2449489.04	24.92 ± 0.07	25.46 ± 0.11	24.94 ± 0.06	25.15 ± 0.05	25.28 ± 0.10	25.11 ± 0.08	24.97 ± 0.06
2449493.53	25.10 ± 0.08	25.37 ± 0.09	24.98 ± 0.06	25.37 ± 0.08	...	25.47 ± 0.10	25.00 ± 0.06
2449498.82	25.15 ± 0.07	25.21 ± 0.09	25.18 ± 0.09	25.54 ± 0.14	25.10 ± 0.07	25.55 ± 0.08	25.25 ± 0.08
2449503.85	25.14 ± 0.07	25.07 ± 0.08	25.14 ± 0.06	25.46 ± 0.08	25.10 ± 0.07	25.59 ± 0.11	24.89 ± 0.05
2449510.82	25.16 ± 0.09	25.00 ± 0.07	25.29 ± 0.07	25.85 ± 0.13	24.73 ± 0.07	25.60 ± 0.12	24.43 ± 0.06
2449520.95	25.19 ± 0.07	24.97 ± 0.07	25.41 ± 0.09	24.99 ± 0.05	24.83 ± 0.06	24.89 ± 0.06	24.72 ± 0.06
2449522.96	25.21 ± 0.08	25.11 ± 0.08	25.35 ± 0.10	24.88 ± 0.05	25.02 ± 0.09	24.83 ± 0.07	24.61 ± 0.07
$V \pm \Delta V$							
JD	C8 $P = 50.3$	C9 $P = 50.3$	C10 $P = 50.0$	C11 $P = 48.0$	C13 $P = 47.0$	C14 $P = 46.5$	C15 $P = 44.0$
2449465.78	24.90 ± 0.08	25.84 ± 0.12	24.76 ± 0.05	25.70 ± 0.11	25.63 ± 0.08	25.16 ± 0.07	26.34 ± 0.22
2449476.71	25.08 ± 0.08	26.35 ± 0.15	25.06 ± 0.06	25.83 ± 0.12	25.62 ± 0.09	25.30 ± 0.08	25.57 ± 0.09
2449478.99	25.00 ± 0.05	26.06 ± 0.12	25.02 ± 0.15	25.65 ± 0.09	25.76 ± 0.09	25.23 ± 0.08	25.09 ± 0.05
2449482.40	25.14 ± 0.08	26.17 ± 0.14	25.08 ± 0.06	25.06 ± 0.06	25.91 ± 0.14	24.83 ± 0.07	25.12 ± 0.06
2449485.22	25.14 ± 0.08	26.26 ± 0.15	25.08 ± 0.06	25.06 ± 0.06	25.91 ± 0.14	24.68 ± 0.06	25.12 ± 0.06
2449489.04	25.14 ± 0.10	26.02 ± 0.12	24.78 ± 0.06	25.18 ± 0.07	25.36 ± 0.07	24.74 ± 0.07	25.11 ± 0.06
2449493.53	25.20 ± 0.07	25.86 ± 0.12	24.43 ± 0.04	25.23 ± 0.08	25.22 ± 0.05	24.59 ± 0.10	25.48 ± 0.09
2449498.82	25.08 ± 0.06	25.53 ± 0.11	24.41 ± 0.04	25.51 ± 0.10	25.16 ± 0.05	24.73 ± 0.06	25.41 ± 0.06
2449503.85	24.80 ± 0.05	25.72 ± 0.11	24.46 ± 0.05	25.56 ± 0.08	25.36 ± 0.05	24.73 ± 0.06	25.67 ± 0.08
2449510.82	24.76 ± 0.05	25.69 ± 0.10	24.68 ± 0.05	25.70 ± 0.09	25.61 ± 0.07	25.17 ± 0.09	25.90 ± 0.12
2449520.95	24.98 ± 0.07	26.09 ± 0.10	24.86 ± 0.05	26.16 ± 0.16	25.70 ± 0.08	25.47 ± 0.10	25.26 ± 0.07
2449522.96	24.95 ± 0.06	26.23 ± 0.15	25.04 ± 0.06	25.86 ± 0.12	25.61 ± 0.09	25.40 ± 0.10	25.28 ± 0.12
$V \pm \Delta V$							
JD	C16 $P = 42.9$	C17 $P = 42.9$	C18 $P = 42.3$	C19 $P = 41.7$	C21 $P = 41.5$	C23 $P = 41.1$	C25 $P = 34.7$
2449465.78	24.57 ± 0.06	25.21 ± 0.11	24.94 ± 0.05	25.92 ± 0.18	24.96 ± 0.07	25.89 ± 0.17	25.74 ± 0.09
2449476.71	24.83 ± 0.08	24.78 ± 0.08	25.29 ± 0.07	25.98 ± 0.18	25.18 ± 0.08	25.90 ± 0.15	26.10 ± 0.11
2449478.99	24.90 ± 0.06	24.83 ± 0.09	25.35 ± 0.07	25.88 ± 0.14	25.40 ± 0.09	25.93 ± 0.13	25.92 ± 0.13
2449482.40	25.13 ± 0.10	24.95 ± 0.09	25.64 ± 0.10	25.42 ± 0.11	25.39 ± 0.11	25.24 ± 0.10	25.96 ± 0.11
2449485.22	25.12 ± 0.09	24.89 ± 0.08	25.64 ± 0.10	25.33 ± 0.09	25.54 ± 0.10	25.24 ± 0.10	26.05 ± 0.10
2449489.04	25.17 ± 0.10	25.05 ± 0.09	25.68 ± 0.09	25.36 ± 0.10	25.67 ± 0.12	25.35 ± 0.08	25.59 ± 0.08
2449493.53	25.24 ± 0.17	25.02 ± 0.09	25.53 ± 0.11	25.71 ± 0.14	25.70 ± 0.13	25.47 ± 0.12	25.63 ± 0.09
2449498.82	25.06 ± 0.07	25.34 ± 0.15	24.80 ± 0.05	25.88 ± 0.16	25.68 ± 0.11	25.81 ± 0.14	...
2449503.85	25.06 ± 0.07	25.41 ± 0.12	24.86 ± 0.05	26.16 ± 0.20	25.04 ± 0.06	25.94 ± 0.15	25.86 ± 0.09
2449510.82	24.67 ± 0.07	24.71 ± 0.07	25.13 ± 0.07	25.97 ± 0.16	25.07 ± 0.08	25.79 ± 0.15	25.94 ± 0.10
2449520.95	24.85 ± 0.07	24.81 ± 0.09	25.31 ± 0.07	25.62 ± 0.14	25.29 ± 0.09	25.63 ± 0.12	25.82 ± 0.10
2449522.96	25.01 ± 0.09	24.83 ± 0.08	25.27 ± 0.08	25.65 ± 0.12	25.31 ± 0.09	25.30 ± 0.11	25.73 ± 0.09
$V \pm \Delta V$							
JD	C27 $P = 33.9$	C31 $P = 32.0$	C32 $P = 31.7$	C33 $P = 31.6$	C35 $P = 30.0$	C37 $P = 29.7$	C39 $P = 28.8$
2449465.78	25.89 ± 0.14	25.36 ± 0.06	26.07 ± 0.12	25.87 ± 0.13	26.80 ± 0.24	26.10 ± 0.17	26.44 ± 0.24
2449476.71	26.27 ± 0.17	25.76 ± 0.10	26.57 ± 0.17	26.54 ± 0.24	25.65 ± 0.08	26.62 ± 0.24	26.40 ± 0.19
2449478.99	26.50 ± 0.24	25.88 ± 0.10	26.40 ± 0.19	26.25 ± 0.20	25.72 ± 0.09	26.72 ± 0.24	26.03 ± 0.12
2449482.40	26.71 ± 0.26	25.83 ± 0.13	25.59 ± 0.09	25.44 ± 0.12	26.12 ± 0.13	25.81 ± 0.12	25.59 ± 0.11
2449485.22	...	25.32 ± 0.07	25.59 ± 0.09	25.24 ± 0.08	26.29 ± 0.16	25.81 ± 0.12	25.89 ± 0.14
2449489.04	26.46 ± 0.20	25.21 ± 0.06	25.86 ± 0.15	25.37 ± 0.10	26.54 ± 0.18	25.85 ± 0.16	26.08 ± 0.13
2449493.53	25.70 ± 0.13	25.25 ± 0.07	26.01 ± 0.14	25.95 ± 0.26	26.61 ± 0.20	25.98 ± 0.16	...
2449498.82	25.70 ± 0.11	25.64 ± 0.07	26.40 ± 0.17	26.04 ± 0.13	...	26.39 ± 0.22	26.42 ± 0.19
2449503.85	26.33 ± 0.19	25.66 ± 0.08	26.74 ± 0.19	26.04 ± 0.13	25.78 ± 0.09	...	26.65 ± 0.24
2449510.82	26.35 ± 0.20	25.81 ± 0.09	26.76 ± 0.22	26.11 ± 0.18	25.93 ± 0.08	26.72 ± 0.25	25.60 ± 0.10
2449520.95	26.73 ± 0.29	25.23 ± 0.06	25.82 ± 0.10	25.42 ± 0.10	26.75 ± 0.22	26.06 ± 0.15	...
2449522.96	26.75 ± 0.29	25.17 ± 0.07	25.86 ± 0.10	25.39 ± 0.10	26.82 ± 0.21	26.14 ± 0.19	26.42 ± 0.27

TABLE 6—Continued

$V \pm \Delta V$							
JD	C40 $P = 28.2$	C41 $P = 28.2$	C42 $P = 26.5$	C43 $P = 26.4$	C45 $P = 25.5$	C46 $P = 25.3$	C47 $P = 25.3$
2449465.78	25.71 ± 0.11	25.13 ± 0.07	25.53 ± 0.10	25.31 ± 0.09	26.31 ± 0.16	25.71 ± 0.09	26.23 ± 0.12
2449476.71	26.44 ± 0.19	24.75 ± 0.04	26.13 ± 0.12	25.72 ± 0.12	25.49 ± 0.08	25.28 ± 0.07	26.58 ± 0.22
2449478.99	26.53 ± 0.17	24.85 ± 0.06	26.11 ± 0.13	25.79 ± 0.13	25.48 ± 0.09	25.34 ± 0.07	25.76 ± 0.08
2449482.40	26.17 ± 0.17	24.86 ± 0.05	26.30 ± 0.16	25.64 ± 0.12	25.79 ± 0.12	25.69 ± 0.10	25.95 ± 0.10
2449485.22	26.29 ± 0.16	25.09 ± 0.06	26.30 ± 0.16	25.10 ± 0.09	25.85 ± 0.10	25.69 ± 0.10	25.95 ± 0.10
2449489.04	26.37 ± 0.18	25.20 ± 0.08	26.18 ± 0.14	25.23 ± 0.09	25.98 ± 0.13	25.70 ± 0.08	25.97 ± 0.13
2449493.53	25.69 ± 0.13	24.93 ± 0.07	25.31 ± 0.07	25.43 ± 0.10	26.03 ± 0.15	25.26 ± 0.07	26.31 ± 0.16
2449498.82	26.04 ± 0.18	24.70 ± 0.06	25.65 ± 0.09	26.08 ± 0.17	25.17 ± 0.06	25.19 ± 0.06	26.55 ± 0.21
2449503.85	26.20 ± 0.18	24.56 ± 0.05	25.91 ± 0.11	25.86 ± 0.13	25.58 ± 0.09	25.35 ± 0.06	26.37 ± 0.15
2449510.82	26.37 ± 0.20	24.82 ± 0.05	26.31 ± 0.13	25.30 ± 0.10	25.86 ± 0.12	25.54 ± 0.08	25.92 ± 0.11
2449520.95	25.93 ± 0.11	25.12 ± 0.07	25.31 ± 0.06	25.61 ± 0.12	26.03 ± 0.22	24.71 ± 0.04	26.45 ± 0.16
2449522.96	25.68 ± 0.14	25.13 ± 0.07	25.47 ± 0.09	25.90 ± 0.18	25.20 ± 0.08	24.98 ± 0.05	26.13 ± 0.13
$V \pm \Delta V$							
JD	C48 $P = 25.1$	C49 $P = 24.8$	C50 $P = 24.5$	C51 $P = 24.0$	C52 $P = 22.4$	C53 $P = 21.8$	C55 $P = 21.0$
2449465.78	25.98 ± 0.11	25.92 ± 0.10	25.73 ± 0.09	26.36 ± 0.19	26.35 ± 0.16	25.94 ± 0.12	26.57 ± 0.18
2449476.71	26.49 ± 0.17	26.67 ± 0.17	26.30 ± 0.16	25.39 ± 0.09	26.85 ± 0.23	26.66 ± 0.18	25.94 ± 0.11
2449478.99	26.62 ± 0.21	26.61 ± 0.21	26.46 ± 0.16	25.53 ± 0.09	26.61 ± 0.17	26.65 ± 0.18	26.28 ± 0.14
2449482.40	25.55 ± 0.08	26.71 ± 0.21	26.90 ± 0.24	26.38 ± 0.20	26.15 ± 0.11	26.86 ± 0.19	26.81 ± 0.19
2449485.22	25.55 ± 0.08	...	27.04 ± 0.29	26.38 ± 0.20	26.26 ± 0.21	26.69 ± 0.23	26.76 ± 0.21
2449489.04	25.92 ± 0.10	26.40 ± 0.15	25.51 ± 0.11	26.30 ± 0.17	26.83 ± 0.17	26.02 ± 0.10	26.78 ± 0.19
2449493.53	26.00 ± 0.12	25.66 ± 0.10	25.88 ± 0.11	26.60 ± 0.22	27.05 ± 0.25	26.53 ± 0.18	26.72 ± 0.22
2449498.82	25.93 ± 0.10	25.98 ± 0.11	26.18 ± 0.13	25.46 ± 0.08	26.81 ± 0.21	26.95 ± 0.20	26.27 ± 0.14
2449503.85	26.33 ± 0.14	26.56 ± 0.22	26.66 ± 0.22	25.74 ± 0.12	26.10 ± 0.13	27.07 ± 0.26	26.71 ± 0.18
2449510.82	25.58 ± 0.09	26.84 ± 0.19	26.44 ± 0.14	26.25 ± 0.17	26.60 ± 0.18	25.90 ± 0.10	26.89 ± 0.25
2449520.95	26.15 ± 0.12	26.17 ± 0.21	26.02 ± 0.11	26.56 ± 0.20	26.72 ± 0.20	26.52 ± 0.18	26.23 ± 0.13
2449522.96	26.23 ± 0.12	26.37 ± 0.15	26.25 ± 0.13	25.32 ± 0.08	26.42 ± 0.13	27.16 ± 0.28	26.55 ± 0.17
$V \pm \Delta V$							
JD	C56 $P = 21.0$	C59 $P = 19.0$	C60 $P = 18.8$	C62 $P = 17.7$	C63 $P = 17.6$	C64 $P = 17.0$	C65 $P = 15.7$
2449465.78	26.05 ± 0.12	25.18 ± 0.07	26.18 ± 0.14	25.54 ± 0.08	25.79 ± 0.09	26.17 ± 0.24	25.95 ± 0.15
2449476.71	26.82 ± 0.19	25.63 ± 0.09	26.04 ± 0.11	26.53 ± 0.20	26.53 ± 0.20	26.01 ± 0.14	25.74 ± 0.11
2449478.99	26.70 ± 0.19	25.55 ± 0.14	26.03 ± 0.12	26.83 ± 0.27	26.66 ± 0.20	26.08 ± 0.21	25.48 ± 0.11
2449482.40	25.92 ± 0.09	25.82 ± 0.14	26.45 ± 0.18	25.80 ± 0.09	25.77 ± 0.11	26.18 ± 0.14	25.87 ± 0.14
2449485.22	25.92 ± 0.09	24.95 ± 0.07	26.45 ± 0.18	25.80 ± 0.09	25.77 ± 0.11	25.69 ± 0.10	26.14 ± 0.15
2449489.04	26.23 ± 0.13	25.13 ± 0.08	26.24 ± 0.18	26.15 ± 0.14	25.99 ± 0.13	25.60 ± 0.09	26.20 ± 0.17
2449493.53	26.64 ± 0.19	25.67 ± 0.12	25.83 ± 0.11	26.50 ± 0.20	...	25.78 ± 0.12	25.56 ± 0.14
2449498.82	26.96 ± 0.24	25.86 ± 0.13	26.26 ± 0.13	26.59 ± 0.19	26.54 ± 0.22	26.24 ± 0.17	25.92 ± 0.16
2449503.85	25.40 ± 0.07	25.77 ± 0.10	26.29 ± 0.17	25.76 ± 0.10	25.85 ± 0.10	25.46 ± 0.08	26.29 ± 0.19
2449510.82	26.32 ± 0.14	25.25 ± 0.08	25.87 ± 0.10	26.52 ± 0.20	26.38 ± 0.16	25.75 ± 0.13	25.68 ± 0.13
2449520.95	27.11 ± 0.29	25.73 ± 0.11	26.57 ± 0.20	25.60 ± 0.12	25.78 ± 0.10	25.27 ± 0.09	26.08 ± 0.16
2449522.96	27.03 ± 0.28	25.93 ± 0.13	26.69 ± 0.20	26.00 ± 0.13	25.99 ± 0.12	25.65 ± 0.11	26.01 ± 0.16
$V \pm \Delta V$							
JD	C66 $P = 15.5$	C68 $P = 10.9$	C70 $P = 7.3$				
2449465.78	26.47 ± 0.14	26.47 ± 0.19	26.13 ± 0.13				
2449476.71	26.98 ± 0.25	26.29 ± 0.16	26.56 ± 0.20				
2449478.99	26.73 ± 0.19	25.77 ± 0.12	25.73 ± 0.10				
2449482.40	26.40 ± 0.18	25.67 ± 0.09	26.91 ± 0.30				
2449485.22	25.80 ± 0.11	26.02 ± 0.14	26.70 ± 0.18				
2449489.04	26.32 ± 0.14	26.08 ± 0.14	...				
2449493.53	26.77 ± 0.20	25.97 ± 0.14	26.03 ± 0.14				
2449498.82	25.73 ± 0.08	26.58 ± 0.18	26.84 ± 0.22				
2449503.85	26.26 ± 0.14	25.58 ± 0.10	26.64 ± 0.18				
2449510.82	26.68 ± 0.19	26.37 ± 0.17	26.35 ± 0.20				
2449520.95	26.42 ± 0.16	26.31 ± 0.20	26.55 ± 0.19				
2449522.96	26.34 ± 0.15	25.54 ± 0.10	25.82 ± 0.12				

NOTES.—The V photometry for the Cepheids listed in Table 5. We only list the DoPHOT magnitudes and errors. The period listed in the table heading is the DoPHOT period. The V photometry for the Cepheids found by only one of the two photometry packages can be found in the Appendix (Table 11).

TABLE 7
I PHOTOMETRY FOR THE FINAL SAMPLE

$I \pm \Delta I$							
JD	C1 $P = 85.0$	C2 $P = 76.3$	C3 $P = 63.5$	C4 $P = 53.1$	C5 $P = 52.8$	C6 $P = 52.0$	C7 $P = 51.0$
2449465.91	23.65 \pm 0.06	23.76 \pm 0.05	23.88 \pm 0.07	23.82 \pm 0.06	23.80 \pm 0.07	24.94 \pm 0.17	23.72 \pm 0.05
2449485.35	23.67 \pm 0.05	24.03 \pm 0.08	23.73 \pm 0.05	23.89 \pm 0.05	24.10 \pm 0.08	24.23 \pm 0.09	24.04 \pm 0.06
2449510.81	24.23 \pm 0.14	23.81 \pm 0.07	24.16 \pm 0.12	24.21 \pm 0.07	23.80 \pm 0.08	24.88 \pm 0.19	23.66 \pm 0.05
2449523.09	24.22 \pm 0.11	23.73 \pm 0.06	24.17 \pm 0.08	23.84 \pm 0.06	23.93 \pm 0.07	24.19 \pm 0.12	23.71 \pm 0.06
$I \pm \Delta I$							
JD	C8 $P = 50.3$	C9 $P = 50.3$	C10 $P = 50.0$	C11 $P = 48.0$	C13 $P = 47.0$	C14 $P = 46.5$	C15 $P = 44.0$
2449465.91	24.00 \pm 0.09	24.86 \pm 0.12	23.74 \pm 0.08	24.56 \pm 0.10	24.26 \pm 0.07	23.97 \pm 0.07	24.61 \pm 0.09
2449485.35	24.21 \pm 0.10	25.19 \pm 0.13	24.04 \pm 0.06	24.13 \pm 0.06	24.52 \pm 0.08	23.82 \pm 0.06	24.14 \pm 0.06
2449510.81	23.90 \pm 0.09	24.75 \pm 0.10	23.69 \pm 0.05	24.56 \pm 0.08	24.19 \pm 0.06	24.00 \pm 0.07	24.89 \pm 0.13
2449523.09	23.89 \pm 0.09	25.02 \pm 0.10	23.83 \pm 0.06	24.40 \pm 0.09	24.45 \pm 0.08	24.09 \pm 0.08	24.30 \pm 0.07
$I \pm \Delta I$							
JD	C16 $P = 42.9$	C17 $P = 42.9$	C18 $P = 42.3$	C19 $P = 41.7$	C21 $P = 41.5$	C23 $P = 41.1$	C25 $P = 36.4$
2449465.91	23.67 \pm 0.07	24.02 \pm 0.10	24.07 \pm 0.06	24.65 \pm 0.17	24.03 \pm 0.07	24.53 \pm 0.10	25.18 \pm 0.14
2449485.35	23.87 \pm 0.06	23.77 \pm 0.07	24.46 \pm 0.08	24.70 \pm 0.14	24.54 \pm 0.09	24.46 \pm 0.09	25.55 \pm 0.15
2449510.81	23.68 \pm 0.06	23.64 \pm 0.07	24.14 \pm 0.06	24.96 \pm 0.20	24.21 \pm 0.09	24.87 \pm 0.16	25.23 \pm 0.12
2449523.09	23.85 \pm 0.08	23.68 \pm 0.07	24.28 \pm 0.08	24.79 \pm 0.17	24.35 \pm 0.10	24.50 \pm 0.08	25.15 \pm 0.12
$I \pm \Delta I$							
JD	C27 $P = 33.9$	C31 $P = 33.1$	C32 $P = 31.7$	C33 $P = 31.6$	C35 $P = 30.0$	C37 $P = 29.7$	C39 $P = 28.8$
2449465.91	24.94 \pm 0.12	24.70 \pm 0.09	24.82 \pm 0.12	24.68 \pm 0.14	25.28 \pm 0.17	25.07 \pm 0.21	25.04 \pm 0.19
2449485.35	25.07 \pm 0.16	24.68 \pm 0.09	25.00 \pm 0.21	24.51 \pm 0.11	24.80 \pm 0.12	24.64 \pm 0.12	24.95 \pm 0.14
2449510.81	25.07 \pm 0.14	25.02 \pm 0.10	25.63 \pm 0.27	...	24.74 \pm 0.11	24.83 \pm 0.16	24.63 \pm 0.13
2449523.09	25.34 \pm 0.20	24.48 \pm 0.08	24.84 \pm 0.13	24.55 \pm 0.14	24.90 \pm 0.15	24.93 \pm 0.18	24.97 \pm 0.16
$I \pm \Delta I$							
JD	C40 $P = 28.2$	C41 $P = 28.2$	C42 $P = 26.5$	C43 $P = 26.4$	C45 $P = 25.5$	C46 $P = 25.3$	C47 $P = 25.3$
2449465.91	24.83 \pm 0.14	24.41 \pm 0.09	25.20 \pm 0.14	24.82 \pm 0.13	25.13 \pm 0.15	25.10 \pm 0.15	25.23 \pm 0.12
2449485.35	25.20 \pm 0.20	24.18 \pm 0.07	25.17 \pm 0.17	24.61 \pm 0.13	24.65 \pm 0.12	25.30 \pm 0.14	25.09 \pm 0.14
2449510.81	25.37 \pm 0.24	24.08 \pm 0.08	25.10 \pm 0.16	24.85 \pm 0.16	24.63 \pm 0.14	24.85 \pm 0.15	24.94 \pm 0.12
2449523.09	24.73 \pm 0.12	24.22 \pm 0.08	24.61 \pm 0.14	25.35 \pm 0.22	24.47 \pm 0.12	24.51 \pm 0.09	...
$I \pm \Delta I$							
JD	C48 $P = 25.1$	C49 $P = 24.8$	C50 $P = 24.5$	C51 $P = 24.0$	C52 $P = 22.4$	C53 $P = 21.8$	C55 $P = 21.0$
2449465.91	24.76 \pm 0.10	25.13 \pm 0.17	25.03 \pm 0.11	25.10 \pm 0.16	25.52 \pm 0.19	25.18 \pm 0.14	25.28 \pm 0.16
2449485.35	24.71 \pm 0.13	25.66 \pm 0.20	25.60 \pm 0.18	25.11 \pm 0.16	25.56 \pm 0.17	25.57 \pm 0.15	25.39 \pm 0.15
2449510.81	24.94 \pm 0.11	25.19 \pm 0.15	25.47 \pm 0.16	25.21 \pm 0.17	25.57 \pm 0.15	25.15 \pm 0.11	25.47 \pm 0.19
2449523.09	24.82 \pm 0.12	...	25.33 \pm 0.14	24.77 \pm 0.13	25.79 \pm 0.18	26.00 \pm 0.25	25.06 \pm 0.14
$I \pm \Delta I$							
JD	C56 $P = 21.0$	C59 $P = 19.0$	C60 $P = 18.8$	C62 $P = 17.7$	C63 $P = 17.6$	C64 $P = 17.0$	C65 $P = 15.7$
2449465.91	25.16 \pm 0.14	24.57 \pm 0.10	24.80 \pm 0.12	25.00 \pm 0.15	24.81 \pm 0.12	25.61 \pm 0.21	25.42 \pm 0.26
2449485.35	25.17 \pm 0.12	24.44 \pm 0.10	25.11 \pm 0.15	24.90 \pm 0.12	24.78 \pm 0.12	25.09 \pm 0.17	25.29 \pm 0.22
2449510.81	24.93 \pm 0.12	24.61 \pm 0.10	24.84 \pm 0.12	25.01 \pm 0.14	25.13 \pm 0.16	25.70 \pm 0.28	25.15 \pm 0.22
2449523.09	25.91 \pm 0.26	...	25.35 \pm 0.18	24.92 \pm 0.14	24.98 \pm 0.14	25.18 \pm 0.22	25.35 \pm 0.27
$I \pm \Delta I$							
JD	C66 $P = 15.5$	C68 $P = 10.9$	C70 $P = 7.3$				
2449465.91	25.97 \pm 0.25	24.92 \pm 0.14	25.54 \pm 0.25				
2449485.35	25.53 \pm 0.16	24.73 \pm 0.12	25.85 \pm 0.25				
2449510.81	...	24.76 \pm 0.11	25.60 \pm 0.20				
2449523.09	25.90 \pm 0.23	24.80 \pm 0.12	25.54 \pm 0.23				

NOTES.—The I photometry for the Cepheids listed in Table 5. We only list the DoPHOT magnitudes and errors. The period listed in the table heading is the DoPHOT period. The I photometry for the Cepheids found by only one of the two photometry packages can be found in the Appendix (Table 12).

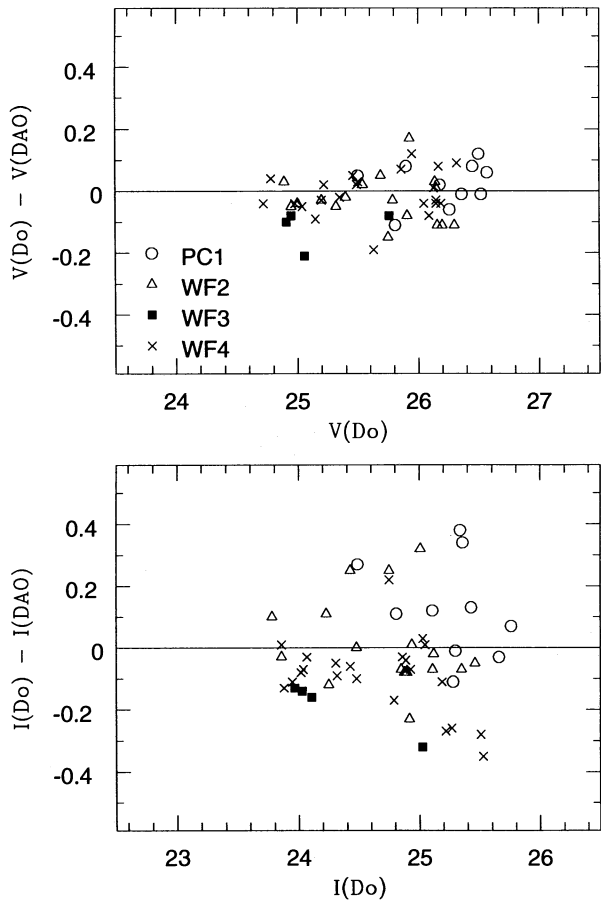


FIG. 6.—Comparison between the DoPHOT and DAOPHOT mean magnitudes for the 52 Cepheids identified from both the DoPHOT and DAOPHOT photometry. Excellent agreement is found for the mean V magnitudes, except for WF3, and for the mean I magnitudes in WF2.

σ^2 . We only report the distance moduli obtained for the sample of Cepheids with periods between 20 and 70 days; as can be seen, these distance moduli are in excellent agreement with the one derived from the unweighted fit.

As mentioned in § 5, there is a systematic difference (0.11 mag in V and -0.19 mag in I) between the DoPHOT and DAOPHOT mean magnitudes for the WF3 Cepheids. Since only four Cepheids are found in WF3, this discrepancy should not impact the distance modulus. In fact, we found that if these Cepheids are dropped from the sample, and the PL relation is then fitted to the remaining Cepheids, the final distance modulus is unaltered.

7. THE EXTINCTION AND THE TRUE DISTANCE MODULUS

In order to derive a true distance modulus to M100, the observations need to be dereddened. The extinction law derived by Cardelli, Clayton, & Mathis (1989), applied to the Cousins I and Johnson V passband, gives

$$A(I)/A(V) = 0.773 - 0.587/R_V, \quad (6)$$

with $R_V = A(V)/E(B-V)$. The absolute distance modulus to M100, μ^{M100} , can be expressed as a function of the relative apparent distance modulus $\Delta\mu$ between the LMC and M100, the absolute distance modulus μ^{LMC} to the LMC, and the absolute extinctions A^{M100} and A^{LMC} for M100 and the

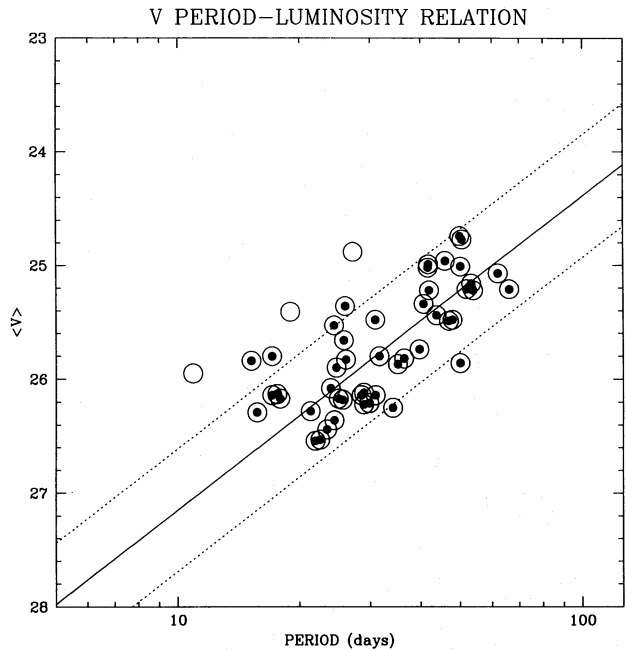


FIG. 7.— V PL relation for the sample of Cepheids listed in Table 5. For reasons discussed in the text, only the Cepheids with periods between 8 and 70 days are plotted. The solid line represents the best unweighted fit to the Cepheids with periods between 20 and 70 days, using phase weighted mean magnitudes, and corresponds to an apparent distance modulus of 31.31 ± 0.06 mag. The dashed lines, drawn at ± 0.54 mag, reflect the finite width of the Cepheids instability strip, and thus the expected intrinsic 2σ scatter around the best-fitting PL relation. The three points plotted as open circles mark outliers falling more than 4σ away from the mean, in either the V or the I PL plots.

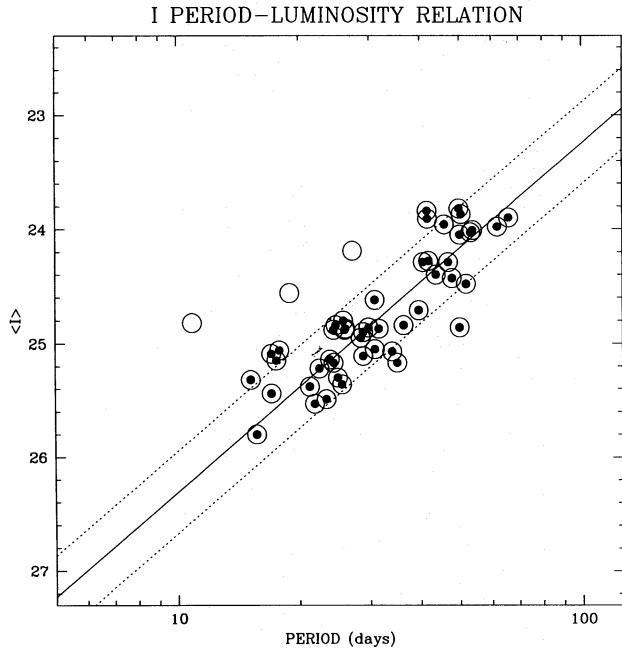


FIG. 8.— I PL relation for the sample of Cepheids listed in Table 5. For reasons discussed in the text, only the Cepheids with periods between 8 and 70 days are plotted. The solid line represents the best unweighted fit to the Cepheids with periods between 20 and 70 days, using phase weighted mean magnitudes, and corresponds to an apparent distance modulus of 31.18 ± 0.05 mag. The dashed lines, drawn at ± 0.36 mag, reflect the finite width of the Cepheids instability strip, and thus the expected intrinsic 2σ scatter around the best-fitting PL relation. The three points plotted as open circles mark outliers falling more than 4σ away from the mean, in either the V or the I PL plots.

TABLE 8
DISTANCE MODULI AND REDDENING

Sample (1)	Number (2)	rms _V (3)	rms _I (4)	μ_V (5)	μ_I (6)	μ (7)	d(Mpc) (8)	$E(B-V)$ (9)
ALL, $8 < P < 70$, P	50	0.42	0.37	31.21 ± 0.06	31.09 ± 0.05	30.93 ± 0.17	15.3 ± 1.3	0.09 ± 0.06
ALL, $20 < P < 70$, P	42	0.36	0.29	31.31 ± 0.06	31.18 ± 0.05	30.99 ± 0.17	15.8 ± 1.3	0.10 ± 0.06
ALL, $25 < P < 70$, P	33	0.37	0.31	31.29 ± 0.07	31.17 ± 0.05	30.99 ± 0.17	15.8 ± 1.3	0.09 ± 0.06
ALL, $30 < P < 70$, P	24	0.32	0.31	31.32 ± 0.06	31.20 ± 0.06	31.03 ± 0.17	16.0 ± 1.3	0.09 ± 0.06
ALL, $35 < P < 70$, P	20	0.31	0.33	31.29 ± 0.07	31.18 ± 0.07	31.01 ± 0.18	16.0 ± 1.3	0.08 ± 0.07
PC1, $20 < P < 70$, P	7	0.29	0.30	31.54 ± 0.11	31.43 ± 0.11	31.27 ± 0.19	18.0 ± 1.5	0.08 ± 0.11
WF2, $20 < P < 70$, P	12	0.47	0.36	31.26 ± 0.12	31.12 ± 0.09	30.91 ± 0.18	15.2 ± 1.3	0.11 ± 0.11
WF3, $20 < P < 70$, P	4	0.25	0.26	31.12 ± 0.11	30.98 ± 0.11	30.78 ± 0.19	14.3 ± 1.2	0.10 ± 0.11
WF4, $20 < P < 70$, P	19	0.29	0.19	31.29 ± 0.07	31.17 ± 0.04	30.98 ± 0.17	15.7 ± 1.3	0.10 ± 0.06
ALL, $20 < P < 70$, I	42	0.36	0.29	31.30 ± 0.06	31.18 ± 0.05	31.01 ± 0.17	15.9 ± 1.3	0.09 ± 0.06
ALL, $20 < P < 70$, P, σ^2	42	0.34	0.25	31.21 ± 0.08	31.14 ± 0.06	31.04 ± 0.17	16.1 ± 1.3	0.05 ± 0.08
ALL, $20 < P < 70$, P, χ^2	42	0.35	0.32	31.31 ± 0.08	31.20 ± 0.06	31.04 ± 0.18	16.2 ± 1.3	0.08 ± 0.08

NOTES.—The distance moduli and reddening derived from fitting PL relations to the sample of Cepheids listed in Table 5. Col. (1) describes the sample used in the fit, col. (2) the number of Cepheids in that particular sample. “ALL” refers to the sample of Cepheids drawn from all WFPC2 chips, “PC1,” “WF2,” “WF3,” and “WF4” refer to the samples of Cepheids divided into the four chips. In addition, the period range in which the fit was performed is noted; a “P” means that phase weighted mean magnitudes were used in the fits, while an “I” means that intensity averaged mean magnitudes were used. A χ^2 or σ^2 following the period range indicate, that the fits were weighted by $1/\chi^2$ or $1/\sigma^2$, respectively. The apparent distance moduli in V and I are reported in cols. (5) and (6). Col. (3) reports the rms for each fit, calculated for the M100 data alone, not for the M100 and LMC samples combined. The errors associated with the apparent distance moduli are derived from the fits themselves, as $\sigma/(n-1)^{1/2}$. The true distance modulus is listed in col. (7), and the associated error is discussed in § 7 and summarized in Table 9. The distance to M100 in megaparsecs is listed in col. (8), while the color excess $E(B-V)$ is reported in col. (9). The apparent distance moduli, dereddened distance, and color excess have been calculated assuming a dereddened modulus to the LMC $\mu_{LMC} = 18.50 \pm 0.10$ mag, a mean color excess to the LMC Cepheids $E(B-V) = 0.10$ mag, and adopting the extinction law given by Cardelli et al. 1989.

LMC, respectively, as

$$\begin{aligned}\mu^{M100} &= \Delta\mu_V + \mu^{LMC} + A^{LMC}(V) - A^{M100}(V) \\ &= \Delta\mu_I + \mu^{LMC} + A^{LMC}(I) - A^{M100}(I).\end{aligned}\quad (7)$$

Equations (6) and (7) can be used to express $A^{M100}(V)$ and $A^{M100}(I)$ as a function of R_V ; therefore, the absolute distance modulus to M100 is a function of R_V , R_V^{LMC} , $A^{LMC}(V)$, the absolute LMC distance modulus, and the apparent M100 distance moduli:

$$\begin{aligned}\mu^{M100} &= \frac{\Delta\mu_I - \Delta\mu_V[A^{M100}(I)/A^{M100}(V)]}{1 - A^{M100}(I)/A^{M100}(V)} \\ &\quad + \frac{0.59A^{LMC}(V)(1/R_V^{LMC} - 1/R_V)}{1 - A^{M100}(I)/A^{M100}(V)} + \mu^{LMC},\end{aligned}\quad (8)$$

and thus the unreddened distance modulus to M100 will in general depend on the absolute absorption $A^{LMC}(V)$ to the LMC [or on the reddening $E(B-V)$ to the LMC], unless R_V is the same for the LMC and M100. It is therefore rather unfortunate that the value of $E(B-V)$ for the LMC is still a subject of debate. According to Bessell (1991), the foreground (Galactic) reddening to the LMC ranges between $0.04 < E(B-V) < 0.09$ mag, while the mean internal reddening is 0.06 mag but highly variable with position, reaching values as high as 0.3 mag in some regions. The problem is further complicated by the fact that the intrinsic colors of Cepheids may be affected by metallicity, as will be discussed later on in this section.

In Table 8, we have calculated the dereddened distance modulus, color excess $E(B-V)$, and the distance to M100 in megaparsecs, assuming $R_V = R_V^{LMC} = 3.30$. If $R_V = 3.10$ is used, assuming $E(B-V) \sim 0.12$ mag for the LMC, the true distance modulus is 0.01 mag larger than the value obtained for $R_V = 3.30$, for typical values of the apparent distance moduli.

Since incompleteness is important for Cepheids with

periods less than 20 days but is not an issue for Cepheids with larger periods, as discussed in § 6, we adopt for the distance modulus to M100 the value derived from the unweighted fit to the entire sample of Cepheids with periods larger than 20 days, using phase weighted mean magnitudes: $\mu_0 = 30.99 \pm 0.17$ mag, which corresponds to a distance $d = 15.8 \pm 1.3$ Mpc. The distance moduli derived from the same sample but using a weighted fit and/or intensity averaged magnitudes are virtually identical to the value just quoted, since all the Cepheids have very well defined light curves with nearly uniform phase coverage. The derived distance of 15.8 Mpc agrees to within 1σ but is 8% lower than the preliminary result derived by Freedman et al. (1994c) from the same HST observations presented in this paper, but from a smaller (20 instead of 52 with $20 < P < 70$ days) sample of Cepheids; the reasons for this difference are discussed in § 8.

The error budget in the determination of the true distance modulus is given in Table 9. Each source of error has already been discussed in the previous sections, and a brief summary is presented below. Errors on the V and I magnitudes, for both DoPHOT and DAOPHOT, are due to three independent factors: uncertainties in the V and I zero points (Hill et al. 1996), internal reported errors on the DoPHOT and DAOPHOT magnitudes (Hill et al. 1996), and errors introduced by the charge transfer effect (§ 2). Since these three sources of error are uncorrelated, they can be added in quadrature to give the final errors on the V and I magnitudes, which amount to ± 0.06 in both V and I . Since the samples of stars used in determining the V and I apparent moduli are identical, the propagation of their random photometric errors into the error on the true modulus is straightforward: In the dereddening process, these errors are to be combined in quadrature, weighted by the extinction coefficients as given in the formula in Table 9. However, much of the scatter in the individual PL relations is highly correlated (as opposed to the errors in the individual data points, which are largely uncorrelated), where the

TABLE 9
ERROR BUDGET IN THE M100 DISTANCE

Source of Uncertainty	Random Errors	Systematic Errors	Notes
WFPC2 <i>V</i> -band zero point = <i>a</i>	±0.04	...	
WFPC2 <i>I</i> -band zero point = <i>b</i>	±0.04	...	
Error in the <i>V</i> photometry = <i>c</i>	±0.04	...	
Error in the <i>I</i> photometry = <i>d</i>	±0.05	...	
Charge transfer efficiency = <i>e</i>	±0.01	...	
Cumulative error on <i>V</i> magnitudes: $\sqrt{a^2 + c^2 + e^2} = A$	±0.06	...	1
Cumulative error on <i>I</i> magnitudes: $\sqrt{b^2 + d^2 + e^2} = B$	±0.06	...	1
Error on true distance modulus due to <i>A</i> and <i>B</i> : $\sqrt{A^2 \times (1 - R)^2 + B^2 \times R^2}$	±0.17	...	2
Uncertainty in the <i>I</i> -band distance modulus due to metallicity	±0.05	
LMC distance modulus	±0.10	
Uncertainty in LMC + M100 absorption	±0.02	

NOTES.—The error budget in the determination of the true distance modulus. (1) the errors are uncorrelated and therefore summed in quadrature. (2) *R* is defined as $A(V)/E(V-I) = 2.47$, according to the extinction law by Cardelli et al. 1989. The expression for the error is derived from eq. (8), assuming that the errors are uncorrelated.

wavelength-correlated scatter is due to intrinsic color and differential reddening differences from star to star. Several systematic errors also come into play and are listed in Table 9: uncertainties due to metallicity effects (discussed in more detail below), uncertainty in the LMC distance modulus (§ 6), and uncertainty in the LMC+M100 absorption, which we estimate to be ±0.02 mag.

The average total color excess $E(B-V)$ to M100 varies between 0.08 and 0.11 mag, depending on the sample used: a representative value being $E(B-V) = 0.10 \pm 0.06$ mag, derived from the weighted fit to the complete sample for $20 < P < 70$ days, using phase weighted magnitudes. Burstein & Heiles (1984) find $E(B-V) = 0.01$ mag for the Galactic foreground extinction along the line of sight of M100. Given the range of $E(B-V)$ values found for the total color excess to M100, it is clear that most of the measured reddening is intrinsic to M100 itself, although the uncertainty in this estimate remains large.

One systematic effect that may be significant in the determination of the distance modulus is the possible metallicity dependence of the PL relation. Our field in M100 is considerably more metal rich than the LMC sample of calibrating Cepheids. Measurements of H II region abundances in M100 by Zaritsky, Kennicutt, & Huchra (1994) and Skillman et al. (1996) give an oxygen abundance range for our field of $\log_{10}(O/H) = -2.75 \pm 0.2$, including the radial variation in abundance across the field. The H II regions in the LMC have a mean abundance $\log_{10}(O/H) = -3.65 \pm 0.1$ (Dufour 1990), which implies that the M100 Cepheids are about 8 times more metal rich than the LMC calibrating Cepheids. According to the theoretical calculations of Chiosi, Wood, & Capitanio (1993), the effect of this metallicity difference on the *I*-band Cepheid distance modulus should be small, $\ll 0.1$ mag, and this is consistent with an empirical test of the metallicity dependence of the PL relation by Freedman & Madore (1990). However, it would be reassuring to confirm this result by comparing Cepheid moduli across a galaxy spanning a comparable range in abundance as observed between M100 and the LMC. We are performing such a test by measuring two fields in the nearby Sc galaxy M101 (Kelson et al. 1996; Stetson et al. 1996).

In this closing portion of this section, we discuss the

scatter found in the two PL relations. First, we note that much of the residual scatter is correlated between the two bandpasses. Differential reddening, intrinsic positioning within the finite width of instability strip, and/or (nonrandom) photometric errors will all potentially contribute to these types of residuals. However, we point out that the rms scatter calculated for the M100 Cepheids about the mean *V* and the *I* PL relations is somewhat larger (± 0.36 mag in *V* and ± 0.29 mag in *I*) than the scatter observed for the Cepheids in the LMC calibrating sample (where $\sigma_V = \pm 0.27$ mag and $\sigma_I = \pm 0.18$ mag). Reddening and strip position are well understood; indeed, they are very nearly degenerate in their effect on the correlation of residuals: The intrinsic strip widths in the LMC sample have a *V*:*I* ratio of 1.00:0.67, while the ratio of A_V/A_I is 1.00:0.58.

Figure 9 shows a plot of the *I*-band PL relation residuals for the M100 Cepheids plotted against the *V*-band residuals. The heavy solid line shows the slope and full width of the expected correlation of data points if due to intrinsic strip-width (temperature) effects. The dotted line shows the closely degenerate reddening trajectory. The open circles to the lower left of the diagram are the bright (blue) outliers sitting approximately 4σ away from their respective ridge lines. Excluding these outliers, there is now good agreement between the data and the expected width and slope of the residual correlations. Small amounts of differential reddening could only extend the correlation (along the dotted line) but could not increase the vertical scatter. This remaining scatter in the plot is most likely a result of irreducible and uncorrelated photometric errors amounting to ±0.13 mag (if equally assigned to both the *V* and *I* magnitudes).

8. CONCLUSIONS

We have derived a new Cepheid distance to the Virgo galaxy M100 based on *V* and *I* band *HST*/WFPC2 observations. Photometry for all the stars in the field has been performed independently using a variant of the DoPHOT program (Schechter et al. 1993) and the DAOPHOT II/ALLFRAME package (Stetson 1994). The two sets of photometry agree to within 0.05 mag, with the exception of WF3 and the *I* data for WF4, for which the agreement is

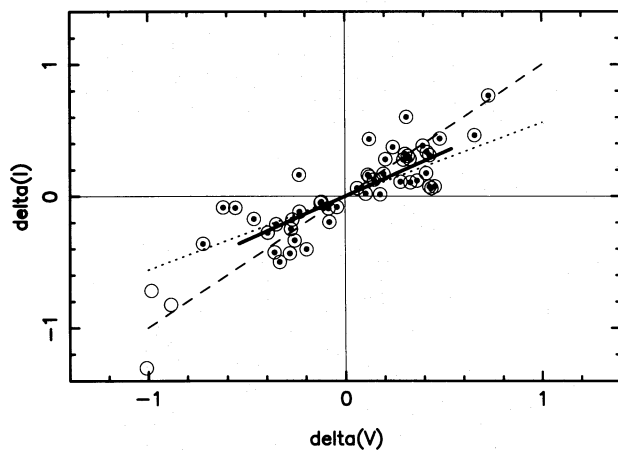


FIG. 9.—Magnitude residuals in I vs. magnitude residuals in V from the corresponding PL relations for Cepheids in M100. Open circles mark outliers falling more than 4σ away from the mean, well outside of the known limits of the intrinsic Cepheid instability strip, which is shown by the heavy solid line. The correlation expected due to differential reddening is shown by the dotted line. The dashed line is a fit to the observed data. The various solutions are statistically indistinguishable.

within 0.09–0.15 mag (Hill et al. 1996). A total of 52 Cepheids have been found in common between the DoPHOT and DAOPHOT samples. For the common Cepheids, excellent agreement in period and good agreement in the mean magnitudes have been found. In order to obtain apparent V and I distance moduli to M100, we compared the M100 sample with the LMC sample defined in Madore (1985) and performed a least-squares fit to the combined sample, constraining the slope of the PL relation to the value derived from a fit to the LMC sample alone (Madore & Freedman 1991) in order to avoid possible biases due to incompleteness in the M100 sample at faint magnitudes. An extinction correction has been applied by fitting the apparent V and I distance moduli to the extinction law given by Cardelli et al. (1989). Both by inspecting the PL relation and by fitting PL relations to samples with increasingly higher period cutoffs, it appears evident that the sample of Cepheids with periods less than 20 days is incomplete. From a fit to all Cepheids in common between the DoPHOT and DAOPHOT samples with periods larger than 20 days, a distance modulus $\mu_0 = 30.99 \pm 0.17$ mag is derived, corresponding to a distance $d = 15.8 \pm 1.3$ Mpc. The total (Galactic plus intrinsic) color excess of M100 is $E(B-V) = 0.10 \pm 0.06$ mag.

The determination of the distance to a Virgo cluster galaxy can be used in estimating the Hubble constant; the problem has already been addressed in detail by Freedman et al. (1994c) and Mould et al. (1996), to which we refer for a complete discussion. Here, we will just note that, for a Virgo cosmic velocity of 1396 ± 96 km s $^{-1}$ (Huchra 1995), a distance of 15.8 Mpc of M100 corresponds to a Hubble constant of 88 ± 24 km s $^{-1}$ Mpc $^{-1}$. The error on the Hubble constant is calculated as in Freedman et al. (1994c); since we use only a single galaxy to estimate the distance to an extended cluster, a conservative uncertainty of 20% in the mean distance to Virgo has been adopted. An alternative approach to determining the Hubble constant makes use of the well-known relative distance between the Virgo and the Coma cluster, therefore avoiding the use of the Virgo cluster recession velocity. Adopting a mean relative Coma-Virgo distance modulus of 3.71 ± 0.10 mag (van den Bergh 1992; de Vaucouleurs 1993), a distance of 15.8 Mpc to Virgo yields a distance to the Coma cluster of 87 Mpc. For a Coma recession velocity of 7200 ± 100 km s $^{-1}$ (Aaronson et al. 1986; Fukugita et al. 1991; Jergen & Tammann 1993), the corresponding value for the Hubble constant is then 83 ± 16 km s $^{-1}$ Mpc $^{-1}$, well in agreement with the value quoted above derived using the Virgo cluster velocity.

The distance modulus to M100 derived in this paper is 0.17 mag lower (or the distance is 8% lower) than the value of 31.16 ± 0.20 mag reported by Freedman et al. (1994c). The two values are consistent within the errors; however, the distance derived in this paper supersedes the Freedman et al. (1994c) value: The sample of Cepheids used in this paper is much larger (42 Cepheids with $20 < P < 70$ days against 20 Cepheids), and, in addition, since the Freedman et al. (1994c) paper was published, more accurate WFPC2 zero points have become available, and considerable improvements have been made to the programs used to obtain the photometry.

Previously published distances to M100 range from 11.8 Mpc (de Vaucouleurs 1982) to 27.7 Mpc (Sandage 1993) and are summarized in Table 10. The Cepheid distance of 15.8 Mpc found in this paper falls toward the lower end of the range, and it agrees very well with the distance derived by applying the EPM to the Type II supernova SN 1979C (15 ± 4 Mpc, Schmidt et al. 1994) and with the distance based on the Tully-Fisher relation reported by Pierce (1994) (14.5 ± 2.7 Mpc). The distance to M100 derived in this paper is also in agreement with the only other Cepheid distance available for a Virgo galaxy, NGC 4571, for which Pierce et al. (1994) estimated a distance of 14.1 Mpc.

TABLE 10
SUMMARY OF DISTANCE DETERMINATIONS TO M100

Distance (Mpc)	Method	Reference
11.8	Tertiary indicators	de Vaucouleurs 1982
14.5 ± 1.1	Tully-Fisher relation	Pierce 1994
15 ± 4	EPM applied to SN 1979C	Schmidt et al. 1994
15.8 ± 1.7	Cepheids	this paper
17.1 ± 1.8	Cepheids	Freedman et al. 1994c
18.4 ± 2.2	Tully-Fisher relation	Pierce & Tully 1988
23 ± 3	Baade method applied to SN 1979C	Branch et al. 1981
27.7 ± 2.8	M100/M101 diameter comparison	Sandage 1993

NOTES.—Estimates of the distance to M100 found in the literature. The Cepheid distance of 15.8 Mpc found in this paper falls toward the lower end of the range, and it agrees very well with the distance derived by applying the EPM to the Type II supernova SN 1979C, and with the distance based on the Tully-Fisher relation.

APPENDIX

THE DoPHOT AND DAOPHOT PL RELATIONS

The selection of a sample of Cepheids common to both the DoPHOT and DAOPHOT samples makes the derivation of the distance modulus and reddening less sensitive to incorrect determinations in the periods and small (about 0.1 mag) systematic errors in the photometry (larger errors are already excluded, see Hill et al. 1996). However, in choosing a common sample, we

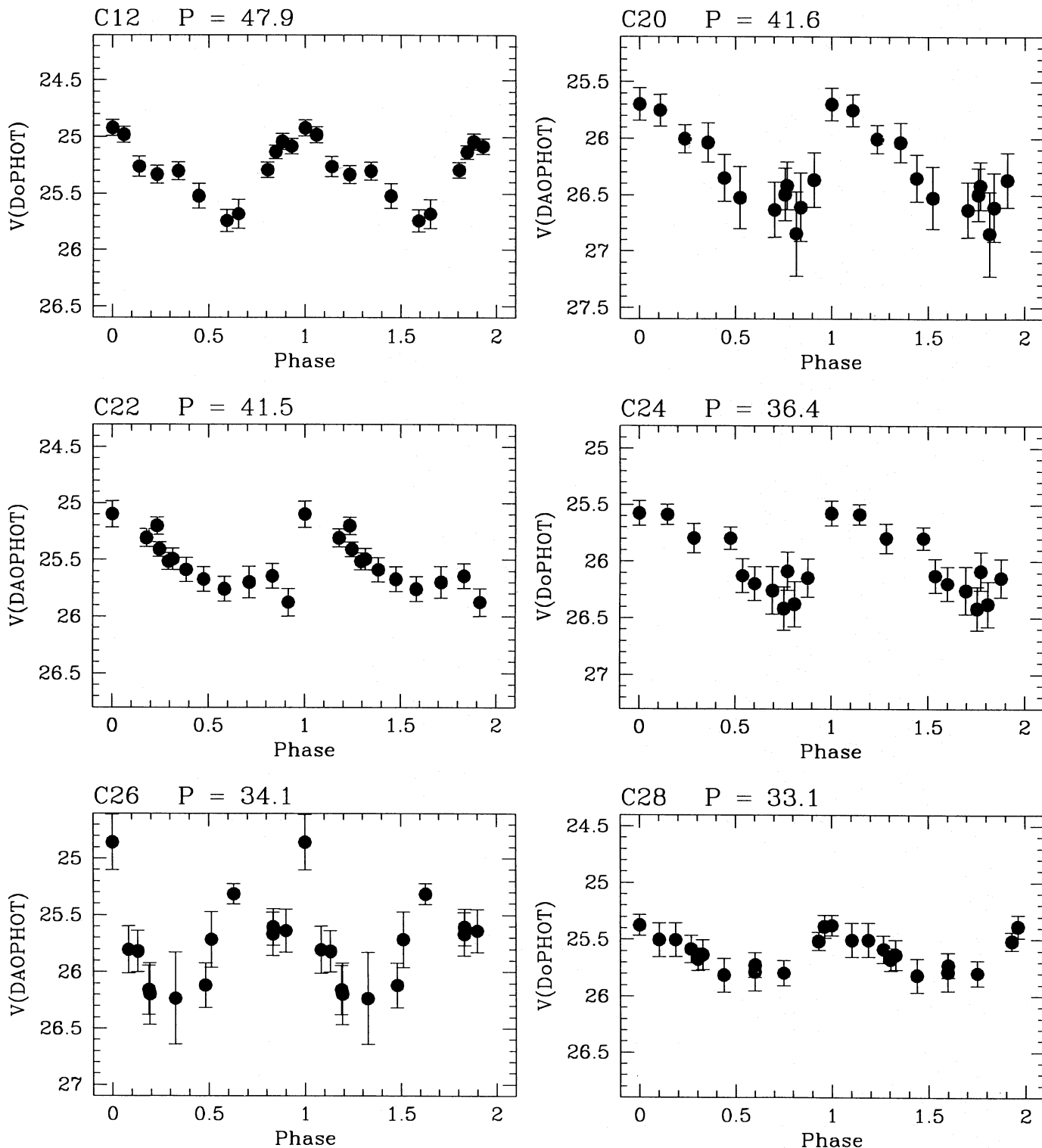


FIG. 11a

FIG. 11.—(a–c) Light curves for the Cepheids that were identified by only one of the two photometry packages. Variables in the plots are labeled with their identification numbers and periods, as in Table 3.

exclude objects that are, without any doubt, Cepheid variables but were not detected by one of the two methods because they fall just short of the selection criteria imposed on the data. In Figures 10a–10c (Plates 30–32), we show the finding charts for the Cepheids that were identified by only one of two packages. Figures 11a–11c show the light curves, while the V and I photometry is given in Tables 11 and 12, respectively.

Both the DoPHOT and DAOPHOT samples are larger than the common sample; to make sure that the distance modulus is not sensitive to small changes in the selection criteria adopted for the Cepheids, we fitted PL relations separately for the DoPHOT and DAOPHOT samples, following the procedure outlined in §§ 7 and 8. Neither C26 nor C44 (Table 3) were used in fitting the DoPHOT PL relation, for the reasons discussed at the end of § 4.3. Again, we found that the result is insensitive to the use of either intensity averaged or phase weighted magnitudes, and is insensitive to whether the fit is unweighted or

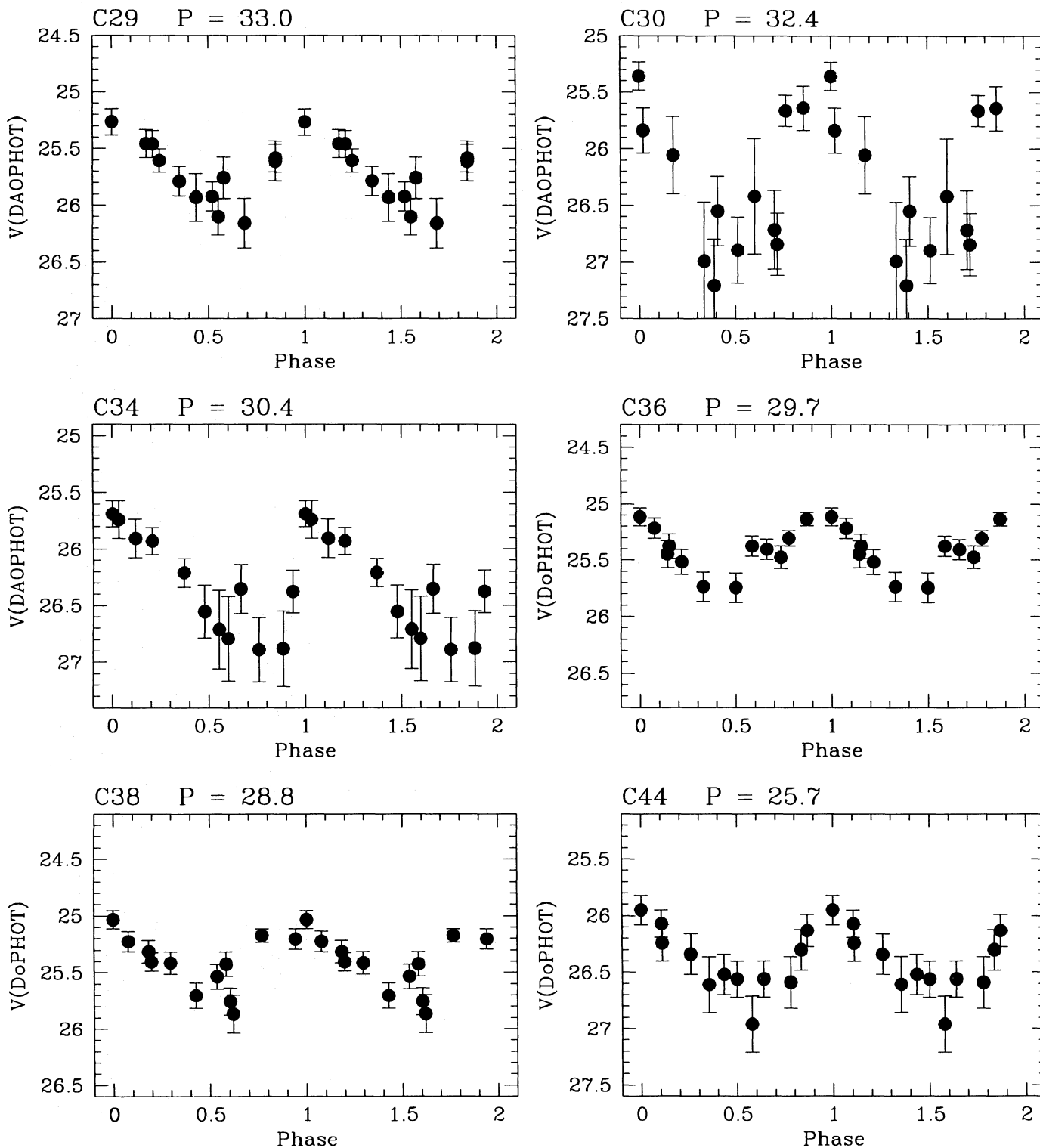


FIG. 11b

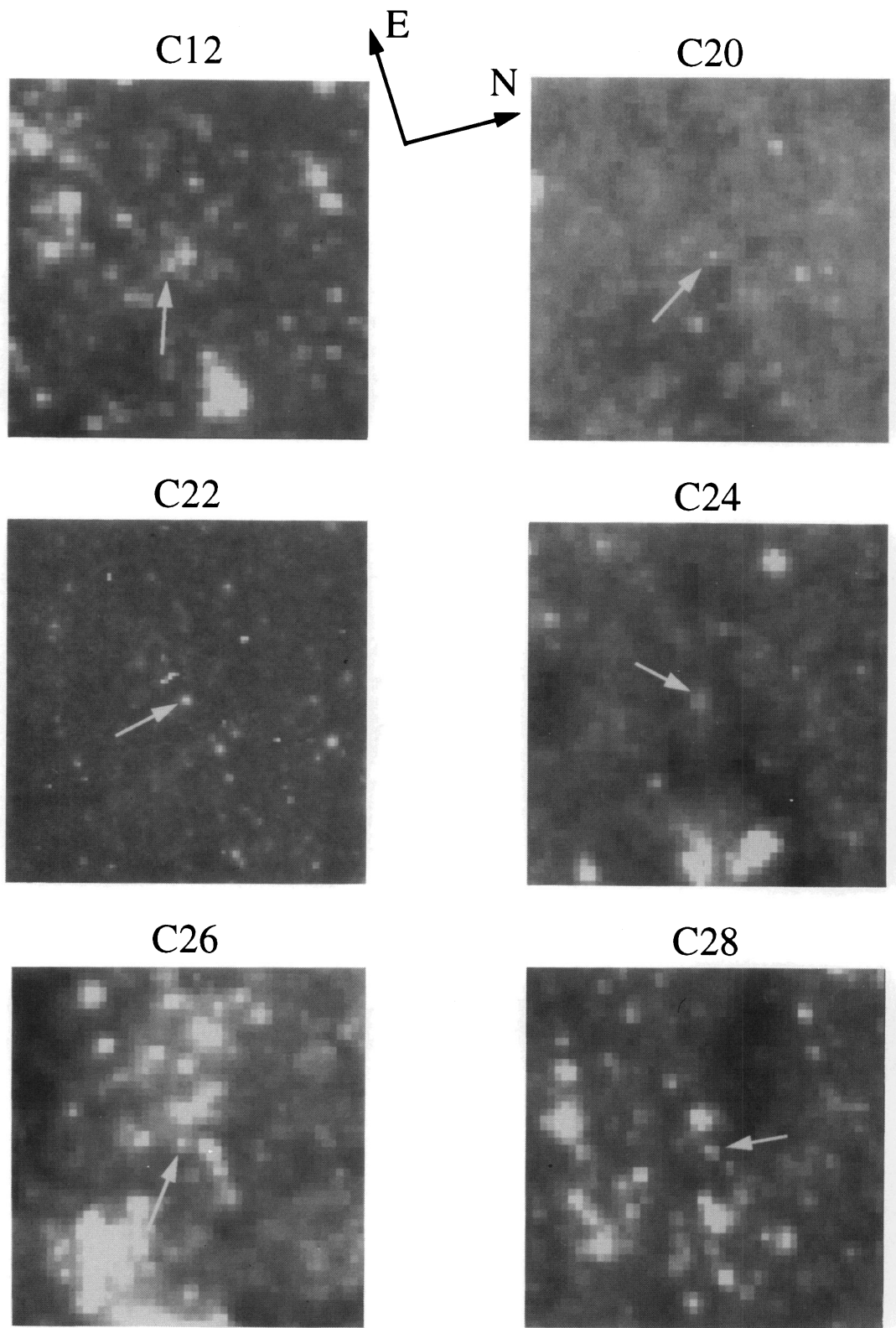


FIG. 10a

FIG. 10.—(a-c) Finding charts for the variable stars that were identified by only one of the two photometry packages. Each finding chart covers a region $4'' \times 4''$ and is oriented as the chips in Figs. 3a-3d. The arrow marks the position of the Cepheid.

FERRARESE et al. (see 464, 595)

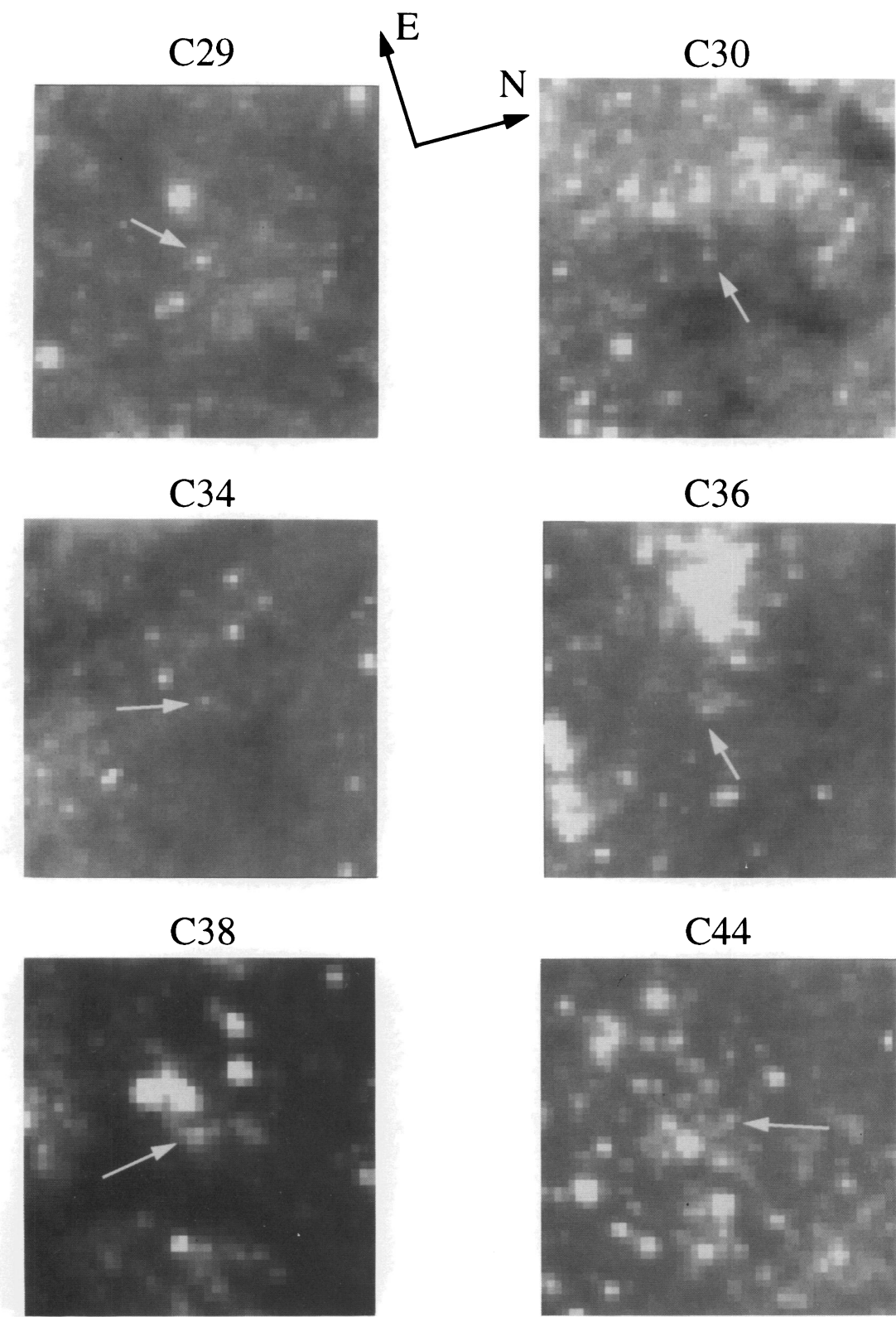


FIG. 10b

FERRARESE et al. (see 464, 595)

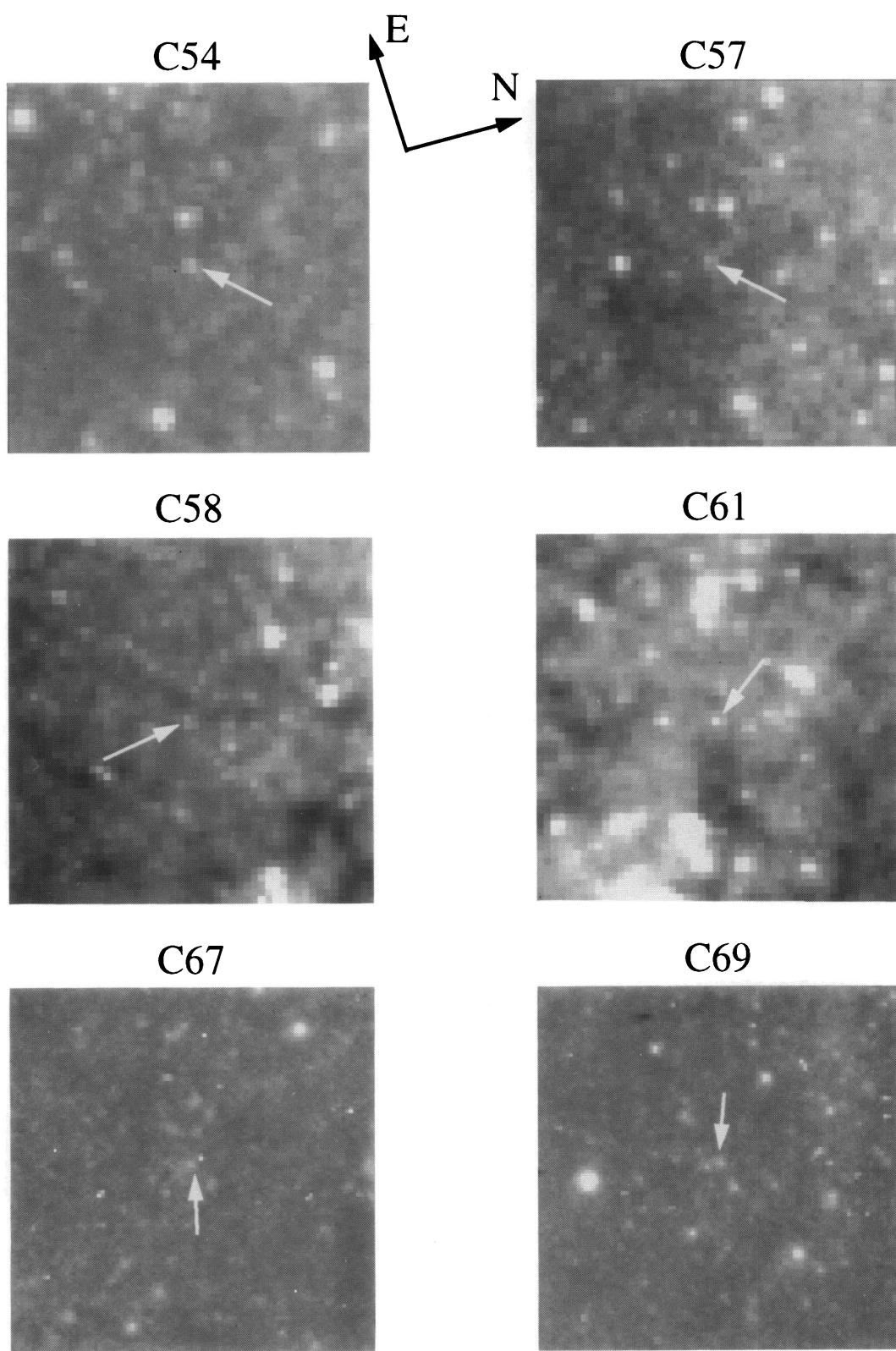


FIG. 10c

FERRARESE et al. (see 464, 595)

weighted on $1/\chi^2$ for DoPHOT, or on $1/\sigma^2$ for DAOPHOT. Also, analogous to what we found when fitting the common sample, a magnitude incompleteness is present for Cepheids with periods shorter than 20 days. In the period range between 20 and 70 days, the unweighted fits to the phase weighted magnitudes yield a true distance modulus $\mu_0 = 30.95 \pm 0.23$ mag (corresponding to a distance $d = 15.5 \pm 1.6$ Mpc) and a reddening $E(B-V) = 0.10 \pm 0.08$ mag for the DoPHOT sample, and a true distance modulus $\mu_0 = 30.96 \pm 0.23$ mag (corresponding to a distance $d = 15.6 \pm 1.6$ Mpc) and a reddening $E(B-V) = 0.11 \pm 0.08$ mag for the DAOPHOT sample. These results are in full agreement with each other and with the results derived from the common sample ($\mu_0 = 30.99 \pm 0.17$ mag, $E(B-V) = 0.10 \pm 0.06$ mag). In Figure 12, we plot the V and I PL relations for both the DoPHOT and DAOPHOT samples.

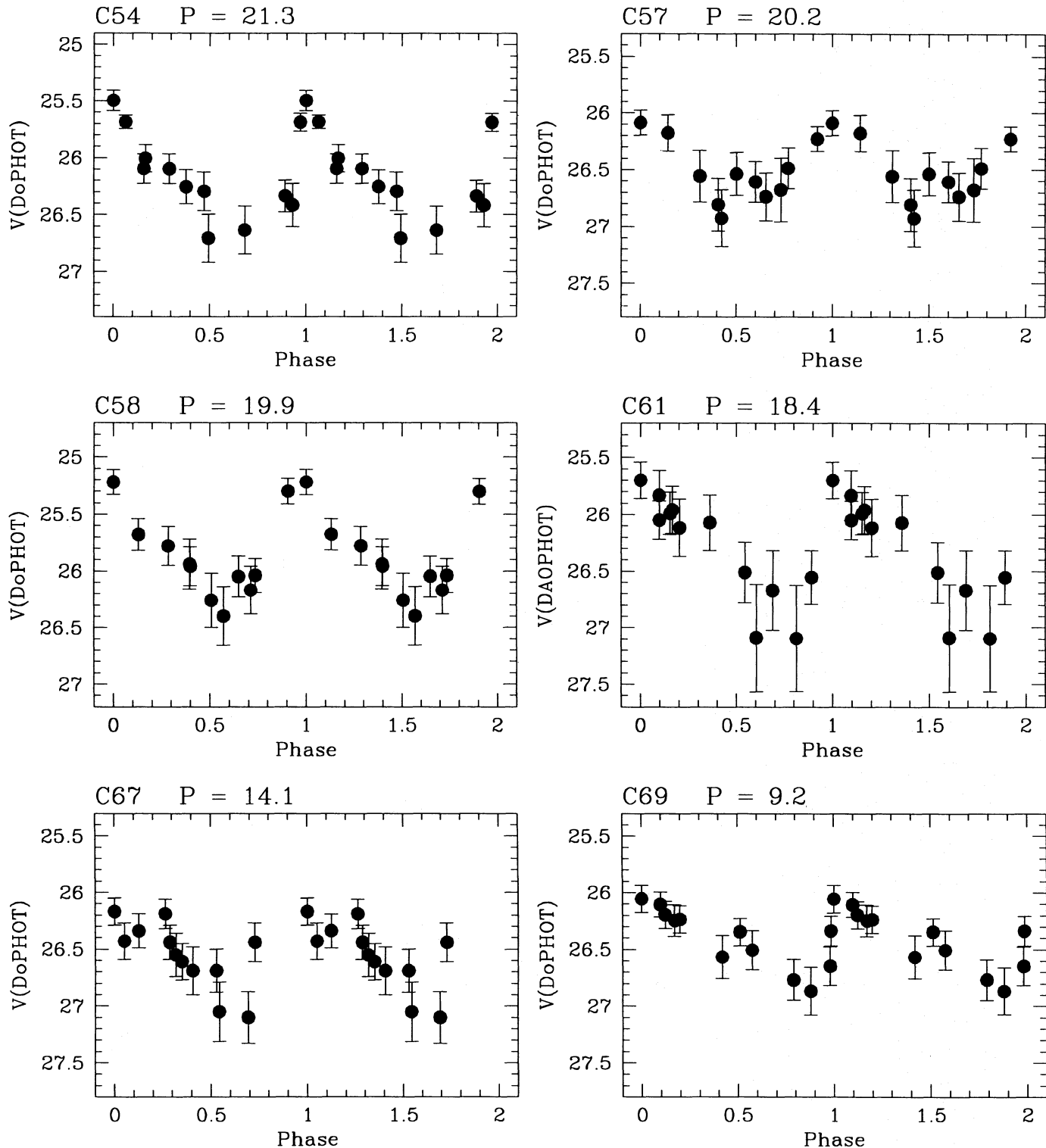


FIG. 11c

TABLE 11
 V PHOTOMETRY

JD	$V \pm \Delta V$						
	C12 $P = 47.9$	C20 $P = 41.6$	C22 $P = 41.5$	C24 $P = 36.4$	C26 $P = 34.1$	C28 $P = 33.1$	C29 $P = 33.0$
2449465.78	25.68 \pm 0.13	26.63 \pm 0.24	25.31 \pm 0.08	25.45 \pm 0.12	...	25.72 \pm 0.11	25.67 \pm 0.19
2449476.71	25.04 \pm 0.07	26.35 \pm 0.21	25.88 \pm 0.12	25.61 \pm 0.18	26.13 \pm 0.15	25.51 \pm 0.08	25.71 \pm 0.24
2449478.99	25.08 \pm 0.07	26.49 \pm 0.23	25.20 \pm 0.08	25.60 \pm 0.10	26.20 \pm 0.15	25.37 \pm 0.09	25.64 \pm 0.19
2449482.40	24.92 \pm 0.07	26.61 \pm 0.30	25.49 \pm 0.09	25.79 \pm 0.13	26.26 \pm 0.21	25.50 \pm 0.15	24.86 \pm 0.25
2449485.22	24.98 \pm 0.07	26.37 \pm 0.24	25.59 \pm 0.11	25.93 \pm 0.21	26.09 \pm 0.17	25.50 \pm 0.15	25.80 \pm 0.21
2449489.04	25.26 \pm 0.09	25.70 \pm 0.14	25.67 \pm 0.11	26.10 \pm 0.16	26.15 \pm 0.17	25.67 \pm 0.10	26.19 \pm 0.27
2449493.53	25.33 \pm 0.08	25.75 \pm 0.14	25.76 \pm 0.11	26.16 \pm 0.22	25.58 \pm 0.11	25.81 \pm 0.15	26.23 \pm 0.41
2449498.82	25.30 \pm 0.08	26.00 \pm 0.12	25.70 \pm 0.14	25.59 \pm 0.12	25.59 \pm 0.09	25.78 \pm 0.17	26.12 \pm 0.20
2449503.85	25.52 \pm 0.11	26.04 \pm 0.17	25.64 \pm 0.11	25.27 \pm 0.12	25.80 \pm 0.13	25.79 \pm 0.11	25.32 \pm 0.09
2449510.82	25.74 \pm 0.10	26.52 \pm 0.28	25.10 \pm 0.12	25.46 \pm 0.12	25.80 \pm 0.10	25.38 \pm 0.10	25.61 \pm 0.16
2449520.95	25.29 \pm 0.07	26.42 \pm 0.21	25.41 \pm 0.07	25.92 \pm 0.13	26.42 \pm 0.19	25.58 \pm 0.12	25.82 \pm 0.18
2449522.96	25.13 \pm 0.06	26.84 \pm 0.38	25.51 \pm 0.08	25.76 \pm 0.18	26.38 \pm 0.20	25.63 \pm 0.13	26.16 \pm 0.22

JD	$V \pm \Delta V$						
	C30 $P = 32.4$	C34 $P = 30.4$	C36 $P = 29.7$	C38 $P = 28.8$	C44 $P = 25.7$	C54 $P = 21.3$	C57 $P = 20.2$
2449465.78	26.99 \pm 0.52	26.55 \pm 0.23	25.51 \pm 0.11	25.86 \pm 0.17	26.58 \pm 0.25	26.26 \pm 0.15	26.49 \pm 0.18
2449476.71	25.36 \pm 0.13	25.91 \pm 0.17	25.37 \pm 0.09	25.03 \pm 0.08	26.56 \pm 0.23	26.34 \pm 0.14	26.56 \pm 0.23
2449478.99	26.55 \pm 0.30	26.71 \pm 0.35	25.40 \pm 0.09	25.22 \pm 0.09	26.10 \pm 0.14	25.50 \pm 0.09	26.93 \pm 0.25
2449482.40	26.89 \pm 0.29	26.35 \pm 0.22	25.30 \pm 0.07	25.40 \pm 0.08	25.92 \pm 0.13	26.10 \pm 0.13	...
2449485.22	26.42 \pm 0.51	26.89 \pm 0.28	25.13 \pm 0.06	25.41 \pm 0.10	26.21 \pm 0.16	26.10 \pm 0.13	26.68 \pm 0.28
2449489.04	26.84 \pm 0.27	26.88 \pm 0.33	25.11 \pm 0.08	25.70 \pm 0.11	26.31 \pm 0.18	26.30 \pm 0.17	26.23 \pm 0.11
2449493.53	25.64 \pm 0.20	25.74 \pm 0.17	25.37 \pm 0.11	25.42 \pm 0.11	26.49 \pm 0.18	26.64 \pm 0.21	26.18 \pm 0.16
2449498.82	25.84 \pm 0.20	25.93 \pm 0.12	25.73 \pm 0.13	25.17 \pm 0.06	26.53 \pm 0.16	26.42 \pm 0.19	26.81 \pm 0.23
2449503.85	26.06 \pm 0.34	26.21 \pm 0.13	25.74 \pm 0.13	25.20 \pm 0.09	26.27 \pm 0.18	26.01 \pm 0.12	26.74 \pm 0.21
2449510.82	27.21 \pm 0.41	26.79 \pm 0.37	25.47 \pm 0.10	25.31 \pm 0.10	26.04 \pm 0.12	26.71 \pm 0.21	26.09 \pm 0.11
2449520.95	26.71 \pm 0.35	26.38 \pm 0.19	25.21 \pm 0.09	25.53 \pm 0.11	26.53 \pm 0.16	25.69 \pm 0.08	26.54 \pm 0.19
2449522.96	25.66 \pm 0.14	25.69 \pm 0.12	25.44 \pm 0.12	25.75 \pm 0.12	26.93 \pm 0.25	25.69 \pm 0.06	26.61 \pm 0.18

JD	$V \pm \Delta V$			
	C58 $P = 19.9$	C61 $P = 18.4$	C67 $P = 14.1$	C69 $P = 9.2$
2449465.78	26.04 \pm 0.15	26.67 \pm 0.35	26.61 \pm 0.16	26.34 \pm 0.13
2449476.71	25.78 \pm 0.17	25.83 \pm 0.22	26.34 \pm 0.15	26.25 \pm 0.14
2449478.99	25.96 \pm 0.17	27.10 \pm 0.47	26.44 \pm 0.15	26.57 \pm 0.19
2449482.40	26.40 \pm 0.26	25.70 \pm 0.16	26.69 \pm 0.19	26.77 \pm 0.18
2449485.22	26.17 \pm 0.21	25.99 \pm 0.18	26.44 \pm 0.17	26.11 \pm 0.11
2449489.04	25.30 \pm 0.11	26.07 \pm 0.24	26.17 \pm 0.12	26.35 \pm 0.12
2449493.53	25.68 \pm 0.14	27.09 \pm 0.47	26.55 \pm 0.19	26.06 \pm 0.12
2449498.82	25.94 \pm 0.22	26.55 \pm 0.24	27.10 \pm 0.23	26.51 \pm 0.17
2449503.85	26.05 \pm 0.18	25.96 \pm 0.21	26.43 \pm 0.16	26.20 \pm 0.12
2449510.82	25.22 \pm 0.11	26.51 \pm 0.27	27.05 \pm 0.26	26.87 \pm 0.21
2449520.95	26.26 \pm 0.24	26.05 \pm 0.17	26.19 \pm 0.13	26.65 \pm 0.17
2449522.96	...	26.12 \pm 0.25	26.69 \pm 0.21	26.24 \pm 0.12

NOTE.—The V photometry for the Cepheids that were identified by only one of the two photometry programs.

Note added in manuscript (1995 September 8).—In the past few months, increasing evidence has been accumulating that leads to the conclusion that the WFPC2 photometric zero points depend on the exposure time of the frame under analysis (Hill et al. 1996). At this time, the effect of changing exposure times on the zero points has not been quantified precisely by the WFPC2 IDT for lack of suitable calibration data and more complete analysis of the problem will likely have to wait for at least another year. However, independent analysis of the data available so far by two of us (P. B. S. and A. S.) and by J. Holtzmann (1995, private communication) leads to the unanimous conclusion that the zero points for frames with exposure time longer than 1200 s, both in V and I and in all four chips, are 0.050 ± 0.007 mag higher than the zero points for shorter exposure times.

Consistent with other recent papers in this series, we are therefore adopting the long-exposure zero points for the M100 frames, all of which were exposed for longer than 1200 s. A 0.05 change in the zero points, in both V and I , brings the distance modulus from 30.99 ± 0.17 to 31.04 ± 0.17 mag, and the distance to M100 from 15.8 ± 1.3 to 16.1 ± 1.3 Mpc. We note that these changes are well within the uncertainty in the distance determinations.

We wish to thank the Director of the Space Telescope Science Institute, Bob Williams, for permission to reschedule the M100 observations, and Doug Van Orsow for his capable help with the scheduling and observing. Many thanks are also due to Jon Holtzman for providing essential information and advice in handling the WFPC2 data. R. Peletier kindly made available the ground-based image of M100 shown in Figure 1. Support for this work was provided by NASA through grant

TABLE 12
I PHOTOMETRY

JD	<i>I</i> ± Δ <i>I</i>						
	C12 <i>P</i> = 47.9	C20 <i>P</i> = 41.6	C22 <i>P</i> = 41.5	C24 <i>P</i> = 36.4	C26 <i>P</i> = 34.1	C28 <i>P</i> = 33.1	C29 <i>P</i> = 33.0
2449465.91	24.06 ± 0.07	24.42 ± 0.10	24.72 ± 0.08	24.86 ± 0.08	...	24.96 ± 0.16	24.43 ± 0.09
2449485.35	23.93 ± 0.07	24.25 ± 0.12	25.13 ± 0.19	24.64 ± 0.09	...	24.85 ± 0.11	24.37 ± 0.08
2449510.81	23.88 ± 0.05	24.51 ± 0.12	24.62 ± 0.07	24.63 ± 0.08	24.60 ± 0.19	24.49 ± 0.10	24.18 ± 0.07
2449523.09	23.87 ± 0.06	24.22 ± 0.10	24.68 ± 0.09	24.40 ± 0.11	25.00 ± 0.23	24.76 ± 0.12	24.12 ± 0.07
<i>I</i> ± Δ <i>I</i>							
JD	C30 <i>P</i> = 32.4	C34 <i>P</i> = 30.4	C36 <i>P</i> = 29.7	C38 <i>P</i> = 28.8	C44 <i>P</i> = 25.7	C54 <i>P</i> = 21.3	C57 <i>P</i> = 20.2
2449465.91	24.91 ± 0.15	24.77 ± 0.17	24.75 ± 0.13	24.62 ± 0.09	...	24.90 ± 0.10	25.04 ± 0.16
2449485.35	24.68 ± 0.09	24.85 ± 0.15	24.62 ± 0.12	24.48 ± 0.09	25.47 ± 0.19	24.90 ± 0.11	25.27 ± 0.18
2449510.81	26.02 ± 0.34	25.31 ± 0.27	24.79 ± 0.15	24.41 ± 0.09	...	25.17 ± 0.15	25.18 ± 0.16
2449523.09	25.62 ± 0.40	25.49 ± 0.17	25.25 ± 0.23	24.49 ± 0.10	...	25.07 ± 0.13	25.19 ± 0.19
<i>I</i> ± Δ <i>I</i>							
JD	C58 <i>P</i> = 19.9	C61 <i>P</i> = 18.4	C67 <i>P</i> = 14.1	C69 <i>P</i> = 9.2			
2449465.91	25.33 ± 0.23	25.00 ± 0.14	25.31 ± 0.19	25.98 ± 0.25			
2449485.35	25.33 ± 0.25	25.05 ± 0.14	25.20 ± 0.15	25.91 ± 0.24			
2449510.81	25.06 ± 0.18	24.69 ± 0.13	25.63 ± 0.23	25.58 ± 0.15			
2449523.09	25.48 ± 0.28	25.62 ± 0.21	25.22 ± 0.13	25.96 ± 0.22			

NOTE.—The *I* photometry for the Cepheids that were identified by only one of the two photometry programs.

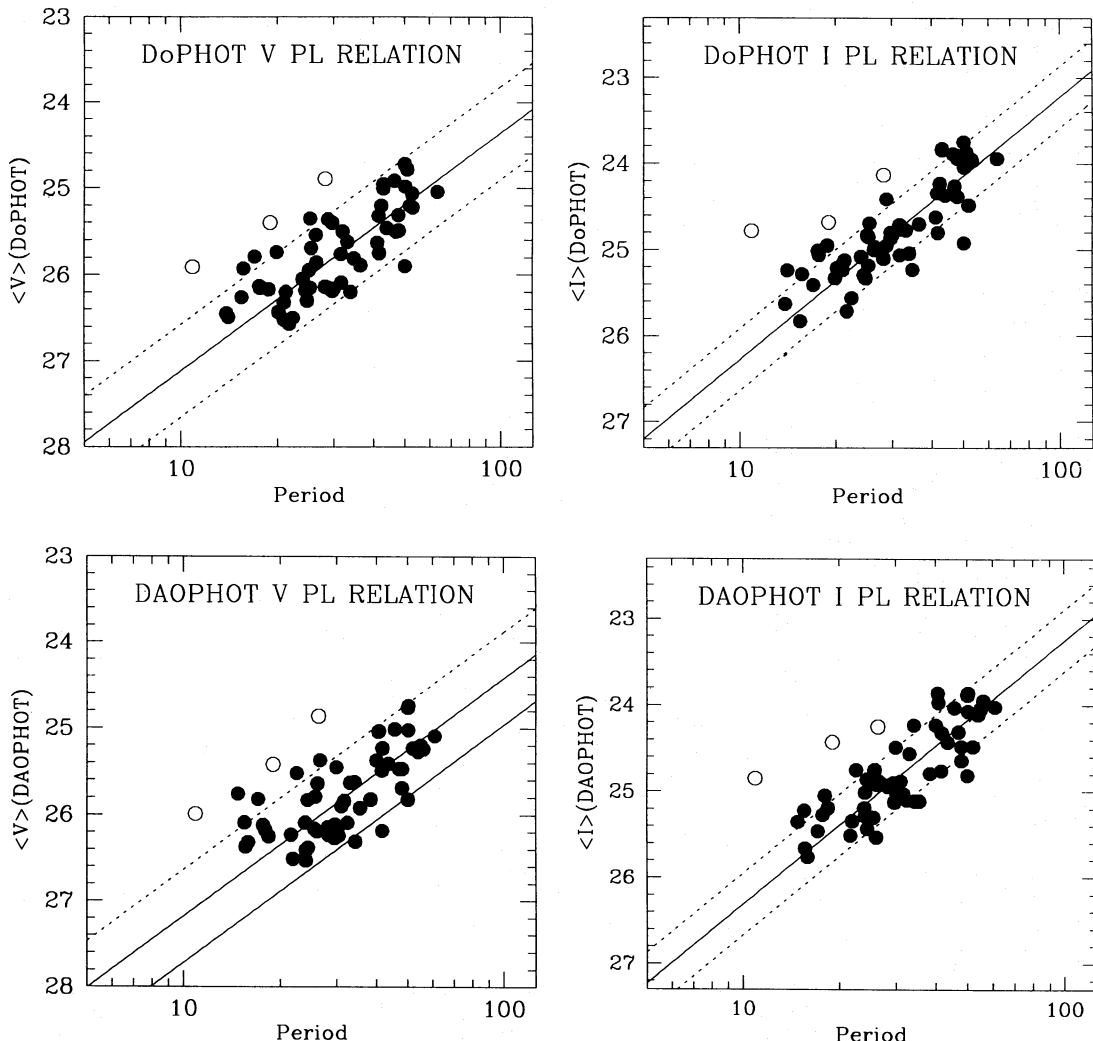


FIG. 12.—The *V* and *I* PL relations for both the DoPHOT and DAOPHOT samples. Symbols are as for Figs. 7 and 8. The solid lines represent the best unweighted fits to the Cepheids with periods between 20 and 70 days, using phase weighted mean magnitudes. The apparent and dereddened distance moduli derived from fitting the DoPHOT and DAOPHOT samples separately agree fully with the results obtained from the common sample (Figs. 7 and 8).

2227-87A from the Space Telescope Science Institute, which is operated by the Association of Universities for Research in Astronomy, Inc., under NASA contract NAS 5-26555. The ground-based calibration was funded in part by NSF grants AST 87-13889 and AST 91-16496 to W. L. F.

REFERENCES

- Aaronson, M., Bothun, G., Mould, J., Huchra, J., Schommer, R. A., & Cornell, M. E. 1986, *ApJ*, 302, 536
 Bessell, M. S. 1991, *A&A*, 242, L17
 Branch, D., et al. 1981, *ApJ*, 244, 780
 Burrows, C. J., et al. 1994, Wide Field and Planetary Camera 2 Instrument Handbook (Baltimore: STScI)
 Burstein, D., & Heiles, C. 1984, *ApJS*, 54, 33
 Cardelli, J. A., Clayton, G. C., & Mathis, J. S. 1989, *ApJ*, 345, 245
 Chiosi, C., Wood, P. R., & Capitanio, N. 1993, *ApJS*, 86, 541
 de Vaucouleurs, G. 1982, *ApJ*, 253, 520
 . 1993, *ApJ*, 415, 10
 de Vaucouleurs, G., de Vaucouleurs, A., & Corwin, H. G., Jr. 1976, Second Reference Catalogue of Bright Galaxies (Austin: Univ. Texas)
 Dufour, R. 1990, in Symp. on Evolution in Astrophysics (ESA SP-310)
 Feast, M., & Walker, A. R. 1987, *ARA&A*, 25, 345
 Ferrarese et al. 1996, in preparation
 Freedman, W. L. 1988, *ApJ*, 326, 691
 Freedman, W. L., & Madore, B. F. 1988, *ApJ*, 332, L63
 . 1990, *ApJ*, 365, 186
 Freedman, W. L., et al. 1994a, *ApJ*, 427, 628
 Freedman, W. L., et al. 1994b, *ApJ*, 435, L31
 Freedman, W. L., et al. 1994c, *Nature*, 371, 757
 Fukugita, M., Okamura, S., Tarusawa, A., Rood, H. J., & Williams, B. A. 1991, *ApJ*, 376, 8
 Hill, B., et al. 1996, in preparation
 Holtzman, J. A., et al. 1995, *PASP*, 107, 156
 . 1996, in preparation
 Hubble, E. 1925, *ApJ*, 62, 409
 Huchra, J. P. 1995, in The MSSSO Heron Island Workshop on Peculiar Velocities in the Universe, in press
 Jacoby, G., Ciardullo, R., & Ford, H. 1990, *ApJ*, 356, 332
 Jergen, H., & Tammann, G. A. 1993, *A&A*, 276, 1
 Kelson, D., et al. 1996, *ApJ*, in press
 Kennicutt, R. C., Freedman, W. L., & Mould, J. R. 1995, *AJ*, 110, 1476
 Knapen, J. H., Cepa, J., Beckman, J. E., Soledad, del Rio, M., & Pedlar, A. 1993, *ApJ*, 416, 563
 Lafler, J., & Kinman, T. D. 1965, *ApJS*, 11, 216
 Madore, B. F. 1985, in IAU Colloq. 82, Cepheids, Theory and Observations, ed. B. F. Madore (Cambridge: Cambridge Univ. Press), 166
 Madore, B. F., & Freedman, W. L. 1991, *PASP*, 103, 933
 Mould, J. R., et al. 1996, *ApJ*, submitted
 Pierce, M. J. 1994, *ApJ*, 430, 53
 Pierce, M. J., & Tully, R. B. 1988, *ApJ*, 330, 579
 Pierce, M. J., Welch, D. L., McClure, R. D., van den Bergh, S., Racine, R., & Stetson, P. B. 1994, *Nature*, 371, 385
 Saha, A., & Hoessel, J. G. 1990, *AJ*, 99, 97
 Saha, A., Labhardt, L., Schwengeler, H., Macchetto, F. D., Panagia, N., Sandage, A., & Tammann, G. A. 1994, *ApJ*, 425, 14
 Sandage, A. 1993, *ApJ*, 402, 3
 Sandage, A., Saha, A., Tammann, G. A., Labhardt, L., Schwengeler, H., Panagia, N., & Macchetto, F. D. 1994, *ApJ*, 423, L13
 Sandage, A., & Tammann, G. A. 1981, A Revised Shapley-Ames Catalogue of Bright Galaxies (Washington, DC: Carnegie Institution)
 Schechter, P. L., Mateo, M., & Saha, A. 1993, *PASP*, 105, 1342
 Schmidt, B. P., Kirshner, R. P., Eastmann, R. G., Phillips, M. M., Suntzeff, N. B., Hamuy, M., Maza, J., & Avilés, R. 1994, *ApJ*, 432, 42
 Silberman, N., et al. 1996, in preparation
 Skillman, E. D., Kennicutt, R. C., Shields, G. A., & Zaritsky, D. 1996, *ApJ*, 462, 147
 Smith, H. A., Silberman, N. A., Baird, S. R., & Graham, J. A. 1992, *AJ*, 104, 1430
 Stetson, P. B. 1994, *PASP*, 106, 250
 . 1996, in preparation
 Stetson, P. B., et al. 1996, in preparation
 van den Bergh, S. 1992, *PASP*, 104, 861
 Walker, A. R. 1988, *PASP*, 100, 949
 Warmels, R. H. 1988, *A&AS*, 72, 19
 Zaritsky, D., Kennicutt, R. C., & Huchra, J. P. 1994, *ApJ*, 420, 87